وزارة التعليم العالي و البحث العلمي

BADJI MOKHTAR UNIVERSITY- ANNABA
UNIVERSITE BADJI MOKHTAR - ANNABA

جامعة باجي مختار - عنابة

FACULTE DE TECHNOLOGIE
DEPARTEMENT DE GENIE CIVIL

Année : 2024

THESE

Présentée en vue de l'obtention du diplôme de DOCTORAT en Génie Civil

Thème

Numerical and experimental study of the mechanical behavior of cold-formed steel compressed columns filled and unfilled with concrete

Option : Structure

Par :

HARRAT Oulfa

Directeur de Thèse:
HADIDANE Yazid - Professeur - Université de Badji Mokhtar, Annaba

Co-directeur de Thèse:
GOUIDER Nadia - MCA - Université de Badji Mokhtar, Annaba

Devant le jury:

Président:	**OUCIEF Hocine**	**Pr.**	**Univ. BADJI Mokhtar ANNABA**
Examinateurs:	**BOUHADRA Abdelhakim**	**Pr.**	**Univ. Abbes Laghrour khenchela**
	MENASRIA Abderrahmane	**MCA.**	**Univ. Abbes Laghrour khenchela**
	MENADI Souad	**MCA.**	**Univ. BADJI Mokhtar ANNABA**
Invité :	**SAIDANI Messaoud**	**Pr.**	**Univ. Coventry U.K**

Acknowledgements

I first express my gratitude to the Almighty Allah for granting me the courage, strength, and patience to complete this humble work.

I would like to convey my heartfelt appreciation and thanks to my supervisor, Pr. Hadidane Yazid, for his patience and encouragement especially during the experimental tests, for his invaluable assistance, persistent support, helpful advice, insightful suggestions, motivation and guidance throughout this work.

From the bottom of my heart I would like to express my special appreciation and thanks to my Co-supervisor, Dr. Gouider Nadia, for her unwavering support, guidance, patience, motivation, and assistance. She consistently offered valuable advice, insightful suggestions, encouragement, and was always willing and enthusiastic to assist in any way she could throughout all stages of this research work.

I also want to extend my deepest gratitude and thanks to Dr. Benzerara Mohammed for his priceless help particularly during the procedures of the article's publication, his invaluable support and encouragement throughout this research.

Words cannot express how grateful and thankful I am to my father Mr. Harrat Messauod for his unwavering support and endless encouragement. Your presence by my side has been a source of inspiration and strength, and I will never forget your valuable contributions throughout my academic journey.

I would like to express my sincere gratitude to the members of the jury. First and foremost, I extend my thanks to the president of the jury Pr. Oucief Hocine for the honor of chairing my defense committee, my thanks also go to the examiners Pr. Bouhadra Abdelhakim, Dr. Menasria Abderrahmane, and Dr. Menadi Souad for their expertise in evaluating my work. I am also grateful to the guest member Pr. Saidani Messaoud.

I am deeply grateful to my mother, Lynda, my brother, Nadim, and my sister, Insaf, for their unwavering support, enduring patience, and constant motivation. This achievement belongs to all of us, and I couldn't have done it without you.

Finally, my heartfelt gratitude goes out to those who have also contributed in this research work, including Dr. S.M. Anas from India, graduated student Righi Anes, Dr. Melais Fatma Zohra, and laboratory technicians Mr. Akroum Kamel and Mr. Khoualdi Keireddine.

Abstract

Built-up cold-formed steel sections (CFS) have been increasingly developed and utilized in recent years, especially in the construction industry, due to their numerous functional and architectural advantages, such as improved load-bearing capacity and increased resistance to elastic instability modes. This thesis presents an experimental and numerical study of two built-up cold-formed steel C-sections with different slenderness and configurations (back-to-back, face-to-face, and box). These columns were assembled using double-row rivets for back-to-back and box configurations, while they were welded together for the face-to-face design. The assembled columns were filled with high-strength ordinary concrete (C25/30). Finite element models were validated using ABAQUS software to evaluate mechanical performances and study the influence of assembly methods on the behavior of cold-formed columns under axial compression. The study also evaluated analytical methods derived from the guidelines of Eurocode 3 and Eurocode 4 for unfilled and filled concrete columns, respectively. Additionally, the effects of concrete confinement were analyzed in accordance with the standards set by the American Concrete Institute (ACI) for both face-to-face and box configurations. The findings demonstrated a strong correlation between the numerical and experimental results, with discrepancies not surpassing 5%. Failure modes showed that the tested columns exhibited instabilities such as local and distortional buckling.

Keywords: Built-up sections; CFS; instability modes; experimental; configurations; finite element; axial compression; confinement.

Résumé

Les sections assemblées en acier formé à froid (PAF) ont été de plus en plus développées et utilisées ces dernières années, notamment dans l'industrie de la construction, grâce à leurs nombreux avantages fonctionnels et architecturaux, tels qu'une capacité portante améliorée et une résistance accrue aux modes d'instabilité élastique. Cette thèse présente une étude expérimentale et numérique de deux sections en forme de C assemblées en acier formées à froid avec différents élancements et configurations (dos-à-dos, face-à-face et en caisson). Ces colonnes ont été assemblées par des rivets en double rangée pour les configurations dos-à-dos et en caisson, tandis qu'elles ont été soudées ensemble pour la conception face-à-face. Les colonnes assemblées étaient remplies de béton ordinaire de bonne résistance (C25/30). Des modèles par éléments finis ont été validés en utilisant le logiciel ABAQUS, pour évaluer les performances mécaniques et étudier l'influence des moyens d'assemblage sur le comportement des colonnes formées à froid sous compression axiale. L'étude a également évalué les méthodes analytiques dérivées des lignes directrices de l'Eurocode 3 et de l'Eurocode 4 pour les colonnes en béton non remplies et remplies, respectivement. De plus, les effets du confinement du béton ont été analysés conformément aux normes établies par l'American Concrete Institute (ACI) pour les configurations en face-à-face et en caisson. Les résultats ont révélé une bonne corrélation entre les résultats numériques et expérimentaux, les écarts ne dépassant pas 5%. Les modes de défaillance ont montré que les colonnes testées ont présenté des instabilités telles que le flambage local et distortional.

Mots-clés: Sections assemblées; PAF; modes d'instabilité; expérimentale; configurations; éléments finis; compression axiale; confinement.

.

الملخص

تم تطوير واستخدام أقسام الصلب المجمعة المشكلة بالبارد (CFS) بشكل متزايد في السنوات الأخيرة، خاصة في البناء و الصناعة، نظرًا لمزاياها الوظيفية والمعمارية العديدة، مثل زيادة قدرة تحمل الحمولة وزيادة مقاومتها لأوضاع عدم الاستقرار المرونية. تقدم رسالة الدكتوراه هذه دراسة تجريبية و رقمية لقسمين على شكل C من أقسام الصلب المجمعة المشكلة بالبارد مع إختلاف الإرتفاعات و التكوينات (ظهرًا لظهر، وجهًا لوجه، وصندوق). تم تجميع هذه الأعمدة باستخدام براشم ذات صفين مزدوجة لتكوينات ظهرًا لظهر وصندوق، بينما تم لحامها معًا لتصميم التكوين وجه لوجه. تم ملء الأعمدة المجمعة بخرسانة عادية ذات قوة عالية (C25/30). تم التحقق من نماذج العناصر المحدودة باستخدام برنامج ABAQUS لتقييم الأداء الميكانيكي ودراسة تأثير طرق التجميع على سلوك الأعمدة المشكلة بالبارد تحت الضغط المحوري. كما قامت الدراسة بتقييم الأساليب التحليلية المستندة إلى إرشادات اليورودكود 3 واليورودكود 4 لعمود الخرسانة غير المملوء والمملوء على التوالي. بالإضافة إلى ذلك، تم تحليل تأثيرات حبس الخرسانة وفقًا للمعايير المحددة من قبل المعهد الأمريكي للخرسانة (ACI) للتكوينات وجهًا لوجه و على شكل صندوق. أظهرت النتائج وجود ارتباط قوي بين النتائج الرقمية والتجريبية، حيث لم تتجاوز الفروقات 5%. أظهرت أوضاع الفشل أن الأعمدة المختبرة تعاني من عدم استقرار مثل الإنحناء المحلي و التشويهي.

الكلمات المفتاحية: الأقسام المجمعة; الصلب المُشَكَّل بالبارد; أوضاع عدم الاستقرار; تجريبية; التكوينات; العناصر المحدودة; الضغط المحوري; الحصر.

NOTATIONS AND ABBREVIATIONS

CFS	Cold-formed steel
CF-CFS	Concrete-filled cold-formed steel
DSM	Direct strength method
FEM	Finite element method
FSM	Finite strip method
ACI	American Concrete Institute
AISI	American Iron and Steel Institute
AS/NZS	Australian/New Zealand Standard
ASD	Allowable stress design
LRFD	Load and resistance factor design
LSD	Limit states design
f_{yb}	Yield strength of steel
E_s	Elastic modulus of steel
G_s	Shear modulus of steel
ν_s, ν_c	Poisson's coefficients of steel and concrete respectively
α	Linear expansion coefficient
ρ_s, ρ_c	Density of steel and concrete respectively
A_{eff}	Effective area of the cross-section
$N_{c,Rd}$	Compressive strength of the cross-section
$\bar{\lambda}$	Reduced slenderness
λ	Slenderness
l_f	Buckling length
i	Radius of gyration
A_s	Cross-section of steel
γ_{M0}, γ_{M1}, and γ_{M2}	Partial material safety factor of steel
ℓ_{cr}	Critical length
N_{cr}	Euler's critical load
σ_{cr}	Euler's critical stress
λ_1	Eulerian slenderness
χ, χ_d	Reduction coefficient
α	imperfection factor

f_{ya}	Average yield strength
β_A	Coefficient of reduction of the section
ε_c	Compressive strain of unconfined concrete
f_c	Compressive strength of unconfined concrete
ε_{cc}	Compressive strain of confined concrete
f_{cc}	Compressive strength of confined concrete
f_l	Confining pressure of the concrete
k_1, k_2	Constants were set as 4.1 and 20.5 respectively
k_3	Degradation parameter
B	Width of the cross-section
t	Thickness of the cross-section
f_u	Tensile strength of steel
b_{eff}	Effective width
b_p	Notional flat of plane element
b	Total wall width
c	Total width of stiffener
k	Coefficient dependent on the type of forming process
n	Number of 90° bends in the cross-section with an inner radius r<5t
ψ	Stress ratio
k_σ	Buckling coefficient
K	Rigidity of the elastic support per unit length
$\bar{\lambda}_d$	Relative slenderness
d	Diameter of the rivet
p	Pitch
m	Margin
p_t	Transverse pitch
p_d	Diagonal pitch
$\sigma_\perp$	Perpendicular component to the section
$\tau_\perp$	Component in the plane of the section perpendicular to the longitudinal axis of the weld bead
$\tau_{//}$	Component in the plane of the section parallel to the longitudinal axis of the weld bead
β_w	Correlation factor of the weld bead

γ_{Mw}	Partial safety factor of the weld bead
N_{sd}	Calculated axial force
$N_{Pl,Rd}$	Plastic resistance normal force
$N_{Pl,R}$	Value of the plastic resistance normal force $N_{Pl,Rd}$ considering all partial safety factors γ_{M1} and γ_c equivalent to 1,0
γ_c	Partial material safety factor of concrete
$(EI)_e$	Flexural rigidity of the composite column relative to the considered buckling plane
I_s, I_c	Respective flexural inertias of the steel profile and concrete are considered for the given bending plane
E_c	Elastic modulus of concrete
E_{cm}	Secant modulus of concrete
A_c	Cross-section of concrete
b_p	Width of the profile
H	Height of the cross-section
C	Length of dropped edge
R	Bend radius
B’	Width of the concrete
H’	Height of the concrete
ε_y	Yield strain of the steel
ε_u	Ultimate strain of the steel
σ_y	Yield stress of steel
G	Gage length of the specimen
W	Width of the specimen
R	Radius of fillet of the specimen
L	Overall length of the specimen
A	Length of reduced section of the specimen
B	Length of grip section of the specimen
C	Width of grip section of the specimen
TEST BE	Experimental results of cold-formed steel built-up back-to-back empty columns
TEST BF	Experimental results of cold-formed steel built-up back-to-back filled with concrete columns

TEST FE	Experimental results of cold-formed steel built-up face-to-face empty columns
TEST FF	Experimental results of cold-formed steel built-up face-to-face filled with concrete columns
TEST BOE	Experimental results of cold-formed steel built-up box section empty columns
TEST BOF	Experimental results of cold-formed steel built-up box section filled with concrete columns
FEA BE	Numerical results of cold-formed steel built-up back-to-back empty columns
FEA BF	Numerical results of cold-formed steel built-up back-to-back filled with concrete columns
FEA FE	Numerical results of cold-formed steel built-up face-to-face empty columns
FEA FF	Numerical results of cold-formed steel built-up face-to-face filled with concrete columns
FEA BOE	Numerical results of cold-formed steel built-up box section empty columns
FEA BOF	Numerical results of cold-formed steel built-up box section filled with concrete columns

TABLE OF CONTENTS

CHAPTER I

Bibliographic research

CHAPTER II

Concrete-filled cold-formed steel built-up columns

CHAPTER III

Regulatory aspects

CHAPTER IV

Numerical study of cold-formed steel built-up columns

CHAPTER V

Experimental study and validation

LIST OF FIGURES

LIST OF TABLES

GENERAL INTRODUCTION

GENERAL INTRODUCTION

Cold-formed steel profiles (CFS) are extensively utilized in the construction of residential and industrial buildings owing to their notable benefits. These advantages include a remarkable strength-to-weight ratio, effortless assembly, precise dimensional accuracy, and the ability to achieve a wide range of shapes. The widespread adoption of CFS profiles in the construction industry is a testament to their effectiveness and versatility. Cold-formed steel is also known as light-gauge steel. In civil engineering, cold-formed steel elements are typically used in industrial buildings as purlins, columns, trusses, or frame elements, as well as in storage supports, vehicle bodies, and various types of equipment. These profiles are manufactured through a cold-forming process, where steel sheets are stamped, rolled, or pressed to achieve the desired product. Different profiles, such as C-sections and Z-sections, are commonly used as purlins and baseboards in roofing and wall systems, where they serve as secondary load-bearing elements. On the flip side, there is a growing preference for thin-walled cold-formed profiles within the metal construction field. These profiles come with highly sought-after attributes, such as lightweight composition, simple assembly, precise dimensions, and a wide array of achievable shapes. Nonetheless, the thin nature of these profiles can lead to instability in the flat sections when exposed to external loads, underscoring the necessity for a detailed examination of the structural behavior and stability of such elements.

Nowadays, the use of cold-formed steel built-up columns as compression elements is increasing due to their several advantages over individual columns. These elements, assembled through various methods (riveting, bolting, welding, etc.), can span greater distances, offer higher load-bearing capacities, and provide practical solutions in light steel construction when a single section cannot meet load-bearing or serviceability requirements. Due to the narrowness of the web and the high width-to-thickness ratio, built-up compressed columns are susceptible to various types of instability, such as global, distortional, and local buckling. Global buckling is characterized by translation as a rigid body (translation and/or rotation without deformation) without invariability of the cross-section at the flanges and the web. Additionally, distortional buckling involves movements at the linear junction between the edge stiffener and the flange, without translation of the cross-section or rotation of the rigid body. In contrast, local buckling consists of deformations of the flange, web, and edge elements without movement at the linear junction between the web and the flange, or between the edge stiffener and the flange.

In the design of modern slender structures, steel-concrete composite structures are increasingly being incorporated. These structures offer multiple advantages, including high strength, excellent ductility, and superior stiffness, all while allowing for significant material optimization. Additionally, composite columns can serve as formwork, leading to cost savings and accelerated construction schedules. Recently, concrete-filled cold-formed steel (CF-CFS) built-up columns have been increasingly used in various civil engineering structures due to their exceptional mechanical and economic efficiency. The appropriate combination of steel and concrete provides crucial stability to the overall structure by supporting compressive loads with their concrete core, which enhances ultimate strength, deformability, and energy absorption capacity under extreme loads. Moreover, the confinement effect of the concrete filling can prevent or at least delay local buckling of the steel column. Extensive research on these concrete-filled profiles, such as the studies by Rahnavard et al. (2022), has provided a better understanding of the behavior of these structures under various conditions, as well as their resistance to instability phenomena. Furthermore, the use of concrete further enhances the performance of these structures.

OBJECTIVE OF THE THESIS

The objective of this thesis is to study the mechanical performance and the influence of assembly techniques on the behavior of cold-formed steel unfilled and concrete-filled columns, with C-shaped sections in different configurations (back-to-back, face-to-face, and box) under axial compression. Additionally, it aims to identify a stronger element that enables the creation of more durable, lighter, and material-efficient cross-sections. The thesis also seeks to increase the lateral rigidity of built-up cold-formed steel columns through concrete filling and encasement. Finally, it presents the standard regulatory design method for structures using cold-formed steel profiles, in accordance with the Eurocodes, the most widely adopted European standard.

THESIS STRUCTURE

This thesis is structured into five chapters:

- Chapter one provides a detailed literature review on cold-formed steel profiles, focusing on their manufacturing techniques and applications. It describes the various

configurations of these profiles, highlights their benefits, and discusses potential issues related to instability.

- Chapter two focuses on cold-formed steel built-up columns, both empty and filled with concrete. It also address various types of available columns, the properties of the materials composing them, the effects of slenderness and buckling calculation codes, confinement effects, as well as their significance in modern construction.

- Chapter three elaborates on the regulatory aspects based on European standards (EN 1993-1-3 and EN 1994-1-1) concerning the behavior of cold-formed steel assembled columns, unfilled and filled with concrete. It also highlights the concept of effective width as well as the development of different types of connections, including rivets and welds.

- Chapter four elucidates the three-dimensional nonlinear numerical analysis of cold-formed steel built-up columns, both unfilled and concrete-filled. It provides a comprehensive overview of the various numerical models developed utilizing the ABAQUS software. The numerical results obtained are validated through analytical approaches based on European standards (EN 1993-1-3 and EN 1994-1-1).

- Chapter five delves into an experimental study of the models under investigation, involving various stages of specimen preparation and testing procedures. Thus, validation and interpretation of the results are carried out by comparing the numerically obtained results with those obtained experimentally.

- At the conclusion of this thesis, a comprehensive synthesis of the significant results obtained in the studied subject is presented in the general conclusion, accompanied by recommendations and perspectives for future studies.

CHAPTER I

Bibliographic research

I.1 INTRODUCTION

At present, the structural elements used in steel frameworks can be manufactured either hot at high temperatures or cold by bending simple metal sheets to obtain the desired shapes. Hot-rolled profiles are more commonly used than cold-formed profiles in practice. But with the current trend towards building stronger and lighter, cold-formed steel profiles, particularly those with thin-walled, are beginning to gain in popularity in the steel construction market. These profiles offer several compelling features that make them highly competitive, including their lightweight design, ease of assembly, precise dimensions, and the wide range of shapes they can produce (Mansuri and Parmar, 2017).

The United States and the United Kingdom used cold-formed steel elements in construction in the 1850s. In the 1920s and 1930s, cold-formed steel was not yet accepted as a building material because there were no design standards for it and little information on its use in building codes. The Virginia Baptist Hospital, built around 1925 in Lynchburg, Virginia, was one of the first uses of cold-formed steel as a building material. Lustron Corporation built nearly 2,500 cold-formed steel frame homes in Albany, New York, just 20 years later. These affordable homes were built for veterans returning from the Second World War. It was the beginning of the cold-formed steel construction adventure (Dubina et al., 2012).

Recently, cold-formed steel profiles are increasingly used as major structural components, such as wall stud systems in housing, trusses and racking structures. They are rigid and strong, in addition the profiles are generally light and thin, as the cold-formed steel can be less than 1mm thick. To improve load-bearing capacity and diversify their application in civil engineering, research into CFS elements is currently underway.

In addition, due to the production of more economical steel coils, particularly in zinc-coated or aluminium/zinc-coated form, the use of cold-formed steel structures is increasing worldwide. The cold forming process is used to form these coils into thin-walled sections. Their thickness is generally less than 3mm, which is why they are often referred to as thin sections. However, new advances have made it possible to cold-form 25mm thick sections. However, open sections around 8mm thick have become more common in building construction (Yu, 2016).

The steel used recently for thin-walled sections is high-strength steel with a yield strength of 250MPa to 550MPa. However, engineers and designers of these structures encounter design problems when using thin sections with high-strength steel. Steel structures do not generally encounter these problems when they are designed. Due to the thinness of the sections, which

reduces loads and buckling stresses, structural instability of these sections is more likely to occur. Furthermore, using higher-strength steel typically balances the buckling stress and yield strength of thin-walled sections (Dubina et al., 2012).

The American Iron and Steel Institute's design specifications for cold-formed steel structural members were first published in 1946 and have been regularly updated based on research until the latest edition in 2016 ("North American Specification for the Design of Cold-Formed Steel Structural Members, 2016 Edition," 2016).

A design standard AS/NZS4600 for the design of cold-formed steel structures was published in December 2005 in Australia and New Zealand (*Cold-formed steel structures*, 2005).

The European standard EN1993-1-3 was created and published in 2006 as the European design code Eurocode 3 for the design of steel structures. General rules, part 1-3. Additional rules for cold-formed thin-gauge members and plates (European Committee for Standardization, 2006).

I.2 COLD-FORMED STEEL SECTIONS

Because of its many advantages, cold-formed steel (CFS) is frequently used in both residential and commercial construction. The use of thin-walled constructions has increased recently because of their excellent strength-to-weight ratios, formability, and speed of assembly. Moreover, because cold-formed steel be recycled, it is cheap and eco-friendly (Schafer, 2011). Prismatic elements made up of a succession of flat walls of constant thickness and folds are called cold-formed elements and are intended to fulfil a structural function as a framing element or sometimes as a roof (Figure I.1).

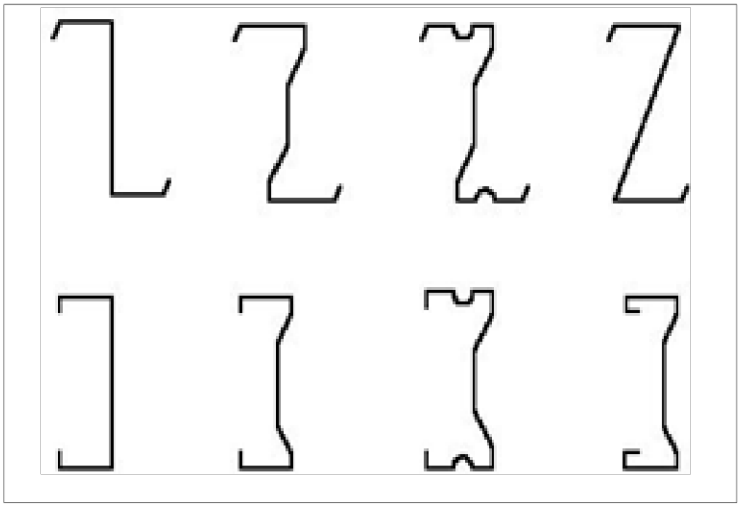

(a)

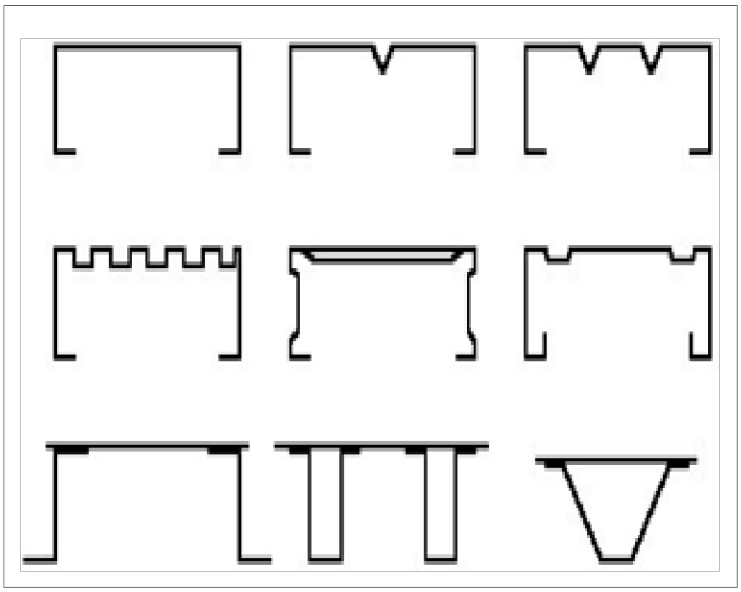

(b)

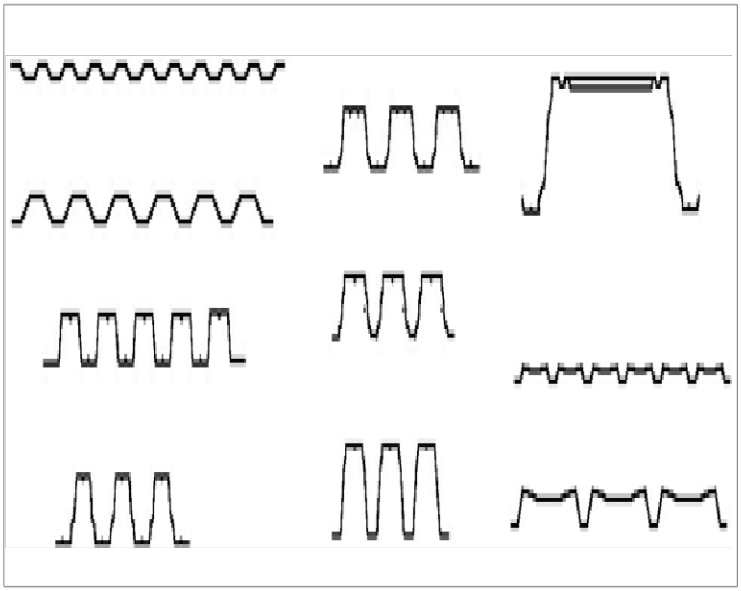

(c)

Figure I.1. The different forms of cold-formed steel sections: (a) Beam type; (b) Load-bearing for roofing; (c) Panels (European Committee for Standardization, 2006).

Folds acting as stiffeners (edge stiffeners or full flat wall stiffeners) are a feature of cold-formed sections in panels subjected to compression. The purpose of these folds is to delay or prevent premature buckling of the panels concerned (Figure I.2).

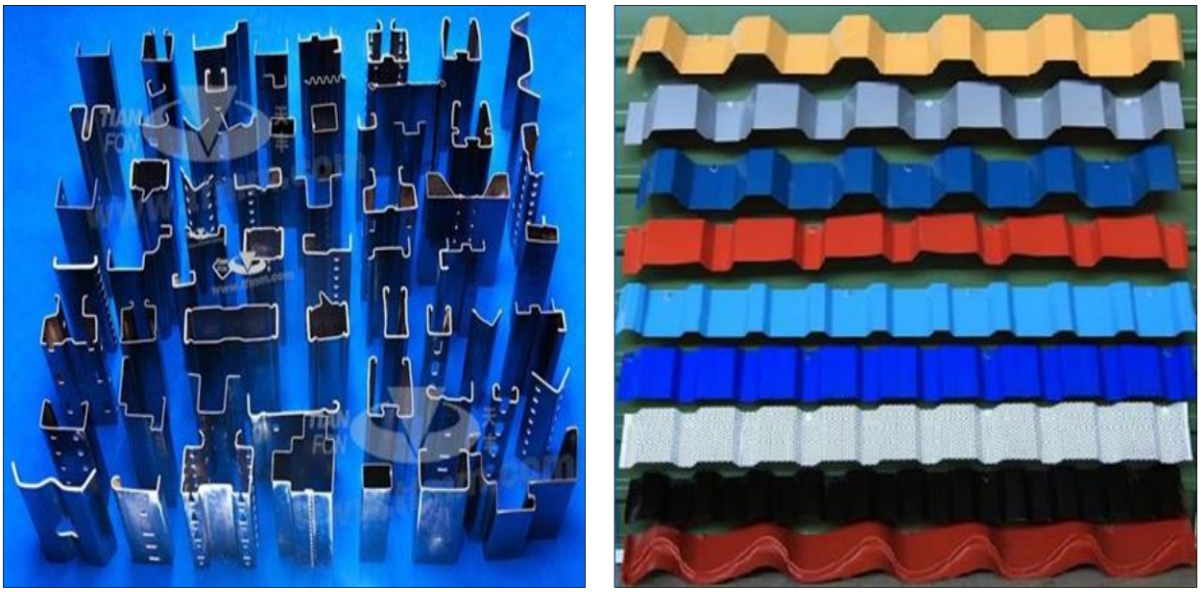

Figure I.2. Types of cold-formed profiles.

I.2.1 Manufacturing

Advancements in industrial processes have introduced cutting-edge, fast, and more energy-efficient manufacturing techniques. These methods have facilitated the creation of sections with innovative and optimized geometric shapes, some reaching thicknesses of up to 25mm (Becque, 2019; Xie et al., 2018). Furthermore, the possibility of mass production has allowed for the optimization of section shapes based on structural or economic criteria, thus offering remarkable architectural possibilities for structures. However, since current manufacturing technologies enable the production of sections with unusual configurations, the sizing and analysis of these elements can be considered a complex and demanding task.

The simplest manufacturing process involves folding a sheet of material through a series of bends to produce samples of reduced length and simple geometry. This process only works with very simple cross-sections, such as angles, C-sections and Z-sections (Alex and Iyappan, 2016).

In addition, press brake bending is the most commonly used manufacturing method because it can produce a greater variety of cross-sectional shapes. Each fold is usually formed separately. It is forbidden to bend sections longer than 5m using a press brake.

However, very large quantities of sections with a specific shape are usually produced by rolling. The initial cost of tooling is high, but labour costs are low. Folding with a press brake is typically used for small production runs where various section shapes are needed, and where the process is more cost-effective than the initial method (Kouider et al., 2021).

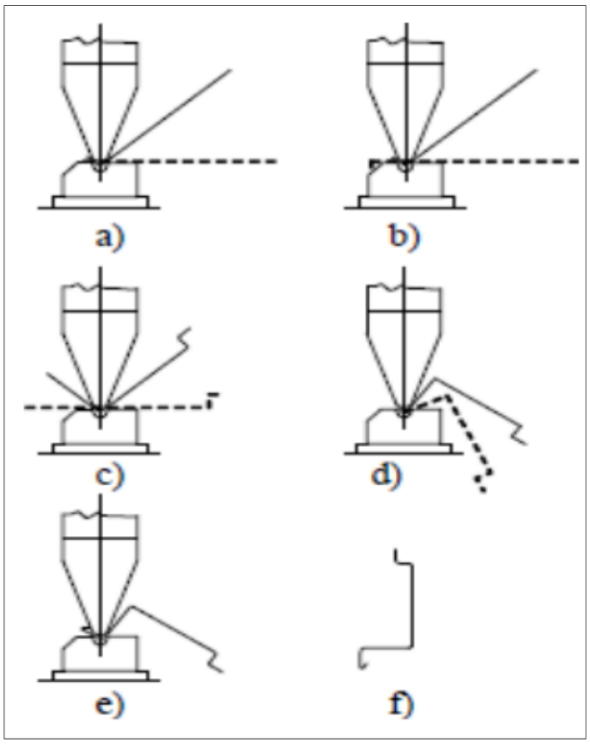

Figure I.3. Forming steps in the press-brake process (Veríssimo, 2008).

I.2.2 Applications

Thus, where the combination of such profiles and panels offers the greatest advantage, thin cold-formed elements are mainly used in the construction of low-rise buildings with modest spans. The most common applications of cold-formed steel profiles can be summarized as follows:

I.2.2.1 Roof and wall components

In traditional practice, cold-formed steel profiles are primarily utilized as purlins and cladding rails to reinforce coverings in structures, particularly in industrial buildings, as depicted in Figure I.4.

The profiles designed for this purpose come in the form of Z-sections and their variations, which streamline the integration of sleeves and overlaps to enhance the efficiency of the profiles in multi-bay applications.

Figure I.4. Cold-formed steel profiles used as purlins and cladding rails.

I.2.2.2 Cold-formed steel frameworks

An expanding market for cold-formed steel profiles involves on-site prefabricated frames and panels for walls, roofs, and standalone structures. This approach has been embraced in the construction of small-scale industrial and commercial buildings (Figure I.5).

Figure I.5. Cold-formed steel framing.

I.2.2.3 Partition walls

A particular application involves the use of extremely lightweight sections in combination with plasterboard panels in constructing partition walls, thus creating a thin yet sturdy wall (Figure I.6).

Figure I.6. Cold-formed steel partition walls.

I.2.2.4 Floor joists, large panels for housing envelope

Cold-formed steel profiles provide an alternative to wooden joists in small-scale residential and commercial building floors with limited space, as depicted in Figure I.7.

Figure I.7. Floor joists made of cold-formed steel.

Furthermore, these products can be utilized in the production of prefabricated wall panels, which are factory-assembled and then installed on-site within housing units, as illustrated in Figure I.8.

Figure I.8. Wall panels made of cold-formed steel profiles.

I.2.2.5 Flooring for composite concrete/steel slabs in multi-story buildings

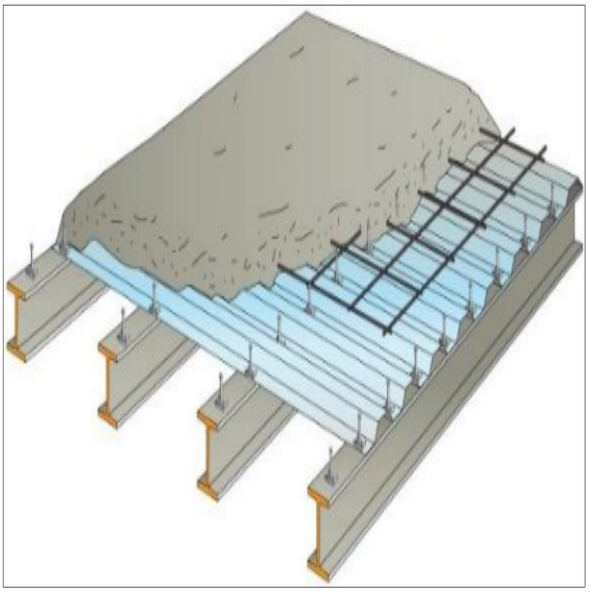

Figure I.9. Composite floors (steel-concrete).

I.2.2.6 Trusses

Cold-formed steel profiles also find application in truss beam systems and roof trusses, as illustrated in Figure I.10.

Figure I.10. Roof truss using C-sections.

I.2.2.7 Storage shelving

Shelving systems designed for warehouses and industrial facilities are typically constructed from perforated cold-formed steel profiles (Figure I.11). Most of these systems come with special clip fastenings or bolted joints for easy installation.

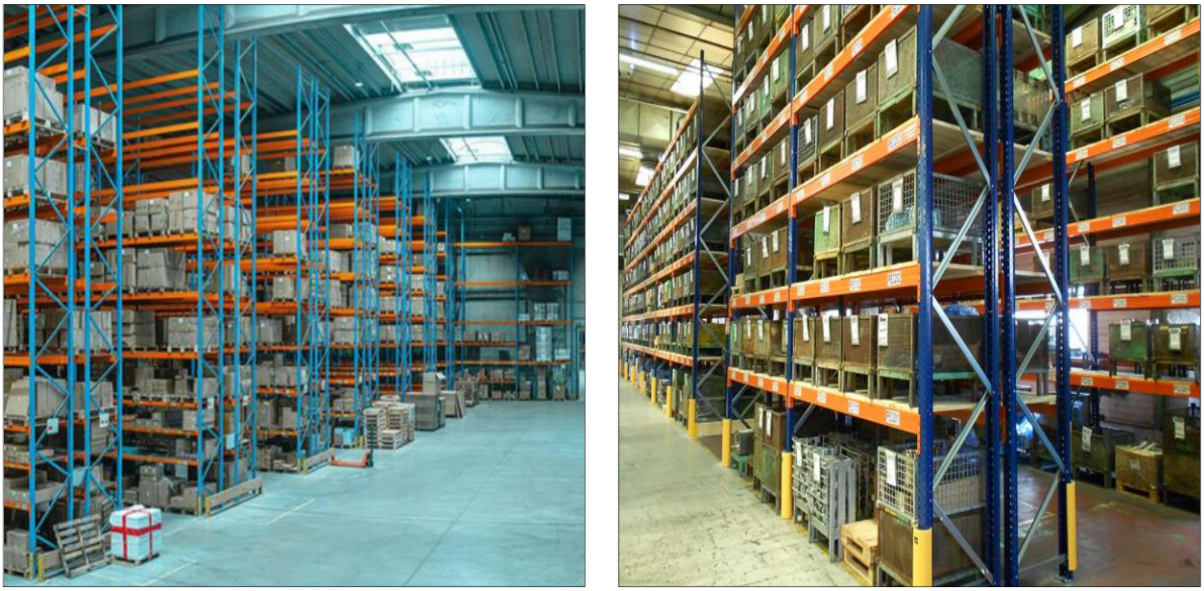

Figure I.11. Storage shelving systems.

I.2.2.8 Prefabricated buildings

A common application of cold-formed steel products is in the construction of prefabricated units (Figure I.12).

Figure I.12. Prefabricated modular units used for buildings, schools, and offices.

I.2.3 Advantages of cold-formed steel elements

Light-frame construction systems, such as those using cold-formed steel members, offer a number of inherent advantages over heavy-frame construction, including design flexibility and shorter construction cycles, light weight, ease of fabrication and assembly, and economy of transport and handling (Dar, 2021). Cold-formed steel profiles generally offer the following structural advantages:

I.2.3.1 Lateral loads resistance

Structures are designed to absorb the energy produced by ground and wind movements, while experiencing varying degrees of deformation. The level of deformation varies according to the materials used in the construction, the design of the structure, the quality of the construction and the requirements of the design code in force. Cold-formed steel is the ideal material for this purpose because it is ductile, making it more resistant than other more brittle materials to earthquakes and high winds, and it has inherent resistance to uplift and gravity loading (Yu, 2016).

I.2.3.2 Consistent performance

When subjected to structural loads and movements caused by high winds and earthquakes, steel behaves in a very predictable way. Indeed, because steel is an inherently stable material with consistent chemical and mechanical properties, the fasteners and joints used to join cold-formed steel framing members retain their strength and reliability over time (Kanthasamy et al., 2022).

I.2.3.3 Strength-to-weight ratio

This ratio is calculated by dividing the maximum load imposed by the weight of the material in order to compare the advantages of different materials. All commonly used construction materials have the highest strength-to-weight ratio. CFS corners considerably increase the strength of the walls in a C-pillar, which offers a strength-to-weight ratio up to seven times greater than that of timber used in construction framing (Shanmugam et al., 2021).

I.2.3.4 Cold-formed steel recycling

According to the study, the Steel Recycling Institute claims that steel is more recyclable than paper, plastic, glass, copper, lead, and aluminum. All CFS products, including frames, are made from recycled steel. A steel structure is 100% recyclable at the end of its life and typically contains at least 25% recycled steel.

I.2.4 Disadvantages of cold-formed steel elements

I.2.4.1 Corrosion resistance

When moisture encounters bare steel, it initiates a chemical process known as corrosion, which gradually deteriorates the metal's structural characteristics. Typically, CFS components are shielded from moisture through a thin coating of zinc applied using a procedure called galvanization.

Zinc provides dual protection for steel. Firstly, it acts as an excellent shield against moisture due to the superior adhesion properties and exceptional resistance to abrasion found in galvanized coatings (Figure I.13). Unlike paint, a galvanized coating remains intact over time, without cracking, peeling, discoloration, or mechanical deterioration. Furthermore, when the underlying steel becomes exposed due to cuts, scratches, or other surface damage, zinc offers cathodic protection through its sacrificial reaction. This occurs because zinc is more electronegative (reactive) than steel in the galvanic hierarchy, preventing steel from corroding when in close proximity to zinc. Consequently, this negates the need for additional corrosion

protection on the edges of metal-clad steel structural members, even if they undergo cutting, stamping, or drilling during fabrication or on-site (Yu, 2000).

In enclosed areas such as walls, attics, and floors, zinc coatings have the potential to safeguard steel for a remarkable span of up to 1150 years. When it comes to outdoor locations that are either fully exposed or partially so, particularly in harsh environments with elevated humidity and external pollutants, we can project significantly accelerated corrosion rates, yet the coating's lifespan can still extend beyond 150 years, surpassing the expected service life of contemporary buildings.

Figure I.13. Typical spangle of a galvanized coating.

I.2.4.2 Thermal conductivity

The management of energy consumption, as an essential element of sustainability, has risen to the top of global regulatory priorities. Buildings have now become a leading target for energy efficiency advocates. New codes and standards continue to evolve, and stakeholders in construction, as well as regulatory bodies, are increasingly knowledgeable about energy consumption issues in buildings (Moradibistouni et al., 2021). In wall design, the focus is typically on managing energy efficiency by limiting thermal transfer between the interior and exterior surfaces of the wall, or between both sides of an interior wall. Every component of a wall, whether it be wooden or steel studs, joists, rafters, concrete beams, masonry blocks, bricks, or even nails and screws, has the potential to create a thermal bridge, allowing heat and cold to propagate from one side to the other. In some scenarios, additional heat losses have a

minimal impact on actual energy consumption, but in other cases, particularly in cold climates, they can be significant. Steel, in particular, is a highly efficient conductor of heat and cold. One of the most common methods to mitigate thermal transfer in a cold-formed steel wall structure is the use of continuous insulation. When applied to the exterior side of the cold-formed steel studs, this insulation creates a thermal break, enabling the system to meet desired energy performance requirements (Liang et al., 2022).

An alternative that has been studied but is seldom used in Scandinavia and cold climates is the split stud (Figure I.14), where staggered longitudinal openings are made in the stud's web during manufacturing. These openings create a longer path for the circulation of thermal energy, thereby reducing the amount of heat or cold reaching the sole plate on the opposite side of the stud. However, this product is rarely utilized due to the additional manufacturing costs and reduced load-bearing capacity resulting from the openings in the web.

Figure I.14. Split stud for thermal energy circulation.

I.3 CONNECTION AND ASSEMBLY METHODS

Assembly technique plays a widely incredible role in producing an array of products, from electronic devices to automotively. These method, sometimes highly complexed, aiming at combining various components in a dependable and efficient manner. Among one of the most common approaches, welding is quite distinguished for its aptitude to weld metal parts collectively with heat and pressure, thus fostering a sturdy connection. Conversely, mechanical assembly leans on fasteners like screws, bolts, or rivets to bind parts together. The usage of

adhesive assembly techniques is also extensively favoured, utilizing unique glues to form a lasting bond among materials (Yu et al., 2019).

Welding, bolts, and rivets represent common methods employed for joining components within cold-formed steel structures. Rivets and welds are typically utilized for connecting braces, attaching posts to either the top or bottom runner, assembling window lintels, and securing studs. Conversely, bolts are typically employed to fasten a bottom rail to concrete or masonry.

I.4 CHARACTERISTIC PROPERTIES OF COLD-FORMED STEEL PROFILES

When considering the use and design of structures made from cold-formed steel profiles, it's important to recognize that the technology employed in their manufacture imparts distinct features. To begin with, the process of cold forming alters the steel's stress-strain curve. In contrast to the original material, cold rolling enhances both the yield strength and, in certain instances, the ultimate strength. These strengths remain particularly high in the corners and curved edges, and they remain appreciable in the flanges. However, it's worth noting that these characteristics remain mostly unaffected during the compression bending process in the flanges. These effects, of course, are absent in the case of hot-rolled sections (Yu et al., 2019).

The rise in yield strength results from work hardening and varies based on the specific steel employed in the cold rolling process. Conversely, the elevation in ultimate strength is associated with plastic deformation, a process that typically goes hand in hand with reduced ductility and relies primarily on the metallurgical characteristics of the material.

When a forming force is applied to the sheet, it deforms and plasticizes to achieve the desired shape, reaching a specific stress level. If we reload immediately, this stress level represents the new elastic limit. However, if reloading occurs after a certain duration, the elastic limit will be more significant (Somadasa, 2006). In practice, the increase in tensile strength f_u is much smaller than the increase in yield strength f_{yb}, resulting in a change in the shape of the stress-strain curve of the steel, as illustrated in Figure I.15.

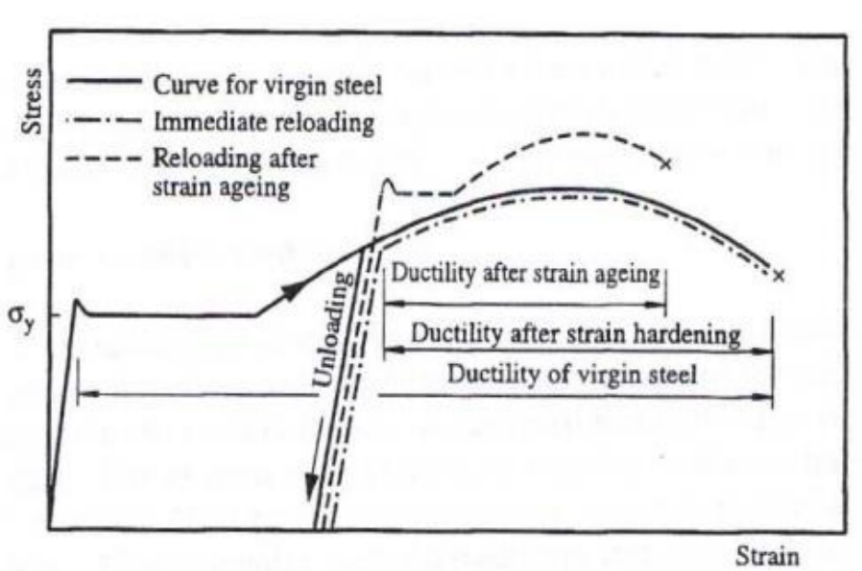

Figure I.15. Effect of strain hardening and strain aging on stress–strain characteristics (Kouider et al., 2021; Somadasa, 2006).

Design standards offer equations to evaluate the boost in yield strength in cold-formed steel profiles when contrasted with the base material. Conversely, hot-rolled profiles are impacted by residual stresses that arise from air cooling following the hot-rolling process. These stresses are primarily of the membrane nature, contingent upon the section's shape, and exert a substantial impact on buckling resistance. Consequently, residual stresses serve as the primary driving factor necessitating the utilization of distinct buckling curves in European design codes for hot-rolled sections (CEN, 2005).

For cold-formed sections, residual stresses primarily take the form of flexural stresses, and their impact on buckling strength is relatively less pronounced compared to membrane-type residual stresses. In contrast, the cold-rolling process generates distinct residual stresses within the section compared to the compression bending process, potentially leading to variations in the section's strength in situations where buckling and plastic deformation come into play together (Weng and Pekoz, 1990).

The European buckling curves have been fine-tuned using experimental data from hot-formed steel profiles. These curves are derived from the established Ayrton-Perry formula, with adjustments made to the imperfection factor α to ensure calibration.

Because of the distinct mechanical characteristics of cold-formed sections, the impact of cold forming and residual stresses differs from that in hot-rolled sections, necessitating the justification of unique buckling curves (Dubina, 1996). Today, there are numerical and

experimental methods accessible to calibrate suitable α factors for cold-formed sections (Dubina, 2001). Nevertheless, in practical design applications, the same buckling curves as those employed for hot-rolled sections are still employed (CEN, 2005; European Committee for Standardization, 2006).

I.5 INSTABILITY MODES OF COLD-FORMED STEEL PROFILES

Over the past decades, with the increasing use of high-strength steel in the steel and metallurgical industry, it has become inevitable to reduce the thickness of sections in thin-walled profiles. Current design and resistance standards have thus facilitated the adoption of cold-formed steel elements with significantly reduced thickness. However, it is crucial to note that the thinner the section, the more susceptible the element is to deformation. In this context, research efforts have been deployed to enhance buckling resistance by incorporating intermediate stiffeners (folds) in the flange and/or web. Nevertheless, the inclusion of intermediate stiffeners may raise the critical constraint of local buckling. Consequently, it is necessary to ascertain whether the use of these reinforcements also provides adequate resistance to the distortional mode (J. Chen et al., 2010).

Most cold-formed steel components have narrow and thin cross-sectional shapes, making them particularly susceptible to various instability phenomena, including local, distortional, and global buckling, along with their potential interactions. Depending on the element's length and cross-sectional dimensions, one of these buckling modes may become critical. Furthermore, the inherent complexity in the design of cold-formed steel profiles is justified by the increasing research efforts aimed at developing a straightforward and rational method that integrates failure mechanisms such as local, distortional, and global buckling into the sizing processes (Moen and Schafer, 2009).

Local buckling is a common occurrence in cold-formed steel profiles, and it is distinguished by the relatively short buckling wavelength of the individual plates within the section. During this instability, the walls bend like plates, yet the junction lines between flat elements remain intact, without undergoing any movement (Figure I.16.a).

Distortional buckling, as implied by its name, is a form of instability arising from the distortion of the cross-section. This mode occurs at intermediate or medium wavelengths, resulting in the rotation and translation of intersection lines between section walls. During this process, the core undergoes excessive deformation while the stiffener's base moves rigidly. The wavelength

associated with distortional buckling typically falls between that of local and global buckling (DJAFOUR, 2015) (Figure I.16.b).

Global buckling, which includes Euler buckling (flexural) and flexional-torsional buckling in columns, as well as lateral-torsional buckling in beams, is also referred to as rigid body buckling. This term is used because, during instability, the entire cross-section experiences movement as a solid body without any deformation (Figure I.16.c).

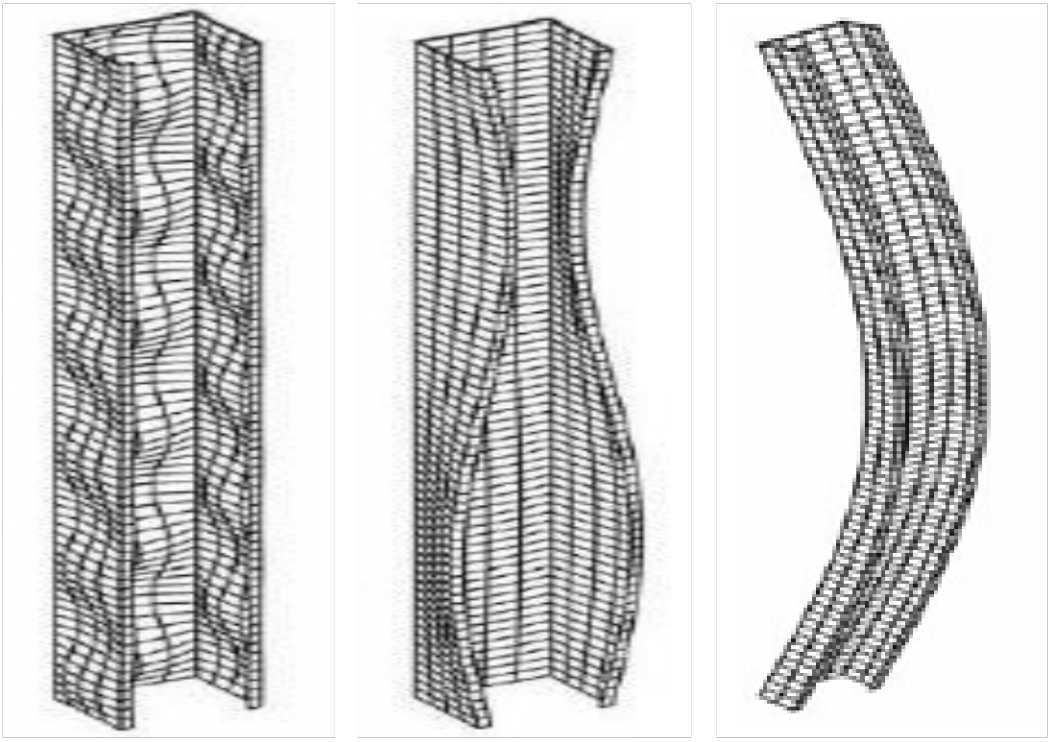

(a) (b) (c)

Figure I.16. Instability modes of CFS: (a) Local; (b) Distortional; (c) Global.

However, scenarios involving the interaction between local and global buckling are significantly better understood and mastered. This is evidenced by the fact that their impacts are already taken into account in virtually all design codes for hot-rolled and cold-formed steel. This is achieved either through the renowned concept of effective plate width or via the more recent and increasingly popular direct strength method (Sujitha et al., 2022). On the other hand, the influence of effects resulting from the interaction of local/distortional mode on the post-buckling behavior and strength of C-section columns has attracted the attention of several researchers in recent years. It is noteworthy that some of these studies have already led to the development and calibration of new applications, such as calculation curves, for the direct strength method.

Figure I.17 illustrates the analysis of a C-section under simple compression using the finite strip method (FSM). The objective of this study is to determine the critical loads for various wavelengths. The lowest points on the resulting curve highlight the different instabilities of the examined column. This analysis demonstrates that buckling modes are primarily influenced by the buckling length (Hancock et al., 2001).

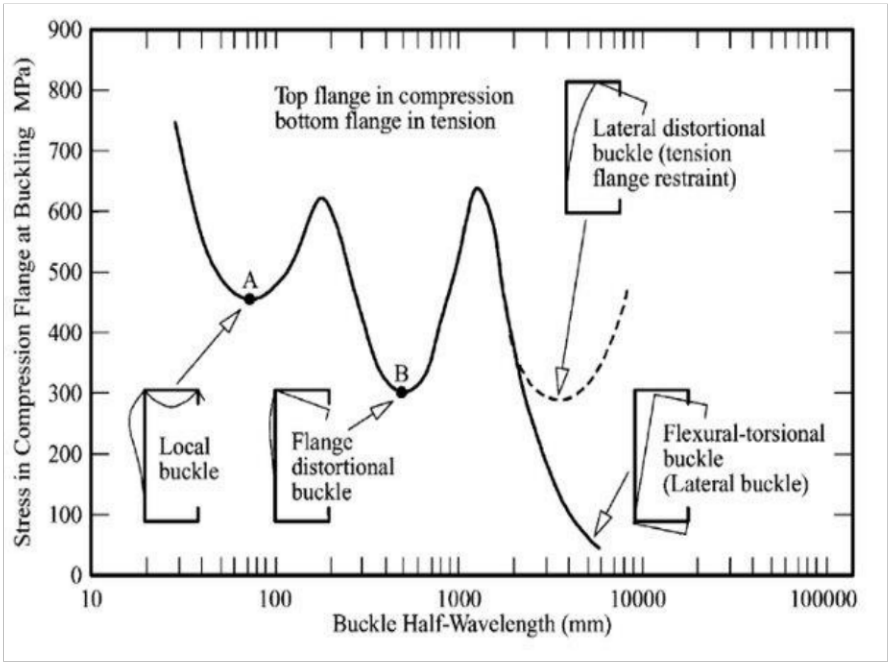

Figure I.17. Buckling modes as a function of the half-wavelength of a C-section profile (Hancock et al., 2001; Saddek et al., 2018).

I.5.1 Combined instability modes

Because of the growing intricacy in the shapes of cold-formed steel sections, determining local buckling is becoming more intricate, and the significance of distortional buckling is on the rise. Local and distortional buckling can be viewed as different sectional buckling modes, and they have the potential to influence each other, along with global buckling.

In Figure I.18, we observe the pure and coupled modes of a C-shaped column under axial load. These findings were obtained through an elastic buckling analysis employing the Finite Element Method (FEM). Specifically, the pure modes encompass (a) local mode, (b) distortional mode, (c) flexural mode, (d) torsional mode, and (e) flexural-torsional mode. Conversely, the combined modes include (f) local + distortional, (g) local + flexural, (h) flexural + distortional, (i) local + flexural-torsional, (j) flexural-torsional + distortional, and (k) flexural + flexural-torsional (DJAFOUR, 2015).

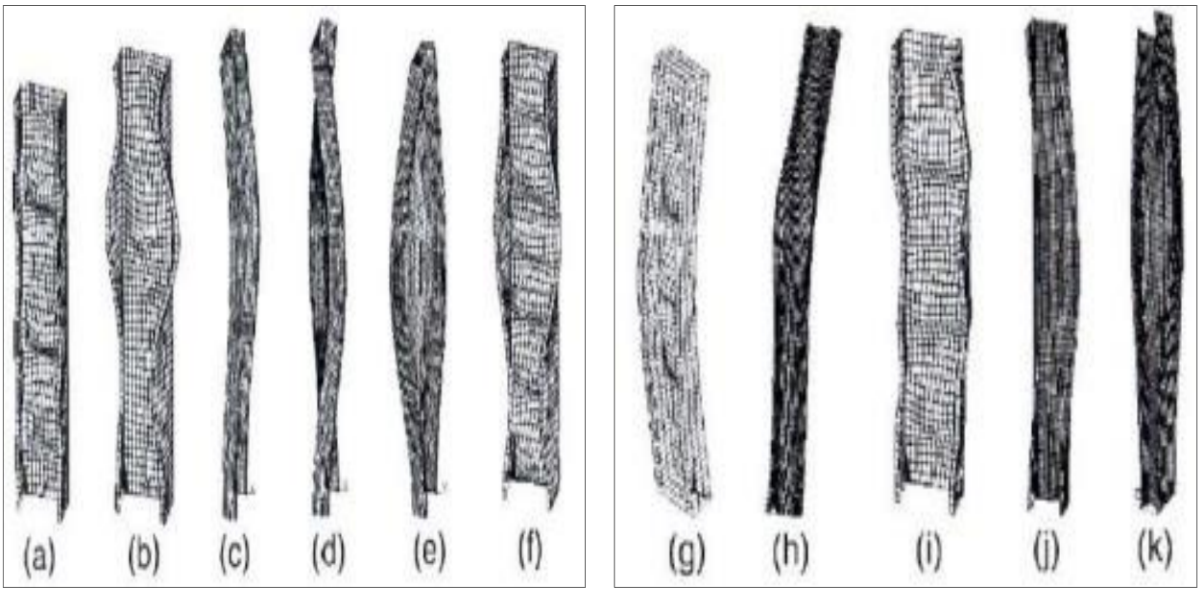

Figure I.18. Instability modes of a compressed C-column (Dubina et al., 2012).

I.6 PROPERTIES OF COMPRESSED ELEMENTS WITH STIFFENED SECTIONS OR UNSTIFFENED SECTIONS

A compressed section's characterization can vary based on the presence or absence of reinforcing elements or stiffeners, ranging from being unreinforced to partially reinforced. The entire width of the wall is considered fully effective when the element has a low width-to-thickness ratio or experiences low compressive stress. However, when the element's width-to-thickness ratio is relatively high and the compressive stress increases, the areas near the edges become more structurally significant once the element undergoes a form of instability. Consequently, the stress distribution within the compressed member is decidedly non-uniform. In the design of such members, the cross-sectional properties are determined based on a reduced effective area (Dubina et al., 2012).

The effective width of a compression element is not solely influenced by the applied stress; it also hinges on its width-to-thickness ratio. When examining a specific beam with a compressed flange characterized by a relatively high width-to-thickness ratio, the effective section modulus diminishes as the yield stress of the steel employed increases. This reduction occurs because the effective width of the compressed flange decreases under higher stress conditions. Consequently, the strength of such a beam doesn't exhibit a direct, linear relationship with the yield strength of the steel. This same principle applies to compression members (Vilnay and Rockey, 1981).

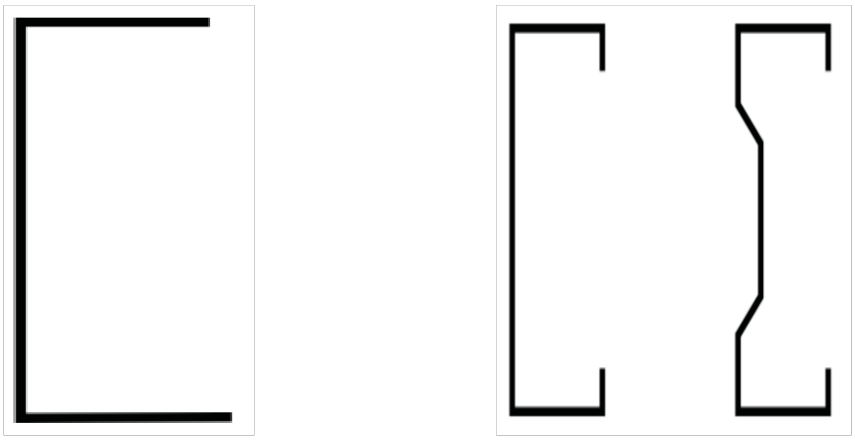

(a) (b)

Figure I.19. Cold-formed steel single sections: (a) Unstiffened section; (b) Stiffened section (Rasmussen et al., 2020).

I.7 DESIGN ASSISTED BY EXPERIMENTAL TESTS

Cold-forming technology can produce unconventional cross-sectional shapes, as shown in Figure I.20. However, from a structural perspective, analyzing and dimensioning these atypical forms can be quite complex. Structural systems often consist of various thin-walled components, such as purlins and wide sheets, which are interconnected. These structures can introduce complex design challenges that aren't fully addressed by established design codes. While numerical analysis via the finite element method is available, it can be notably convoluted in many real-world scenarios. However, for addressing these intricate design problems, contemporary design codes permit the utilization of experimental methods for evaluating the structural performance of such elements. Experiments can either substitute for or complement analytical design approaches. Nevertheless, it's important to note that only laboratories officially sanctioned by competent authorities have the authority to conduct these tests and issue corresponding reports (Laím et al., 2013).

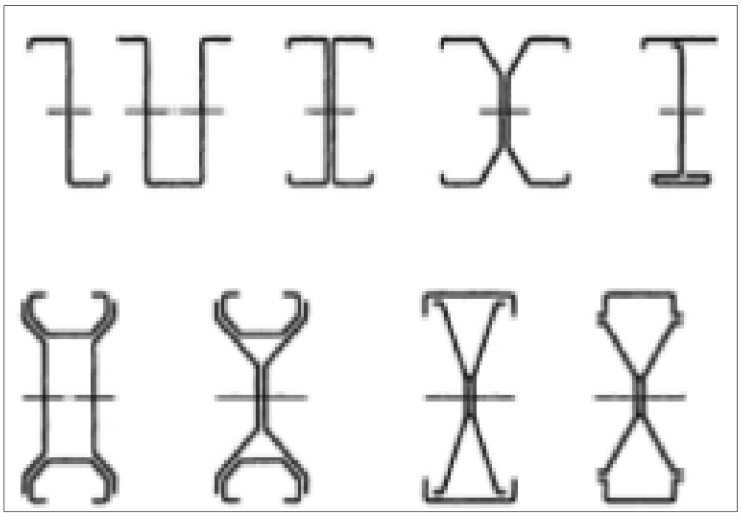

Figure I.20. Different shapes of cold-formed steel profiles (European Committee for Standardization, 2006).

I.8 ECONOMICAL DESIGN

The primary goal of economic design is to achieve the most cost-effective construction that satisfies dimensional specifications. An essential requirement for cost-effective structures is minimizing the material weight while maximizing structural efficiency. Numerous studies have shown that, under a given loading system, optimal efficiency is reached by ensuring that the structural elements can resist any form of failure or failure mode (Loughlan, 2018).

In real-world applications, achieving these "ideal" conditions is not always assured, mainly because unavoidable constraints exist, such as using standard section shapes and adhering to dimensional restrictions imposed by various calculation codes.

The effectiveness of utilizing high-strength steel primarily hinges on the specific type and manner of potential failure. In certain situations, like long columns with relatively high slenderness ratios, failure typically arises from global elastic buckling. In such instances, employing high-strength steel may not lead to a cost-effective design since the performance of structural elements under these conditions remains consistent regardless of the steel grade used. Consequently, using high-strength steel in these scenarios might not be justified in terms of the overall construction cost (Ban and Shi, 2018).

In essence, the overarching goal of cost-effective design is to harness the full strength potential of steel by creating sections that maximize structural efficiency. The versatility of the cold

forming process, allowing the production of a wide range of shapes, is exceptionally well-suited for achieving this objective.

I.9 CALCULATION METHODS

Cross-sectional shapes can be categorized based on their capability to reach a state where they approach their limit. This categorization is determined by the sections' capacity to undergo plastic deformation and the impact of instabilities. The Eurocode defines four types of class, with cold-formed profiles falling into class 4 due to their thickness and vulnerability to local instabilities. Within this class, it's essential to accurately assess the bending moment or compressive strength of a cross-section, while also explicitly considering the effects of local buckling.

I.9.1 Effective width method (b_{eff})

Due to the complexity associated with modeling stress redistribution after the critical point, design methods primarily rely on semi-empirical or analytical approaches. The analytical approach primarily hinges on utilizing the critical buckling stress. This analytical concept is employed in conjunction with the material's yield strength to determine the element's resistance. Current formulas linking the critical stress and yield strength to ultimate strength are predominantly empirical.

The predominant concept in the design of thin-walled structures subjected to local buckling is that of effective width, initially developed by Von Kármán in 1932 for thin steel sheets (Von Kármán et al., 1932). This method was experimentally adjusted for cold-formed steel by George Winter in 1946 (Winter and Pian, 1946). More than 50 years later, it remains the cornerstone of design for most thin-walled structure calculation codes.

The effective width method (b_{eff}) is an approximate technique used to model stress redistribution occurring in the post-buckling phase of thin plates. Considering a thin plate simply supported on all four sides and subjected to longitudinal compression at both ends, when the plate is loaded, its central part deforms and the load is transferred towards the edges. The nonlinear stress resulting from this redistribution is modeled as two effective widths subjected to a constant stress (Yu and Yan, 2011).

I.9.2 Direct strength method (DSM)

The development of the direct strength method (DSM) primarily stems from the emergence of sections with complex shapes, featuring stiffeners at edges or intermediate locations, and the recognition of the distortional mode as a potential source of strength erosion (Schafer, 2006). Indeed, predicting the distortional mode through design methods based on the concept of effective width as described in EC3-1-3 (European Committee for Standardization, 2006) can be perceived as a laborious and inefficient task. It became evident that a more rational approach was necessary. The term "Direct Strength Method" was first coined in the pioneering work of Schafer and Pekoz (Schafer and Pekoz, 1998). The research by these scientists led to the codification of this method for the first time in North American regulations in 2004 (AISI-S100-04, 2004), and it was almost simultaneously integrated into the Australo-New Zealand standard (*Cold-formed steel structures*, 2005). A few years later, it was also adopted in Brazil (ABNT, 2010). The DSM provided a unified approach to the design of cold-formed steel elements, addressing both compression for columns and flexion for beams, while considering local, distortional, global modes, as well as the interaction of local-global types.

On the other hand, the DSM can be seen as an evolution of the approach based on resistance curves for global buckling. It is primarily based on the assumption that the ultimate strength of an element can be predicted by relying exclusively on the elastic stresses of pure buckling modes and the yield limit of the steel. Elastic buckling stresses and the yield stress are considered through simple equations like those of Winter, providing a direct estimate of the final strength of the element instead of the effective section. DSM relies on the precise determination of the critical stress associated with a specific buckling mode, suggesting that computer tools for evaluating these stresses could be deemed essential.

Compared to the effective width method, the DSM method primarily benefits from the ability to address the cross-section as a whole without dividing it. Additionally, the DSM provides four significant advantages.

In DSM, interactions between the section walls are automatically taken into account, eliminating the need to categorize the cross-section or calculate an effective width. This method allows for estimating the resistance of structural elements subjected to the distortion mode, treating distortion buckling as a distinct limit state. Moreover, it explicitly has the capacity to incorporate interactions between buckling modes.

More recently, a second codified generation of DSM resistance curves has been introduced, exclusively present in the current version of the North American specification (AISI-S100-12, 2012) and not yet incorporated into other codes. This new generation addresses the shear resistance of short to moderately long beams and the combined shear-bending resistance of these beams. Additionally, it extends the resistance curves of the first DSM generation to encompass columns and beams with perforated holes.

I.9.3 Finite element method (FEM)

Due to the inherent slenderness of the cross-sections in CFS, the application of the finite element method (FEM) for analysing the stability of these structural elements is typically implemented using finite elements. This allows for a more accurate retention of the deformation of the cross-section.

Due to its robust computational capabilities, the finite element method (FEM) has become widely adopted in the analysis of elastic buckling in thin-walled CFS structures. Its use offers the advantage of handling complex geometries, different types of boundary conditions, and diverse loads. Moreover, its ability to conduct nonlinear analyses leading up to failure, considering material and geometric nonlinearities, makes it particularly powerful for analysing the elastic stability of thin-walled structures. However, modeling and analysing thin-walled structures remain complex tasks influenced by several parameters that can impact the analysis. Among these parameters are boundary conditions, section shape, and meshing, which are three key aspects influencing the analysis of elastic buckling (Dhatt et al., 2012).

Due to the inherent complexity of buckling modes in CFS thin-walled structures (local, global, distortional), it is crucial to accurately identify and classify these modes, as well as precisely calculate the associated elastic critical loads (or moments). This is of fundamental importance in predicting the ultimate strength of these elements.

On the other hand, although this method can accommodate various cross-sectional shapes, boundary conditions, and types of loading, it faces challenges in modeling and identifying characteristic buckling modes (distortional, local, and global). Unlike a method that provides modal identification capabilities, it instead requires a laborious and subjective procedure involving visual inspection to classify buckling modes during elastic stability analysis (Nikishkov, 2004).

I.9.4 Finite strip method (FSM)

The finite strip method (FSM), a variant of the finite element method (FEM), relies on employing a set of trigonometric functions to describe the longitudinal displacement field of the strip (or element), while the shape function in the transverse direction remains similar to that of a conventional finite element. This approach is widely favoured for analyzing instabilities of cold-formed steel elements subjected to various longitudinal constraints such as axial forces, bending, torsion, and deformation (Li and Schafer, 2010).

The popularity of the FSM in the field of elastic stability stems from the work of Hancock. It was he who first introduced the famous signature curve representing the critical buckling stress as a function of the half-wavelength, rather than as a function of the buckling length. In other words, he constrained the structural element or the structure to deform by producing only a single half-sine wave during its instability (Hancock et al., 2001).

I.10 CALCULATION STANDARDS

In-depth research and theoretical advancements have facilitated the development of national design standards for cold-formed steel profiles and structures in numerous countries. Below, we will provide a summary of the key design specifications used worldwide. However, in our research the European standards (Eurocodes 3 and 4) and American code (ACI) were utilized.

I.10.1 North American Specification for the Design of Cold-Formed Steel Structural Members, 2007 Edition

The inaugural version of the consolidated North American NAS/AISI standard was formulated and released in the year 2001 (AISI, 2001), accompanied by explanatory notes. This standard is intended for use in the United States, Canada, and Mexico in the structural design of cold-formed steel components. Given its intended use in these three countries, it was necessary to create a format that accommodates each country's specific requirements. This led to a format comprising a core document, where chapters A to G are intended for use in all three countries, along with three country-specific annexes: Annex A for the United States, Annex B for Canada, and Annex C for Mexico.

Three design methodologies are acknowledged in the field: the ASD approach (Allowable Stress Design), the LRFD approach (Load and Resistance Factor Design), and the LSD approach (Limit States Design). It is important to note that the utilization of ASD and LRFD is

confined to the United States and Mexico, whereas the exclusive implementation of the LSD method is observed solely in Canada. Schafer (Schafer, 2006) developed a new design method for cold-formed steel profiles, adopted in 2004 as Annex 1 of the North American specification (AISI-S100-04, 2004).

Following the publication of the latest trends in cold-formed steel construction, the 2007 editions (AISI-S100-07, 2007) were succeeded by the subsequent release of Supplements 1 and 2 in 2009 and 2010, respectively. A synthesis on these supplements was published by (H. Chen et al., 2010). Consequently, the technical advancements introduced led to the development of the 2012 edition (AISI-S100-12, 2012).

The release of the 2016 edition was characterized by the integration of significant content updates. AISI 2016 ("North American Specification for the Design of Cold-Formed Steel Structural Members, 2016 Edition," 2016) introduced a second-order analysis system to ensure the stability of structural systems. The direct strength method (DSM) was moved from being an appendix to the main body of the specification, and is now presented in parallel with the effective width method. This advancement allows engineers to select the most suitable method for their design, while also opening up new sizing possibilities provided by the direct strength method.

I.10.2 Australian/New Zealand Standard - AS/NZS 4600, 2005 Edition

The Australian/New Zealand standard bears a strong resemblance to the AISI specification, as sections 1 to 5 align with sections A to E of the latter. However, AS/NZS 2005 (*Cold-formed steel structures*, 2005) only allows for design using the limit states method (LSD), excluding the allowable stress method (ASD). Additionally, due to the use of high-strength steel, supplementary provisions have been added to address distortional buckling. Furthermore, the 2005 edition of the Australian/New Zealand standard for cold-formed steel structures (*Cold-formed steel structures*, 2005) has integrated the Direct Strength Method (DSM).

I.10.3 Eurocode 3 - Design of steel structures, Part 1.3 - General rules, Supplementary rules for cold-formed members and sheeting

EN 1993-1-3 (European Committee for Standardization, 2006), functions as the consolidated European standard for the structural design of cold-formed steel structures. This standard includes detailed regulations for structural purposes involving cold-formed steel materials, regardless of whether they are in the shape of sheets or narrow strips, produced through hot or

cold rolling, and with or without coatings. This code is intended to be employed in the design of buildings or civil engineering structures in conjunction with standards EN 1993-1-1 (CEN, 2005) and EN 1993-1-5 (EN 1993-1-5, 2006). In accordance with EN 1993-1-3, only the limit state design (LSD) method is permitted for design purposes. The provisions of the code apply to steel thicknesses ranging from 1.0 to 8.0 mm for steel elements and from 0.5 to 4.0 mm for sheets. However, the use of thicker materials is also feasible, provided that their load-bearing capacity is determined through experimental procedures.

The design provisions for elements in EN 1993-1-3 (European Committee for Standardization, 2006) exhibit similarities with the AISI specification, although the notations and formula formats differ. However, they generally incorporate more advanced design provisions. In certain clauses, particularly those concerning flat elements under compression and edge or intermediate stiffeners, the provisions in EN 1993-1-3 are notably more complex. Additionally, the consideration of distortional buckling is less explicitly addressed in this code compared to design standards such as AISI 2007 (AISI-S100-07, 2007), and AS/NZS 2005 (*Cold-formed steel structures*, 2005).

I.10.4 Eurocode 4 – Design of composite steel and concrete structures, Part 1.1 - General rules and rules for buildings

Eurocode 4 encompasses a comprehensive set of regulations that govern the design of elements and composite structures utilized in the construction of buildings and civil engineering projects. These regulations are in accordance with the principles, safety criteria, and performance requirements outlined in EN 1990 - Basis of Structural Design (Gulvanessian, 2002). Specifically, Eurocode 4 Part 1-1 (Eurocode 4, 2004) offers detailed guidelines pertaining to the safety, performance, and durability of steel and concrete composite structures, with a particular focus on buildings. This code is based on the limit state concept, which is employed in conjunction with a partial coefficients method-based approach.

EN 1994-1-1 proposes two approaches for designing composite columns. The first, a General Method, requires explicit consideration of second-order effects and imperfections. It can be applied to columns with non-symmetric sections or with variable sections along their height. However, it necessitates the use of numerical calculation tools and relies on the availability of appropriate software. The second, a Simplified Method, utilizes European buckling curves for steel columns, implicitly considering imperfections. This method is mainly suited for designing composite columns with doubly symmetric and uniform sections along their height.

I.10.5 Building code requirements for structural concrete (ACI 318-99) and commentary (ACI 318R-99)

In the field of civil engineering, the American Concrete Institute code (ACI) assumes a pivotal role as a primary source of guidance, particularly in relation to the intricate processes involved in the design and construction of concrete structures. It provides detailed guidelines for the design, construction, inspection, and maintenance of concrete works, covering a wide range of applications from foundations to high-rise structures.

ACI 318-99 (ACI Committee, 1999), an important document in civil engineer and constructions arena. It provides guidelines for the design, analysis, and construction of reinforced concrete structures, covering a wide range of applications, from buildings to bridges. This code sets minimum requirements to ensure the safety, durability, and performance of concrete structures, including provisions for materials, structural systems, and construction practices. It incorporates the latest industry research and practices, serving as a valuable resource for engineers, architects, contractors, and construction officials involved in the design and construction of concrete structures.

ACI 318R-99 (ACI Committee, 1999), complementing ACI 318-99 by adding further clarifications and elucidations to assist in understanding and application of the code provisions. Commentary, instances, and adjunct info are provided to aid engineers, architects, and construction experts in interpreting and accomplishment of the requirements laid out in ACI 318-99. The ACI 318R-99 talks about design thoughts, material shapes, building analysis, and construction approaches in relation to reinforced concrete buildings. It is an important thing for making ACI 318-99 clearer and more effective, ensuring that concrete buildings are planned and constructed following the top safety, lastingness, and performance.

I.11 SOME RESEARCH REVIEWS

The use of composite columns made of steel and concrete is becoming increasingly common in various structures. This construction method has attracted the attention of several researchers, including:

J. Zeghiche and K. Chaoui (Zeghiche and Chaoui, 2005), tested twenty-seven tubular steel specimens filled with concrete. The parameters studied in this research included: slenderness, load eccentricity, and eccentric load for the case of single or double curvature, as well as the

compressive strength of concrete. The test results showed the influence of these parameters on the strength and behavior of concrete-filled steel columns. A comparison between the experimentally obtained failure load and the predictions of EN 1994-1-1 revealed that the results were well-approximated in the case of single-curvature bending, whether under axial or eccentric load. However, in the case of double-curvature columns, EN 1994-1-1 predicted a higher load, indicating an overestimation of the load-bearing capacity. This suggests that EN 1994-1-1 may not be conservative in the case of double curvature.

R. Rahnavard et al. (Rahnavard et al., 2022a; Rahnavard et al., 2022b; Rahnavard et al., 2022c), conducted a study on the performance of cold-formed steel built-up columns that were filled with concrete, examining a range of parameters including compression, fire resistance, and equivalent temperature. The findings indicated a strong correlation between the experimental outcomes and the proposed methodology.

H.D. Craveiro et al. (Craveiro et al., 2022), explored the determinants that influence the fire performance of concrete-filled built-up cold-formed steel columns, paying particular attention to dimensions, material characteristics, and geometric design. Their findings revealed that the synergistic effect of steel and concrete components markedly improved fire resistance, thereby delaying structural failure and preserving the columns' integrity in the event of a fire.

M.-T. Chen, T. Zhang, and B. Young (Chen et al., 2023), focused on how axial compression loads affect the structural integrity of stub columns composed of built-up cold-formed steel and concrete infill. Experimental tests were executed to analyze the columns' load-bearing capacity, deformation patterns, and modes of failure. Additionally, the research evaluated the influence of various parameters, including the size of the columns, the thickness of the steel, and the grades of concrete employed.

K.B. Teoh et al. (Teoh et al., 2023), performed experimental tests on concrete-filled cold-formed steel box columns to evaluate their deformation properties, load-carrying capabilities, and failure modes. The outcomes of this study contribute valuable knowledge regarding the structural performance and failure mechanisms of these columns, which can inform improvements in their design and implementation in construction endeavors.

I.12 CONCLUSION

Cold-formed steel profiles offer a versatile and efficient solution for a diverse range of applications across various industrial sectors. Utilizing ambient temperature for their fabrication saves a significant amount of energy compared to hot-forming methods, while ensuring appropriate mechanical properties. Their design flexibility, coupled with high dimensional precision, makes them indispensable in the fields of metal construction, automotive industry, aerospace, and many others.

Concrete-filled cold-formed steel built-up columns offer a flexible solution for structural design challenges. By combining the benefits of steel-concrete composites, such columns address issues related to instability, enhance load bearing capacity, optimize mechanical properties, and promote the use of high-strength steel. This versatility allows for the creation of diverse geometric configurations, further expanding the range of applications for these composite solutions.

CHAPTER II

Concrete-filled cold-formed steel built-up columns

II.1 INTRODUCTION

In the early 19th century, the construction method using hollow profiles filled with concrete was already in use. During that time, the steel crown was initially perceived merely as formwork with no impact on structural resistance. Additionally, the role of concrete was predominantly seen as protecting steel against corrosion. However, over time and through numerous experiments, these assumptions proved to be inaccurate. They were reassessed, taking into account the connection between the two materials and the implications of this connection on their behavior.

II.2 OVERVIEW OF STEEL-CONCRETE COMPOSITE STRUCTURES

A structure is deemed composite when it integrates two distinct materials in terms of nature and properties, such as steel and concrete, during the design of its various elements like beams, columns, slabs, etc. This mechanical combination of the two materials, steel and concrete, serves to enhance both the rigidity and strength of the element, stemming from the connection between the interfaces of the two materials (Johnson and Buckby, 1975).

II.3 MATERIALS USED IN A COMPOSITE ELEMENT

The fabrication of composite structural elements requires the use of four fundamental materials:

- Reinforcing or structural steel
- Structural steel
- Profiled steel sheets
- Concrete

II.4 CHARACTERISTICS OF MATERIALS

These materials are outlined in various design codes, with certain essential requirements also addressed by regulations such as the Eurocodes (Eurocode 4, 2004; European Committee for Standardization, 2006, 2004). The key properties of these materials are detailed below:

II.4.1 Structural steel

Various classifications of steels exist, either based on their chemical composition (alloyed steels, non-alloyed steels, etc.) or on their mechanical properties (tensile strength, yield

strength). In the field of metal construction, the commonly adopted classification is that of "Steel Grade," determined by its yield strength f_y.

The Eurocode 4 addresses the design of composite structures made from commonly graded steels such as S235, S275, S355, S460N, and CR250 as defined in the European standards EN10025, EN10113-2 and ISO 4997.

The design values for the essential properties of structural steels are as follows:

- The elastic modulus E_s=210 000 N/mm^2
- The shear modulus G_s=E/2(1+ν) N/mm^2
- Poison coefficient ν_s=0.3
- Linear expansion coefficient α=12x10^{-6} K^{-1}
- Density ρ_s=7850 kg/m^3

During calculations and design, Eurocode 3 (EC3) allows for the idealization of the stress-strain relationship of structural steel in a perfectly plastic elastic form, as illustrated in Figure II.1.

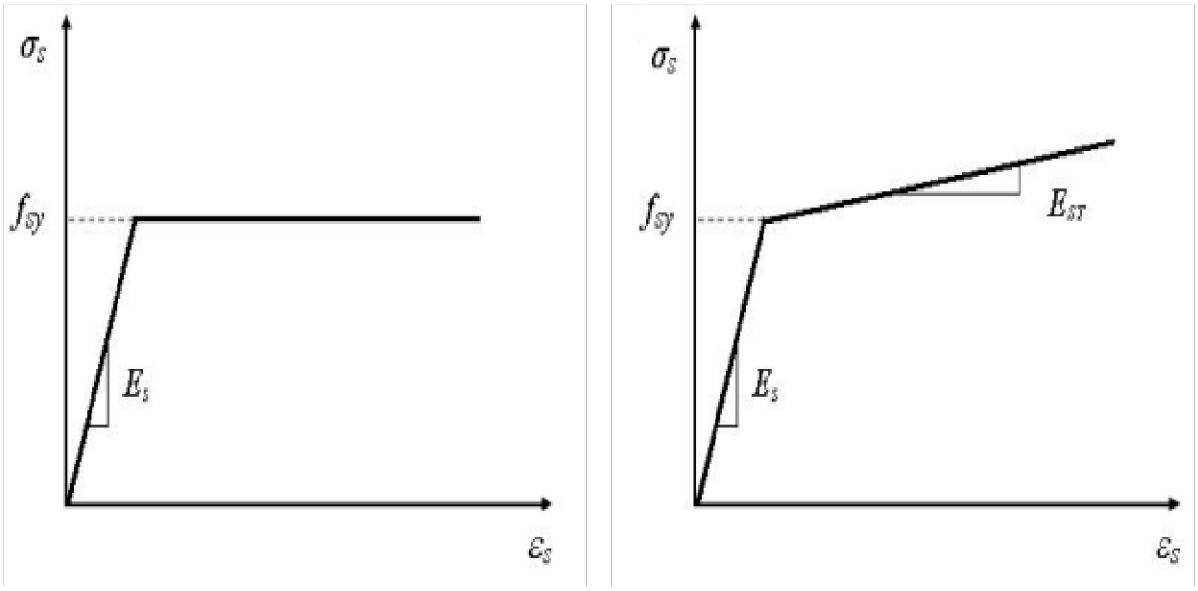

(a) (b)

Figure II.1. Stress-strain relationship specific to structural steels: (a) Bilinear relationship; (b) Idealized diagram (Sæther and Sand, 2012).

II.4.2 Reinforcing steel

Reinforcement steels distinguish themselves from construction steels not only in their configuration but also in their manufacturing process, chemical composition, and mechanical properties. They are notably characterized by their higher yield strength, which, in this context, corresponds to a permanent elongation of 0,2%. Regarding the elasticity modulus, it exhibits minimal variation and can be deemed equivalent to that of construction steel (Figure II.2).

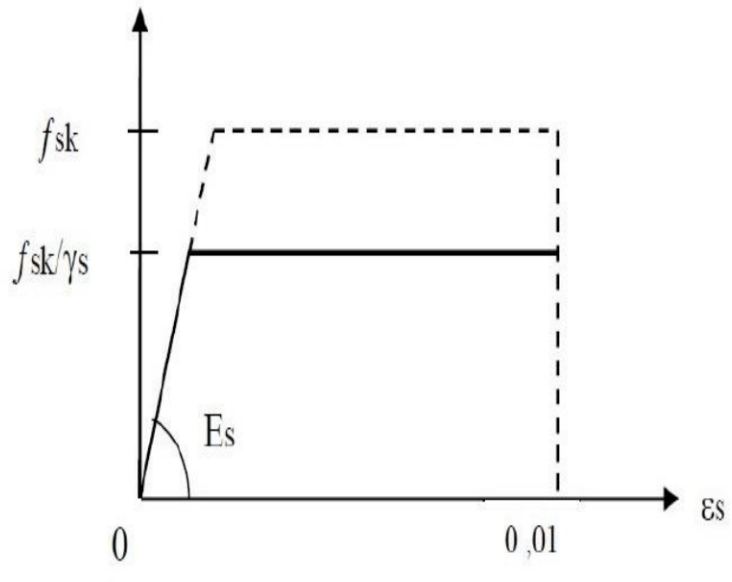

Figure II.2. Stress-strain diagram for reinforcement (CEN, 2005).

II.5 BUILT-UP COLD-FORMED STEEL UNFILLED COLUMNS

In contemporary building construction, cold-formed steel (CFS) sections are gaining widespread adoption, particularly in applications like truss members, floor joists, and wall studs (Zhang and Young, 2012). This surge in usage can be attributed to their numerous benefits, including straightforward assembly, versatile fabrication, and a variety of cross-sectional shapes tailored for diverse purposes. This stands in contrast to traditional rolled sections, primarily focused on enhancing strength-to-weight ratios.

Utilizing Cold-Formed Steel (CFS) built-up sections represents an efficient approach to address the contemporary need for employing cold-formed sections. These sections are created through the assembly of channel sections using screws or fasteners and find frequent application in steel trusses, space frames, and columns (Teoh et al., 2023). Built-up columns are prevalent in structures made of cold-formed steel, offering remarkably efficient strength-to-weight ratios and tailored solutions for diverse structural configurations (Glauz, 2023; Yang et al., 2024).

The columns must absorb compression and bending loads caused by the wind while resisting buckling. Their design should ensure optimal stiffness in compression in all directions, with a particular emphasis on their principal axes.

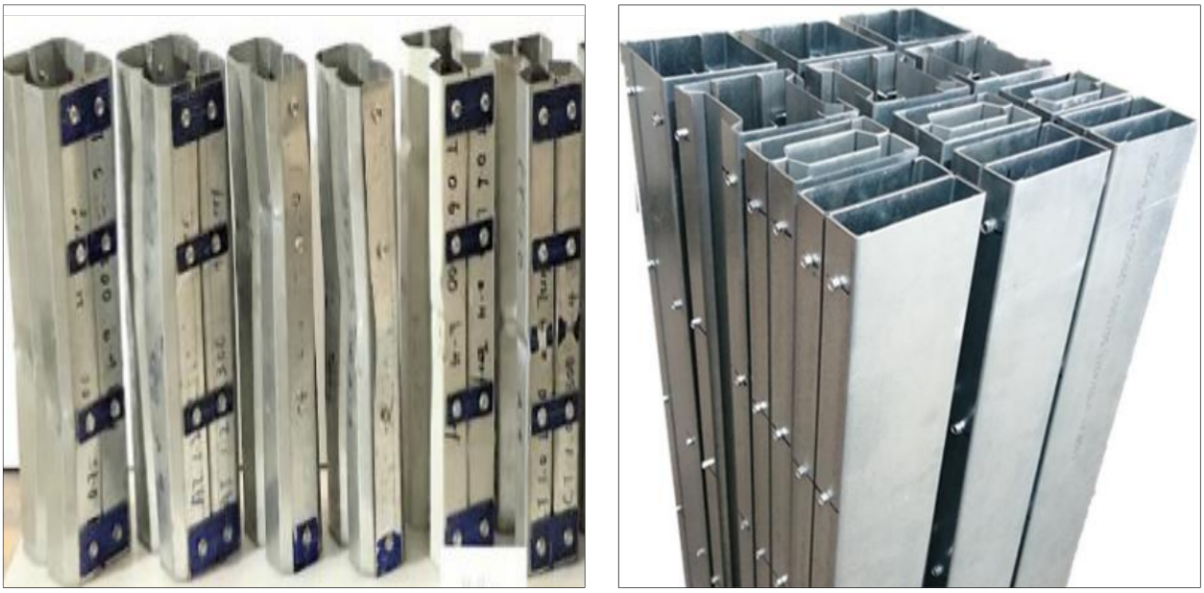

Figure II.3. Cold-formed steel built-up unfilled columns (Chen et al., 2023; Craveiro et al., 2022).

II.5.1 Short columns

Short columns are characterized by a very low slenderness ratio ($\bar{\lambda} \leq 0.2$), making them insensitive to global buckling. In such cases, the compression resistance of the element relies on the compression strength of its cross-section, determined by the section classification. Cross-sections of Classes 1, 2, and 3 do not experience local buckling at this level of axial load; hence, the calculated compression resistance is equivalent to the calculated plastic resistance of the section.

$$N_{c,Rd} = A\frac{f_y}{\gamma_{M0}} \tag{II.1}$$

For cross-sectional profiles classified as Class 4, local buckling in one or more walls of the section prevents reaching the plastic flow load. Consequently, the calculated compression resistance is limited to the local buckling resistance.

$$N_{c,Rd} = A_{eff}\frac{f_y}{\gamma_{M1}} \tag{II.2}$$

With: A_{eff}: effective area of the cross-section.

$N_{c,Rd}$: compressive strength of the cross-section.

II.5.2 Slender Columns

Columns exhibit two distinct behaviors based on their slenderness ratio: those with a high slenderness ratio buckle almost within the elastic range, while others with an intermediate slenderness ratio are particularly susceptible to imperfections.

II.5.2.1 Slenderness λ

The slenderness ratio of the column is given by the following formulas:

$$\lambda = \frac{l_f}{i} = \frac{buckling\ length}{radius\ of\ gyration}\ ;\ i = \sqrt{\frac{I}{A}} \tag{II.3}$$

This gives: $\lambda_z = \frac{l_{fz}}{i_z}$ and $\lambda_y = \frac{l_{fy}}{i_y}$ (II.4)

II.5.2.2 Buckling Length

The buckling length is defined as the greatest distance between two successive points of articulation or inflection along the central line of the element deformed by buckling. It is worth noting that this scenario primarily applies to isolated elements subjected to compression, although this is rarely encountered in practice, typically confined to laboratory tests, as illustrated in Figures II.4 and II.5.

P.S: In the case of compressed elements within metal frame structures, buckling lengths are determined by analyzing the deformation of the entire structure.

Figures II.4 and II.5 illustrate the four buckling modes by presenting the buckling lengths in accordance with EN 1993-1-1 and EN 1994-1-1 standards.

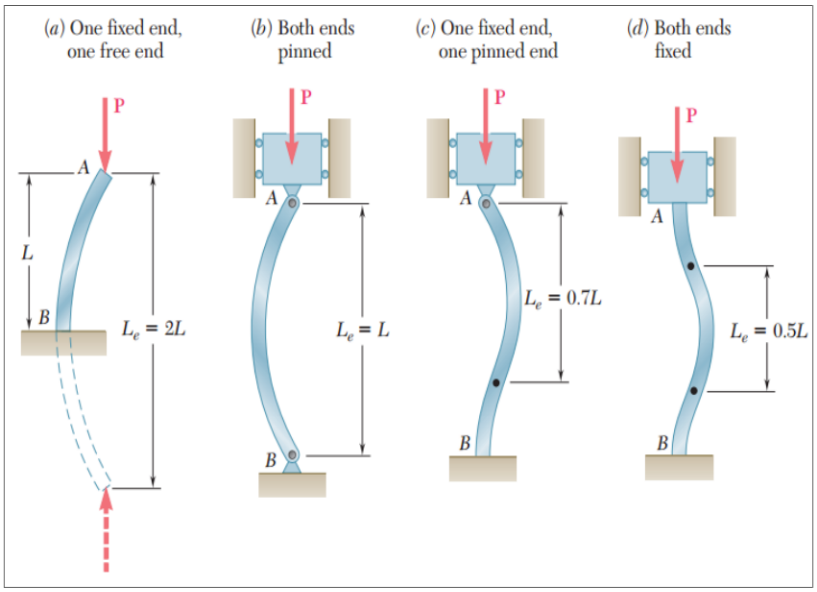

Figure II.4. Different buckling modes (Fadhel, 2014).

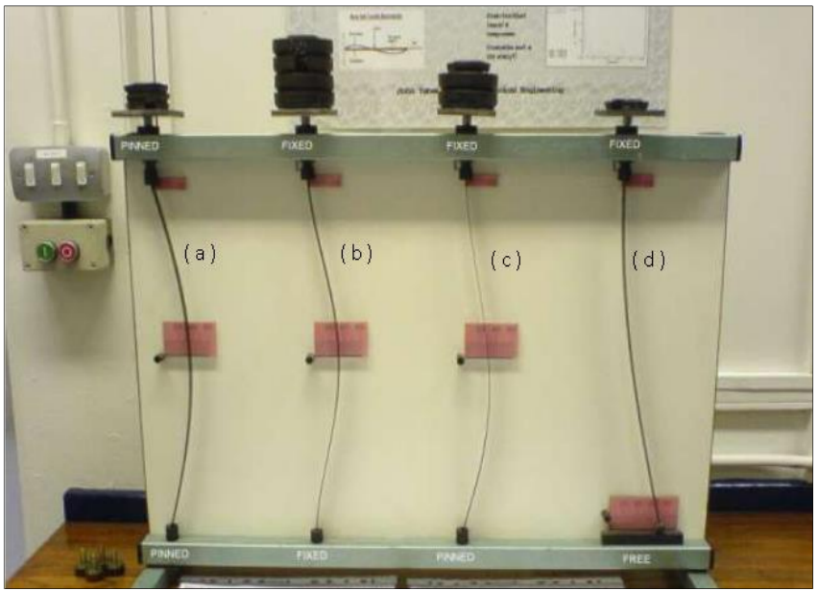

Figure II.5. Experimental test of different buckling modes (BOULMAALI-HACENE CHAOUCHE, 2023).

II.5.3 Theoretical aspect of buckling

At the critical load, the stable equilibrium of the straight column is reached at its limit, and there is a slightly deformed configuration of the column that can also maintain equilibrium (Figure II.6).

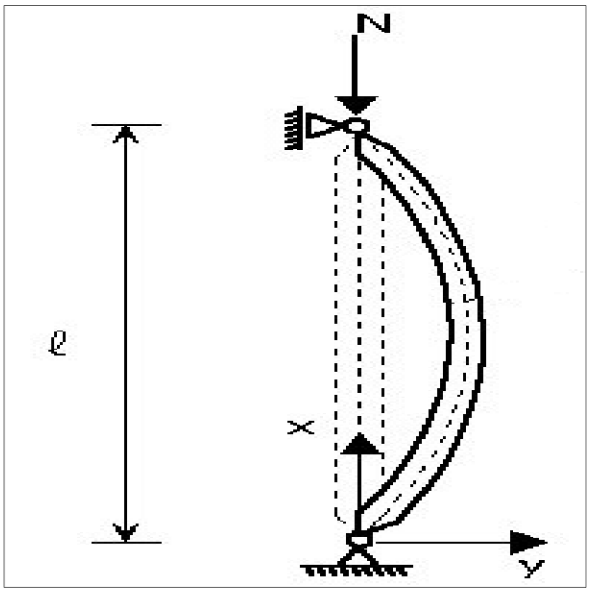

Figure II.6. Deformation mode of a compressed element with bi-articulated supports (Li et al., 2009).

In the context of this arrangement, the bending moment for each position of the cross-sectional area of a bi-articulated bar is determined by:

$$M = N.y \tag{II.5}$$

If we use the differential equation provided by the theory of simple bending:

$$\frac{d^2y}{dx^2} = -\frac{M}{EI} \tag{II.6}$$

Where: EI represents the bending stiffness of the column in the buckling plane.

E: Young's modulus.

I: Moment of inertia about the buckling axis.

The general solution to this equation is:

$$y = A.\sin kx + B.\cos kx \tag{II.7}$$

We assume:

$$k^2 = \frac{N}{EI_z} \tag{II.8}$$

A and B are integration constants adjusted to satisfy the boundary conditions:

y=0 for x=0 → B=0

And y=0 for x=l → A. sin kl=0

$A \neq 0$ (no displacement in this case), we will have: sin kl=0

The root of this equation kl can take an infinite number of values: 0, π, 2π, ...; nπ, meaning:

kl = nπ with n being any integer

$k^2l^2 = n^2\pi^2$

Figure II.7 shows the first three buckling modes (n = 1, 2, and 3 respectively, with n=0 excluded).

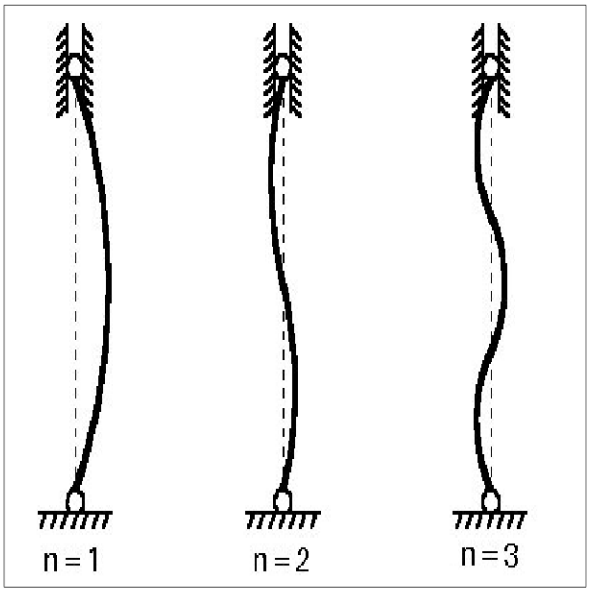

Figure II.7. The buckling modes (De Wilde, 2007).

Ultimately, the critical load is calculated as follows:

$$N_{cr,n} = \frac{n^2\pi^2 EI}{\ell_{cr}^2} \quad \text{(II.9)}$$

Designating ℓ_{cr} as the critical length (i.e., the buckling length), the Euler's critical load N_{cr} for mode 1 is expressed as follows:

$$N_{cr} = \frac{\pi^2 EI}{\ell_{cr}^2} \quad \text{(II.10)}$$

And we can then define Euler's critical stress σ_{cr} as follows:

$$\sigma_{cr} = \frac{N_{cr}}{A} = \frac{\pi^2 EI}{\ell_{cr}^{\,2} A} \tag{II.11}$$

By introducing the radius of gyration, $i = \sqrt{I/A}$ and the slenderness ratio $\lambda = \ell_{cr}/i$ corresponding to the considered buckling mode, σ_{cr} becomes:

$$\sigma_{cr} = \frac{\pi^2 E}{\lambda^2} \tag{II.12}$$

If we plot the variation of σ_{cr} with respect to λ on a graph (Figure II.8), along with the line representing perfectly plastic behavior, $\sigma = f_y$, we can observe the idealized zones associated with failure due to buckling, plasticization, as well as the safety zone. The point of intersection P between these two curves symbolizes the theoretical maximum value of the slenderness ratio for which a column fails due to plasticization. This maximum slenderness ratio, sometimes referred to as Eulerian slenderness and denoted as λ_1 in Eurocode 3, is equivalent to:

$$\lambda_1 = \pi\sqrt{\frac{E}{f_y}} = 93.9\varepsilon \tag{II.13}$$

With :

$$\varepsilon = \sqrt{\frac{235}{f_y}} \tag{II.14}$$

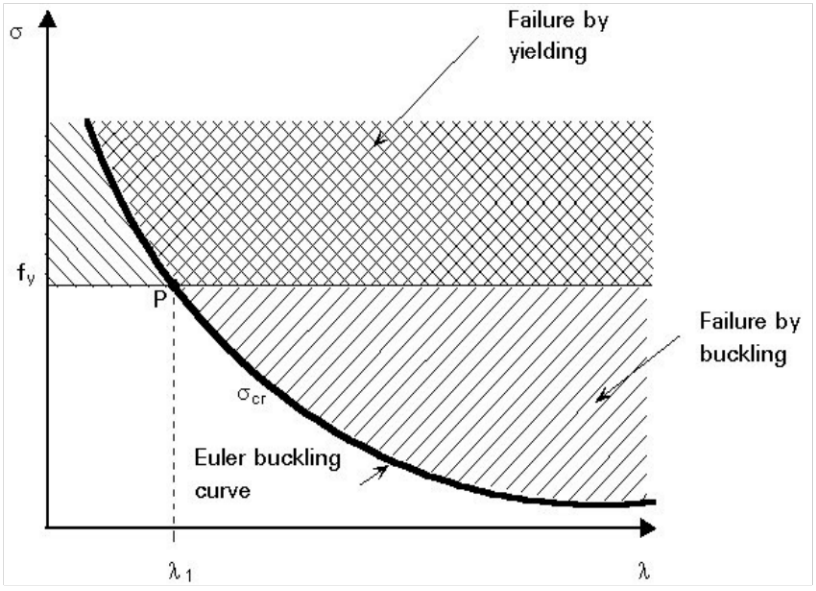

Figure II.8. Plasticization and buckling failure (Henriksson and Panarelli, 2017).

A non-dimensional graph can be created by plotting the values of σ/f_y against λ/λ_1 (Figure II.9). The coordinates of point P are thus defined as P (1;1).

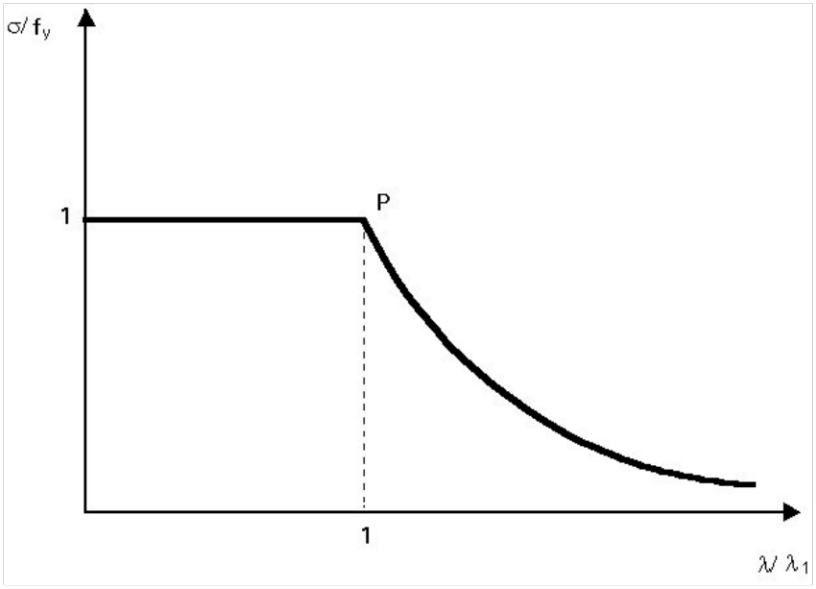

Figure II.9. Non-dimensional diagram (Henriksson and Panarelli, 2017).

II.6 INSTABILITY OF COLUMNS

The actual behavior of steel columns significantly deviates from the description provided earlier, as these columns tend to experience failure, typically through instability in the plastic range, before reaching the Euler buckling load.

The disparity between the actual and theoretical behaviors arises from various imperfections inherent to the "real" column, such as lack of straightness, residual stresses, applied load eccentricity, and yielding. All these imperfections affect buckling and consequently influence the load-carrying capacity of the column. Experimental studies conducted on real columns yield results similar to those depicted in Figure II.10.

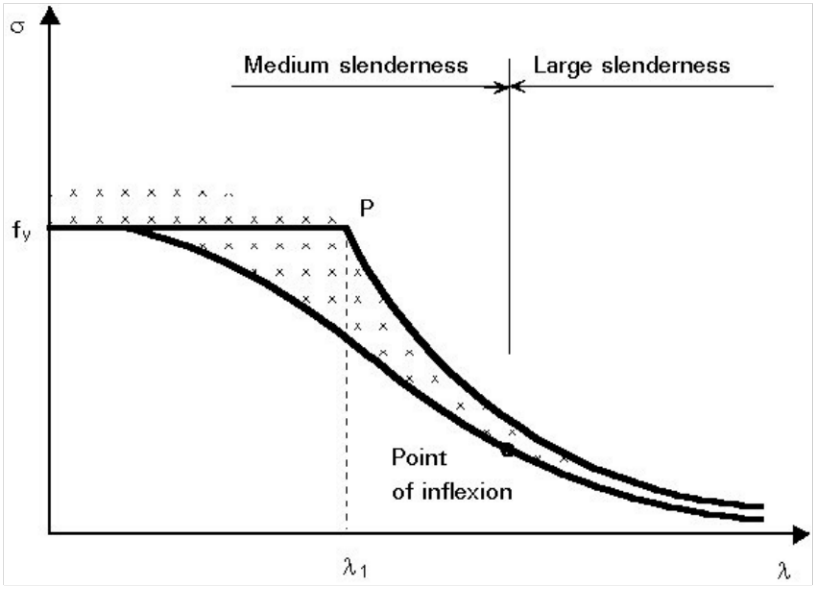

Figure II.10. Euler's buckling curve and actual behavior curve (Henriksson and Panarelli, 2017).

The actual behavior deviates much more significantly from theoretical curves in the range of intermediate slenderness than in the case of high slenderness. In the realm of intermediate λ values (encompassing the majority of columns used in practice), the influence of structural imperfections is notable and must be carefully considered. The most pronounced reduction in the theoretical value occurs around the Eulerian slenderness λ_1. The lower limit curve results from a statistical analysis; it represents the safe loading limit not to be exceeded.

II.7 BUCKLING CURVES

The reduced slenderness $\bar{\lambda}$ is a dimensionless parameter defined as follows for cross-sections of class 1, 2, or 3:

$$\bar{\lambda} = \frac{\lambda}{\lambda_1} \tag{II.15}$$

Where:

λ: Slenderness

λ_1: Eulerian slenderness

$\bar{\lambda}$ can also be expressed in the following form:

$$\bar{\lambda}^2 = \frac{\lambda^2}{\pi^2}\frac{f_y}{E} = \frac{f_y}{\sigma_{cr}} \tag{II.16}$$

$$\bar{\lambda} = \sqrt{\frac{f_y}{\sigma_{cr}}} = \sqrt{\frac{A.f_y}{A.\sigma_{cr}}} = \sqrt{\frac{A.f_y}{N_{cr}}} \tag{II.17}$$

Based on experimental resistance values, a probabilistic approach was employed in conjunction with theoretical analysis to create curves depicting the resistance of a column as a function of its slenderness ratio. Parameters considered in this study include a geometric imperfection shaped like a half-sine wave, with an amplitude set at 1/1000 of the column's length, as well as specific residual stresses unique to each profile type.

The buckling curves (a_0, a, b, or c) are presented in Figure II.11. They illustrate the reduction coefficient of the column's resistance χ, in relation to its reduced slenderness ratio $\bar{\lambda}$ for various cross-sectional types, each corresponding to distinct values of the imperfection factor α as specified in Table II.2. The mathematical expression for χ is formulated as follows:

$$\chi = \frac{1}{\varphi + \sqrt{\varphi^2 - \bar{\lambda}^2}} \leq 1 \tag{II.18}$$

Where: $$\varphi = 0{,}5\left[1 + \alpha\left(\bar{\lambda} - 0{,}2\right) + \bar{\lambda}^2\right] \tag{II.19}$$

Table II.1 presents the appropriate buckling curve for various types of cross-sections, extracted from Eurocode 3 Part 1-3:

Table II.1. Appropriate buckling curve for various types of cross-section.

Type of cross-section		**Buckling about axis**	**Buckling curve**
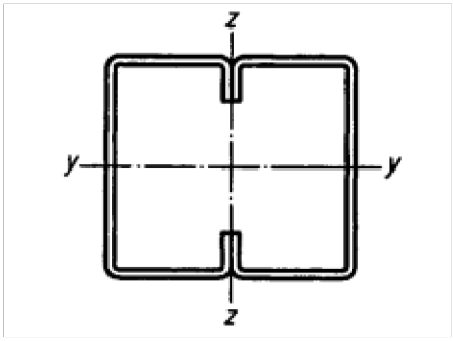	if f_{yb} is used	Any	b
	if f_{ya} is used *)	Any	c

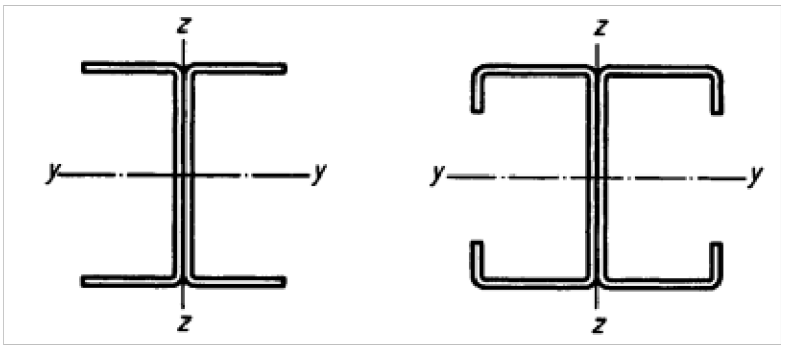	y-y z-z	a b
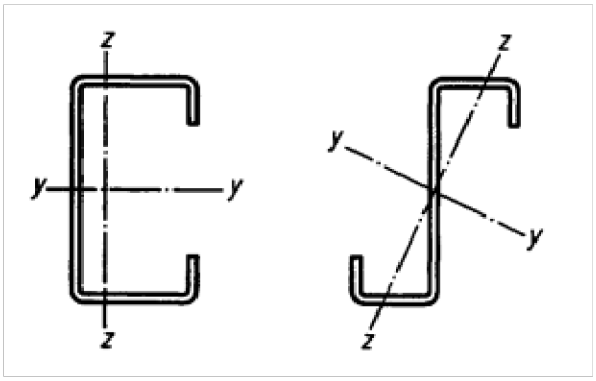	Any	b
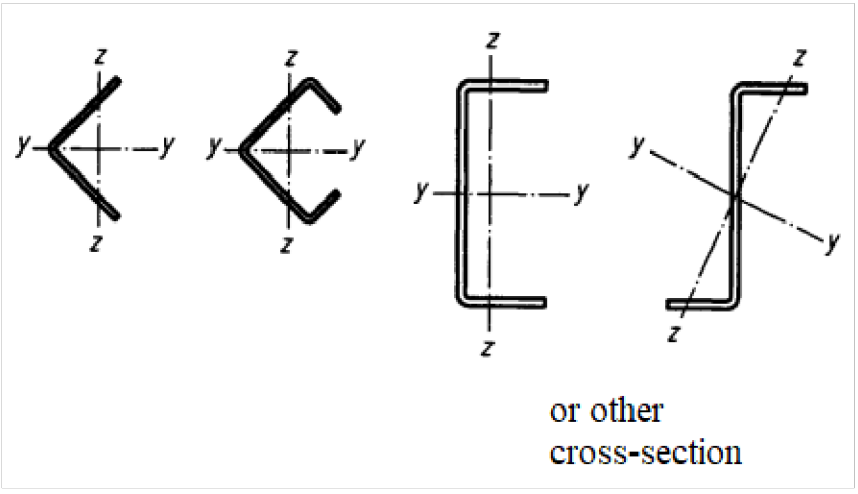	Any	c

*) The average yield strength f_{ya} should not be used unless $A_{eff} = A_g$

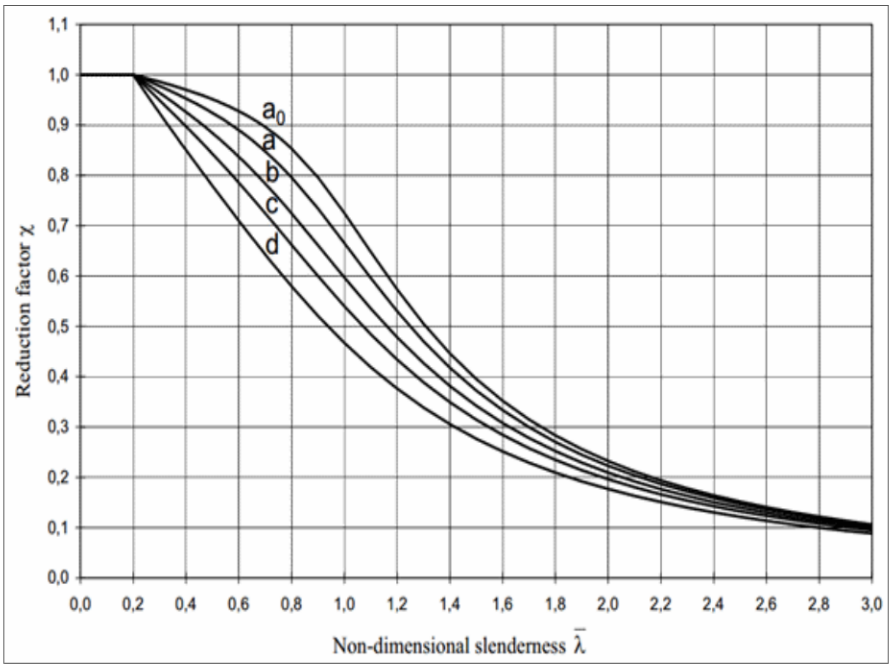

Figure II.11. Buckling curves for various cross-sectional types (CEN, 2005).

The imperfection coefficient α varies based on the configuration of the pole's cross-sectional shape, the direction of buckling (along the y or z-axis), and the manufacturing process employed (hot rolling, welding, or cold forming). The increasing values of α, corresponding to the level of imperfection, are listed in Table II.2:

Table II.2. Imperfection factors (CEN, 2005).

Buckling curve	**a_0**	**a**	**b**	**c**	**d**
imperfection factor α	0,13	0,21	0,34	0,49	0,76

It is crucial to note that buckling curves are established for bi-articulated members subjected to end loads. When these conditions are not met, it becomes necessary to accurately assess the buckling lengths.

II.8 COMPRESSIVE STRENGTH WITH BUCKLING

To design a component subjected to compression, it is essential, firstly, to assess the two buckling lengths corresponding to each of the two principal axes, taking into account the assemblies at its ends. Secondly, calculating the minimum moment of inertia required to withstand Euler's critical loads can be employed for a preliminary sizing of the element. Subsequently, the following verification procedure must be applied:

- The geometric properties of the section and its yield limit enable the calculation of the reduced slenderness ratio $\bar{\lambda}$.

- χ is determined based on the profile manufacturing process and the thickness of its walls, using one of the buckling curves and considering the reduced slenderness ratio $\bar{\lambda}$.

- For an element subjected to a compressive load, the calculated compressive force must satisfy the following condition:

$$N_{Sd} \leq N_{b.Rd} = \chi \cdot \frac{\beta_A \cdot A \cdot f_y}{\gamma_{M1}} \quad \text{(II.20)}$$

β_A=1 for cross-sectional classes 1, 2, and 3

$\beta_A = A_{eff} / A$ for cross-sectional class 4

II.9 CONCRETE-FILLED COLD-FORMED STEEL BUILT-UP COLUMNS

Currently, concrete-filled cold-formed steel (CF-CFS) built-up columns are defined as components composed of two materials, namely cold-formed steel and concrete, intricately connected and working together to withstand applied stresses (Rahnavard et al., 2022b).

Consequently, various types of columns with diverse shapes are utilized, whether they are open or closed cross-sections (C, Z, sigma,…etc), and they may be reinforced with reinforcements (in the case of reinforced concrete) or constructed using metal profiles.

Figure II.12. Built-up cold-formed steel columns filled with concrete.

II.9.1 Definitions and Usage

Steel elements are primarily known for their high tensile strength and ductility, while concrete components are valued for their strength, compressive capacity, and rigidity. The combination of these two materials in a composite structure creates a synergy that optimally leverages the unique qualities of each. Built-up cold-formed steel columns filled with concrete have recently gained popularity in construction due to their advantageous combination of lightness, strength, and durability (Rahnavard et al., 2022a). This hybrid structure leverages the flexibility of steel and the strength of concrete. The presence of concrete in the posts enhances fire resistance, while factory prefabrication ensures efficient manufacturing. These columns provide a more attractive solution, not only allowing for increased load capacity with a reduced cross-sectional area but also delivering cost savings and expedited construction, thereby leading to a significant reduction in overall costs (Rahnavard et al., 2022c).

The flawless adherence between the two materials has enabled their simultaneous use, streamlining their handling while significantly enhancing the performance of structures. This effective adherence prevents any relative slippage between the two materials. Consequently, it is observed that in the contact zone, the deformations ε_s for steel and ε_c for concrete, subjected to an identical load, are equivalent.

II.9.2 Different Types of Composite Columns

There are two main categories of composite columns: those that are partially or fully encased in concrete, and those that are filled with concrete. Figure II.13 illustrates various types of composite columns.

a) Partially concrete-encased columns take the form of I or H profiles, where the space between the flanges is filled with concrete. In fully concrete-encased columns, both the flanges and the webs are coated with a minimum thickness of concrete.

b) Concrete-filled profiles can take on circular, rectangular, or other cross-sectional shapes. The concrete confined within the profile experiences an increase in compressive strength, thereby enhancing the overall compressive strength of the column.

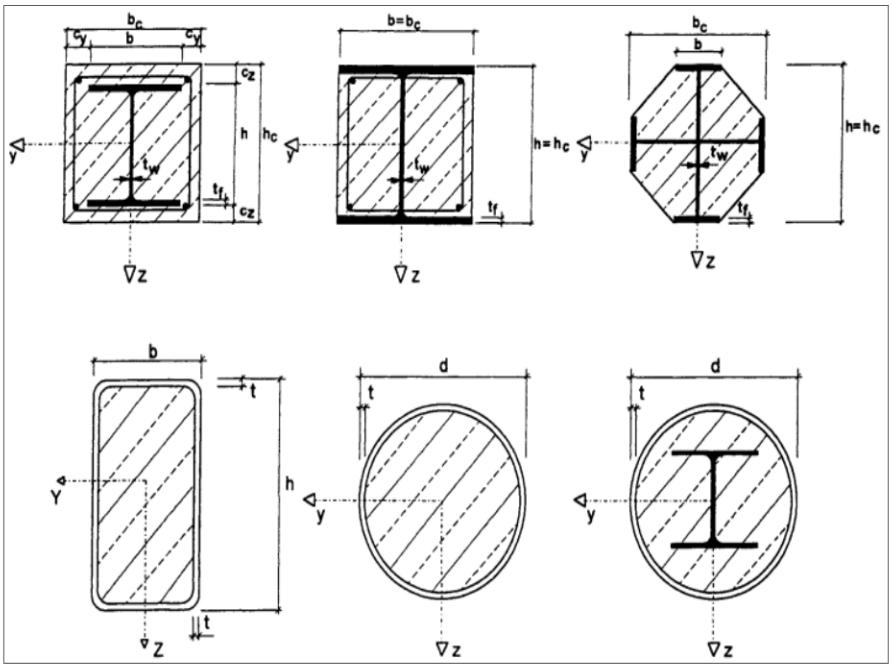

Figure II.13. Typical examples of cross-sectional profiles of mixed columns (Eurocode 4, 2004).

II.10 CONCRETE

Concrete is characterized by its compressive strength. Therefore, our focus is exclusively on the mechanical properties of concrete, as these characteristics determine its strength. The conventional stress-strain relationship is defined as follows:

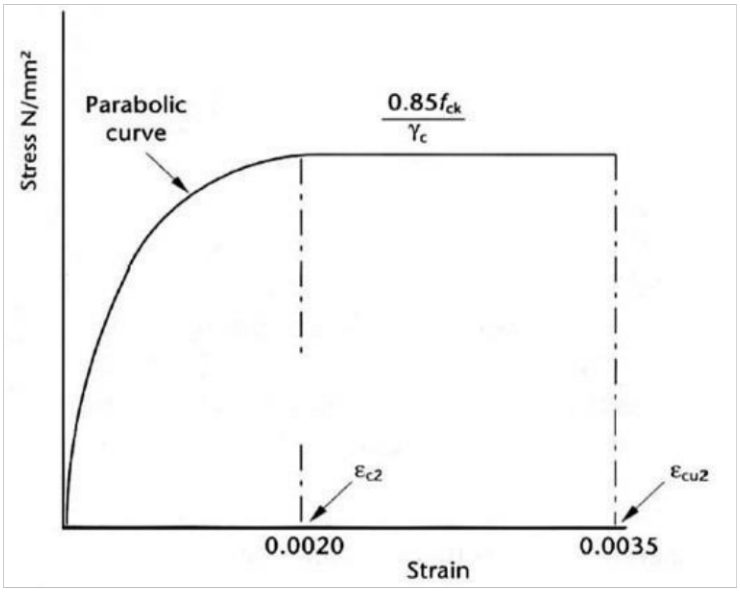

Figure II.14. Parabolic-rectangle diagram for concrete subjected to compression (European Committee for Standardization, 2004).

Concrete exhibits considerable strength in compression, but it remains highly brittle under tensile forces, with an ultimate deformation limited to only 3,5‰. The elasticity modulus E_c of concrete shows significant variability, primarily depending on the compressive strength of cylinders. Nevertheless, the properties of concrete can change over time. Creep and shrinkage are among the key phenomena influencing the behavior of concrete.

In general, concrete failure occurs due to the propagation of cracks, ultimately leading to its deterioration, as soon as its maximum stress, corresponding to a deformation of 2‰, is reached. This results in an irreversible and uncontrollable rupture caused by its disintegration (Figure II.15).

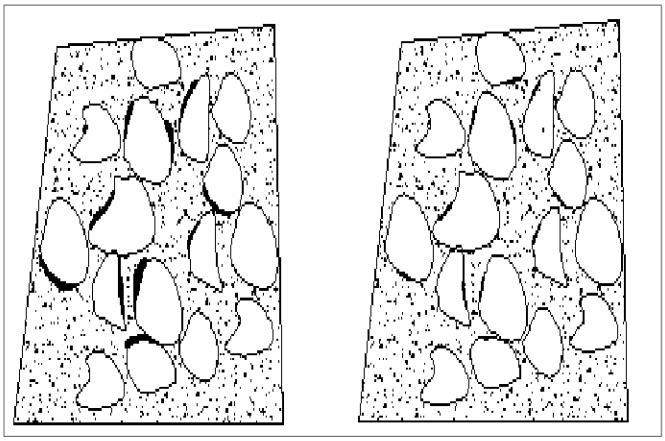

Figure II.15. Scheme of the evolution of micro-cracking in concrete (BOULMAALI-HACENE CHAOUCHE, 2023; KEBAILI, 2013).

II.10.1 Confined concrete

Cross-sections, whether circular or rectangular in shape, provide a form of confinement to concrete known as passive rather than active confinement. This type of confinement is associated with concrete cracking and increases proportionally with it. The use of transverse reinforcements to confine concrete has significantly enhanced its significance in the construction industry. Moreover, this significant improvement in behavior has prompted extensive research efforts focused on demonstrating the material's substantial capacity under stresses induced by confinement. Active confinement occurs through the controlled application of hydrostatic pressure to the concrete core, essentially defined as transverse pre-stressing before loading. In contrast, passive confinement is linked to the longitudinal stress that occurs within the concrete (BOULMAALI-HACENE CHAOUCHE, 2023).

Figure II.16 provides an illustration of confinement in rectangular and circular profiles. Furthermore, for both types of columns, fire resistance can be significantly enhanced compared to that of steel columns.

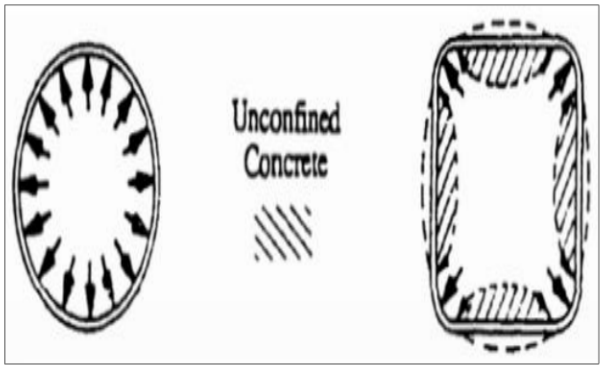

Figure II.16. The confinement in rectangular and circular profiles (BOULMAALI-HACENE CHAOUCHE, 2023; KEBAILI, 2013).

The correlation between stress and deformation in the case of confined concrete is influenced by various parameters. Several research studies have been conducted to develop an analytical model representing this relationship.

The overall performance of the columns filled with concrete depicted in Figure II.17 is primarily based on the restricted concrete recommendations, which are taken from ACI Institute Committee 318 (1999) regulations. The compressive stress f_c and its corresponding strain ε_c of unconfined concrete, which are fixed at 0,003 in accordance with ACI standards, are clearly lower than those of confined concrete (f_{cc} and ε_{cc}) when the stress-strain curves are analyzed. The use of confinement settings is highlighted by this observation (Harrat et al., 2024).

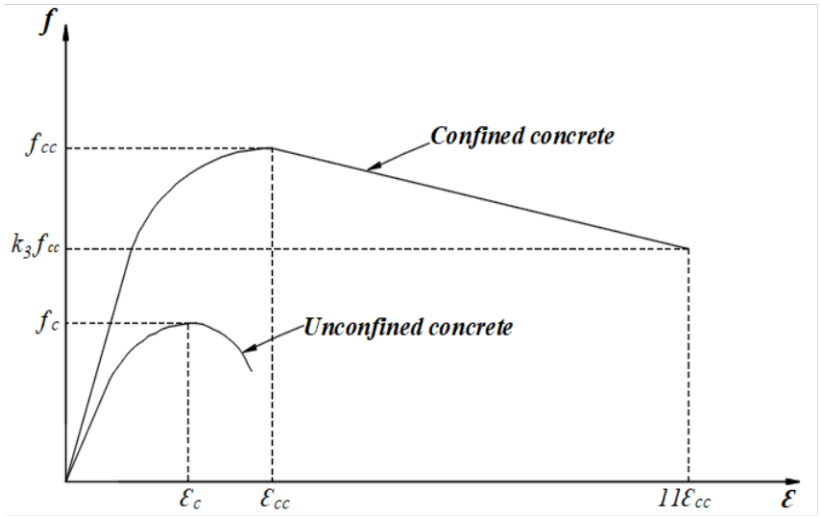

Figure II.17. Stress-strain relationship of unconfined and confined concrete (Hu et al., 2003).

Equations (II.21) and (II.22), which calculate the resistance of restricted concrete and the point at which compressive plastic strain ceases, are proposed based on the consider finished by Mander et al. (Mander et al., 1988):

$$f_{cc} = f_c + k_1 f_l \tag{II.21}$$

$$\varepsilon_{cc} = \varepsilon_c \left(1 + k_2 \frac{f_l}{f_c} \right) \tag{II.22}$$

Where:

k_1 and k_2: Constants based on the studies of Richart et al. (Richart et al., 1928) and were set as 4,1 and 20,5 respectively.

Ɛc and f_c: Compressive strain and strength of unconfined concrete respectively.

Ɛcc and f_{cc}: Compressive strain and strength of confined concrete respectively.

f_l: The confining pressure of the concrete.

In particular, the B/t ratio has a significant role in reducing local instabilities and determining the behavior of concrete-filled columns. Comparing reinforced columns with higher B/t ratios to those with lower ratios, the former are linked to a higher probability of local buckling (Hu et al., 2003).

$$\frac{f_l}{f_y} = 0.055048 - 0.001885\left(\frac{B}{t}\right) \qquad if\left(17 \le \frac{B}{t} \le 29.2\right) \tag{II.23}$$

$$\frac{f_l}{f_y} = 0 \qquad if\left(29.2 \le \frac{B}{t} \le 150\right) \tag{II.24}$$

The degradation parameter k_3 for the material in rectangular sections filled with concrete is defined as per the formulation provided by Hu et al. (Hu et al., 2003):

$$k_3 = 0.000178\left(\frac{B}{t}\right)^2 - 0.02492\left(\frac{B}{t}\right) + 1.2722 \qquad if\left(17 \le \frac{B}{t} \le 70\right) \tag{II.25}$$

$$k_3 = 0.4 \qquad if\left(70 \le \frac{B}{t} \le 150\right) \tag{II.26}$$

II.11 CONCLUSION

Cold-formed steel built-up columns, when unfilled with concrete, offer significant benefits in creating strong and durable structures. Thanks to their modular design and production at ambient temperature, they provide a quick and cost-effective installation on the construction site. When filled with concrete, these columns gain additional strength and stiffness, thereby enhancing their ability to withstand high loads and environmental stresses. This combination of materials also provides remarkable fire resistance and improved sound insulation in the construction industry.

The regulatory aspects regarding cold-formed columns, whether empty or filled with concrete, are extremely important when designing and building constructions. These structural elements are guaranteed to be safe and long-lasting by the American Concrete Institute (ACI) standards and the European construction rules (EN 1993-1-3 and EN 1994-1-1).

CHAPTER III

Regulatory aspect

III.1 INTRODUCTION

To tackle the issue of instability, the regulations governing metal construction provide various methods. This chapter specifically focuses on the regulatory aspects outlined in the European standards Eurocode 3 and Eurocode 4, which pertain to empty and concrete-filled columns respectively. Eurocode 3 encompasses the development of calculation codes, with Part 1-3 dedicated to cold-formed profiles. These profiles are analyzed using the effective width method, which involves iterative calculations to determine their effective properties. This approach adds complexity to the examination of the performance of double C-section columns, whether they are empty or filled with concrete. On the other hand, the simplified method for composite columns proves highly effective. It utilizes European buckling curves for steel columns, which implicitly consider imperfections that impact concrete-filled columns, as per Eurocode 4 Part 1-1.

The numerical and analytical analysis examined the behavior of cold-formed steel double C-columns. Each column consisted of two C-shaped sections assembled in various configurations (back-to-back, face-to-face, and box), connected by rivets and welds. The models accurately predicted the performance of cold-formed posts across different lengths.

III.2 CALCULATION BASIS

Cross-sectional shapes can be categorized based on their ability to reach their strength limit. This categorization is determined by the sections' capacity to undergo plasticization and the impact of instabilities.

III.2.1 Safety factor

For verification in the ultimate limit state, the partial coefficients γ_M should be taken as follows:

- ✓ Resistance of cross-sections when failure is due to plasticisation (γ_{M0}=1)
- ✓ Resistance of profiles and plates when failure is due to instability (γ_{M1}=1.1)
- ✓ Net section resistance at bolt holes (γ_{M2}=1.25)
- ✓ In the service limit state, the coefficient γ is γ_{Mser}=1

III.2.2 Material characteristics

The characteristics and grades of the steels used in the formation of cold and hot-formed profiles recommended by the EN 1993-1-3 are summarised in the following Table III.1:

Table III.1. Nominal values for basic yield strength f_{yb} and tensile strength f_u.

Type of steel	Standard	Grade	f_{yb} N/mm^2	f_u N/mm^2
Hot-rolled structural steel sheet	EN10025	S235	235	360
		S275	275	430
		S355	355	510
Hot-rolled high-strength structural steel sheet	EN10113-2	S275N	275	370
		S355N	355	470
		S420N	420	520
		S460N	460	550
	EN10113-3	S275M	275	360
		S355M	355	450
		S420M	420	500
		S460M	460	530
Cold reduced steel sheet of structural quality	ISO 4997	CR220	220	300
		CR250	250	330
		CR320	320	400
Continuously hot-dip galvanised structural steel sheets	EN 10147	Fe E 220G	220	300
		Fe E 250G	250	330
		Fe E 280G	280	360
		Fe E 320G	320	390
		Fe E 350G	350	420
High yield strength steels for cold forming	EN 10149-2	S315MC	315	390
		S355MC	355	430
		S420MC	420	480
		S460MC	460	520
		S500MC	500	550
		S550MC	550	600
	EN 10149-3	S260MC	260	370
		S315MC	315	430

		S355MC S420MC	355 420	470 530

III.3 EFFECTIVE SECTION

When analyzing the behavior of a cold-formed element and estimating its load-bearing capacity, the first step is to evaluate the effective widths of the compressed walls of its section. This requires an appropriate distribution of stresses within the relevant section. Next, it is necessary to calculate the geometric properties of the effective section, taking into account the displacement of the neutral axis resulting from the redefinition of the section into effective parts. Finally, the same principles and basic rules used for designing and verifying sections with thick walls (hot-rolled sections) are applied to cold-formed walls.

III.3.1 Effective width concept

Considering a plate simply supported at its edges and subjected to compression in one direction, it becomes evident that after reaching the post-critical stage, stresses concentrate along the edges. In this situation, it is possible to determine the plate's capacity based on a uniform stress distribution, but this distribution is limited to a reduced width, referred to as the effective width b_{eff}. This effective width depends both on the critical elastic buckling stress of the plate σ_{cr} and the material's yield strength f_y.

III.3.2 Validity of the effective width concept

Comparative analyses between test results and rupture loads obtained through analytical calculations for C-sections, as well as for other types of sections, have validated the effectiveness of this calculation model. The strength of the effective width concept lies in its ability to facilitate the use of relatively simple calculation methods. Moreover, it allows for highlighting the impact of section geometry on the load-bearing capacity of the studied element.

In Figure III.1, for the C-shaped section, it is necessary to calculate the effective width separately for each component under compression. The ultimate load capacity of the section can then be determined by assuming that the load is solely carried by these effective segments.

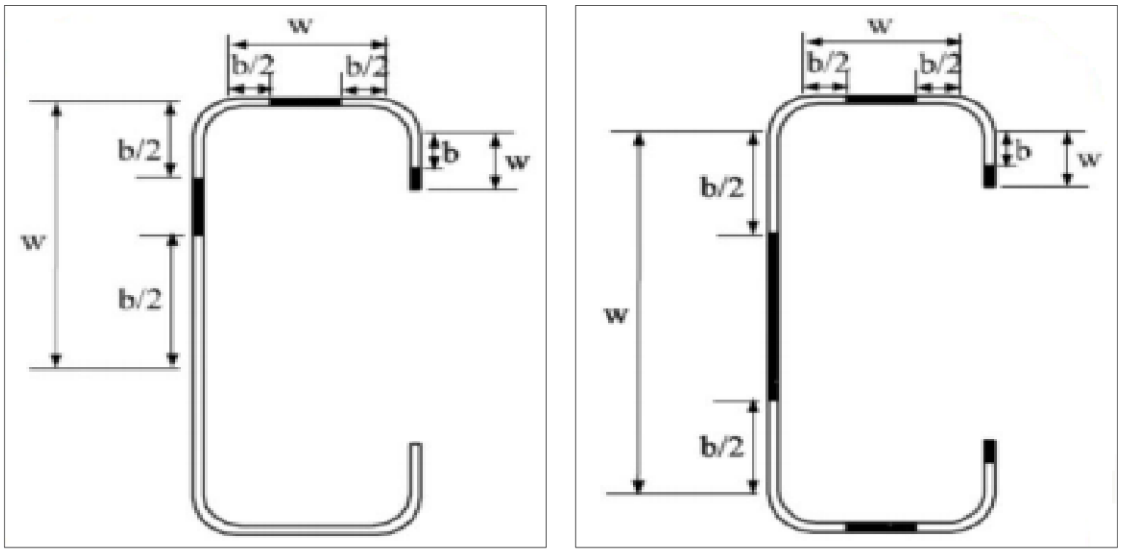

(a) (b)

Figure III.1. Effective widths of C-Section: (a) Bent element; (b) Compressed element (Djelil, 2019).

III.4 CHARACTERISTICS OF SECTIONS

It is essential to assess the characteristics of sections based on the specificities of their cross-sectional shapes, given their direct impact on the strength of the element.

It is crucial to consider the implications of local buckling when selecting cross-sectional shapes that are effective in this regard.

III.4.1 Gross cross-section

The specified nominal dimensions are used to establish the characteristics of the gross cross-section. It is not necessary to subtract fastener holes in this calculation, but it is crucial to consider openings of significant size. Plates used solely for splicing or as connecting gussets should not be included in these calculations.

III.4.2 Net cross-section

The net area of a bar or wall in a cross-section must be calculated by subtracting from its gross area the total surface area of fastener holes and any other openings.

III.4.3 Influence of rounding

In cross-sections with rounded edges, the reference widths of the walls, denoted as b_p, should be defined from the midpoints of the adjacent corner walls.

The properties of the cross-sections must be determined on the basis of the particularities of the cross-sections, as they influence the strength of the element. These characteristics are determined on the basis of the actual geometry of the sections (Figures III.2, III.3, and III.4).

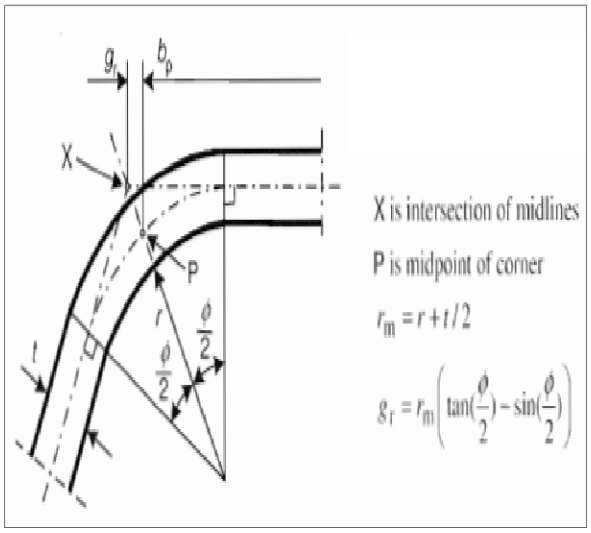

Figure III.2. Midpoint of corner or bend (European Committee for Standardization, 2006).

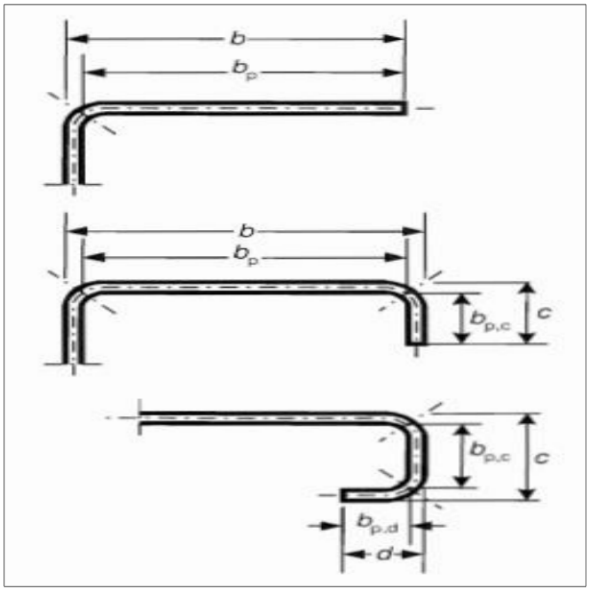

Figure III.3. Notional flat width (European Committee for Standardization, 2006).

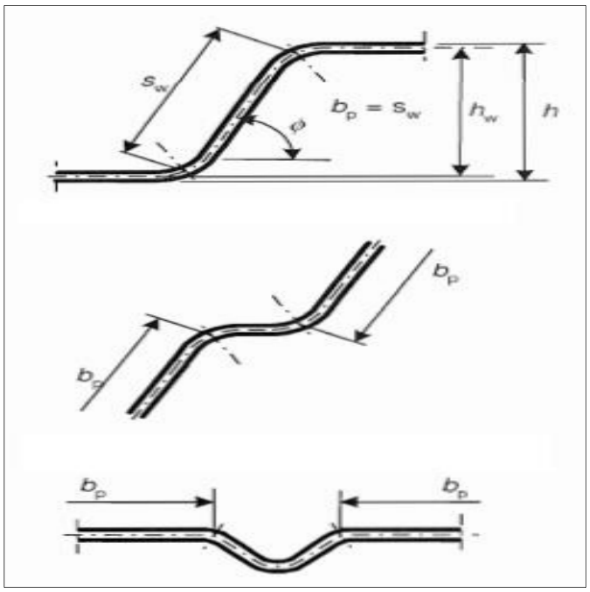

Figure III.4. Notional flat width of adjacent stiffener walls (European Committee for Standardization, 2006).

b_p: Notional flat width of plane element.

b: Total wall width.

c: Total width of stiffener.

III.4.4 Augmented average yield strength

The Eurocode introduces the concept of f_{ya}, which represents the augmented average yield strength of a cross-section after cold forming. Its calculation can be performed using the following method (European Committee for Standardization, 2006):

$$f_{ya} = f_{yb} + \left(f_u - f_{yb}\right) k.n.t^2 / A_g \qquad \text{And} \qquad f_{ya} \le \frac{f_u + f_{yb}}{2} \qquad \text{(III.1)}$$

k=7 for cold profiling or k=5 for other types of profiling.

n: Number of 90° bends in the cross-section with an inner radius r<5t.

t: The nominal thickness of the steel sheet before cold forming.

This increase in the average yield strength is applied when the profile undergoes an axial load, and the effective area of its section A_{eff}, corresponds to the gross area.

When it comes to recommended minimum thicknesses, the Eurocode suggests the following values:

For plates 0,5mm ≤ t ≤ 4mm

For profiles 1mm ≤ t ≤ 4mm

III.4.5 Geometric proportions

The Table III.2 below outlines the maximum limits of geometric proportions that the profiles must adhere to (European Committee for Standardization, 2006):

Table III.2. Maximum width-to-thickness ratios (b/t).

Element of cross-section	Maximum value
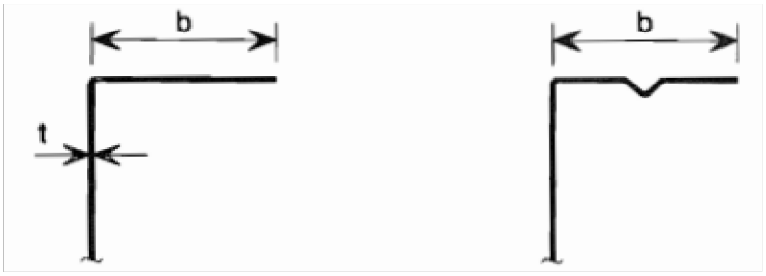	$b/t \leq 50$
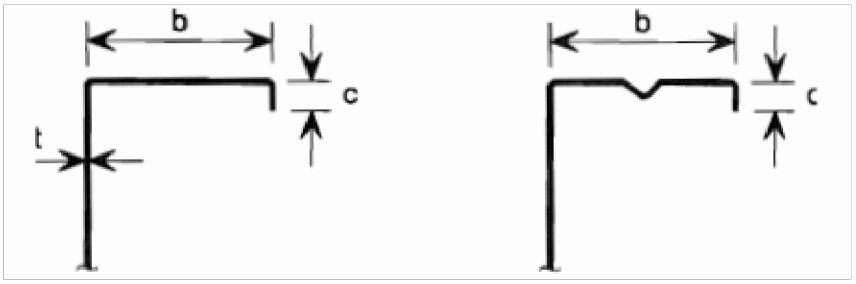	$b/t \leq 60$ $c/t \leq 50$
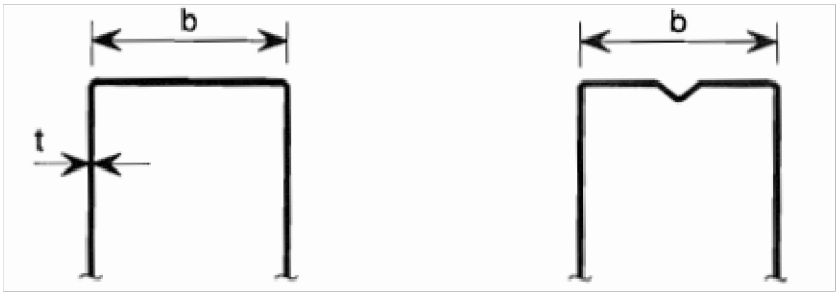	$b/t \leq 500$
	$45° \leq \phi \leq 90°$ $h/t \leq 500 \sin\phi$

Table III.3. Modelling of elements of a cross-section.

Type of element	Model	Type of element	Model
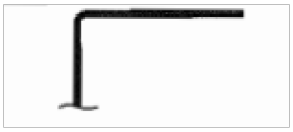		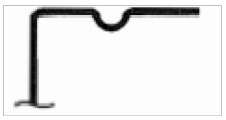	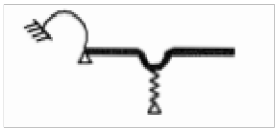
	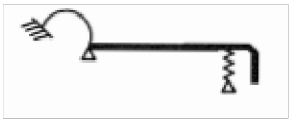		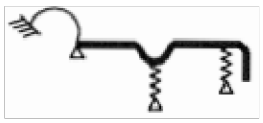
		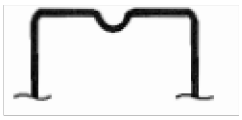	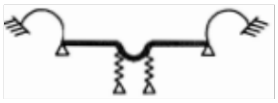
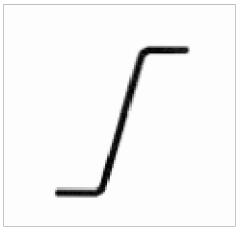	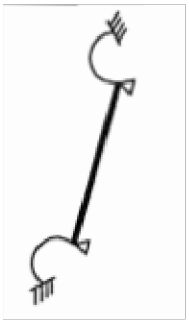	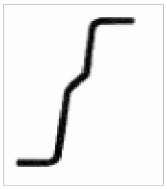	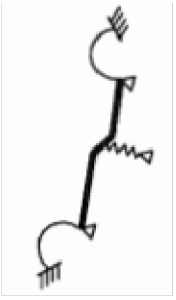

The Table III.3 illustrates the corresponding wall modeling for each type of section. To ensure adequate stiffness and prevent stiffener buckling, the following condition must be met:

$$0{,}2 \leq c/b \leq 0{,}6 \qquad \text{(III.2)}$$

III.5 PRESENTATION OF THE CONCEPT OF EFFECTIVE WIDTH ACCORDING TO EUROCODE 3

The EN 1993-1-3 standard does not provide explicit provisions for distortional buckling. However, a calculation method can be derived by interpreting the rules outlined in this code, specifically for flat elements equipped with compressive stiffeners, regardless of their positioning at the edges or in the center. The design of these compressed elements, which are fitted with either edge or intermediate stiffeners, is based on the assumption that the stiffener behaves similarly to a compressed element with limited restraint. This restraint is represented through a spring stiffness that varies relying on the boundary conditions and the flexural stiffness of adjoining flat factors in the cross-section.

EN 1993-1-3 (European Committee for Standardization, 2006) outlines design specifications for cold-formed profiles and ribbed sheets, encompassing steel products that have undergone cold-forming processes like roll forming or press-brake bending. These processes utilize hot-rolled or cold-rolled steel sheets or strips with thin dimensions, regardless of whether they are coated or uncoated. Additionally, this standard can be employed for shaping profiled steel sheets intended for use in steel-concrete composite slabs during the casting phase. It offers both calculation-based and testing-supported design methods. It is crucial to emphasize that calculation-based approaches are applicable solely within certain ranges of material properties and geometric proportions, provided that there is adequate experience and validation through testing. Nevertheless, these limitations do not extend to design supported by testing. It does not address considerations related to test loads during the execution and maintenance phases.

The critical elastic buckling constraint is given by Timoshenko and Gere (Timoshenko and Gere, 1961):

$$\sigma_{cr} = \frac{\pi^2 EI_s}{A_s \lambda^2} + \frac{I}{A_s \pi^2} K.\lambda^2 \tag{III.3}$$

The critical stress is:

$$\lambda_{cr} = \sqrt[4]{\frac{EI_s}{K}} \tag{III.4}$$

It is advisable to follow the general (iterative) procedure to determine the effective properties of the compressed flange and edge, which is a planar element equipped with an edge stiffener. This assessment takes place in three distinct phases:

In the first step, the initial effective section of the stiffener is acquired by utilizing determined effective widths. It is assumed that the stiffener offers complete restraint and that certain conditions are met:

$$\sigma_{com,Ed} = \frac{f_{yb}}{\gamma_{M0}} \tag{III.5}$$

Effective width of compressed flanges:

The stress ratio, denoted as ψ, is set at a value of 1, signifying a state of uniform compression. As a result, the buckling coefficient k_σ is determined to be 4 for an element experiencing internal compression (Kouider et al., 2021).

$$\varepsilon = \sqrt{\frac{235}{f_{yb}}} \tag{III.6}$$

$$\lambda_{bp} = \frac{b_p / t}{28.4 \times \varepsilon \sqrt{k_\sigma}} \tag{III.7}$$

$$\rho = \frac{\lambda_{bp} - 0.055(3+\psi)}{\lambda_{bp}^2} \tag{III.8}$$

$$b_{eff} = \rho . b_p \tag{III.9}$$

$$b_e = 0.5 \times b_{eff} \tag{III.10}$$

Effective width of the fallen edges:

$$\frac{b_{p,c}}{b_p} \leq 0.35 \qquad k_\sigma = 0.5 \tag{III.11}$$

$$0.35 < \frac{b_{p,c}}{b_p} \leq 0.6 \qquad k_\sigma = 0.5 + \sqrt[3]{\left(\frac{b_{p,c}}{b_p} - 0.35\right)^2} \tag{III.12}$$

$$c_{eff} = \rho . c_p \tag{III.13}$$

The effective section of the stiffener A_s must be obtained from:

$$A_s = t\left(b_{e2} + c_{eff}\right) \tag{III.14}$$

In the second step, the distortion buckling reduction factor (related to the flexural buckling of the stiffener) is calculated by utilizing the initial effective section of the stiffener, while considering the impact of continuous spring restraint (Kouider et al., 2021).

The critical stress of the buckling of the stiffener may be derived, after substitution, as follows:

$$\sigma_{cr} = \frac{2\sqrt{K.E.I_s}}{A_s} \tag{III.15}$$

Where:

I_s: the moment of inertia of the effective section of the stiffener.

Effective width of the fallen edges:

The following expression for the stiffness of the spring K_1:

$$K_1 = \frac{E.t^3}{4(1-\nu^2)} . \frac{1}{b_1^2.h_w + b_1^3 + 0.5.b_1.b_2.h_w.k_f} \quad \text{(III.16)}$$

With:

$$k_f = \frac{A_{s2}}{A_{s1}} \text{ (The lower flange is in compression).} \quad \text{(III.17)}$$

The distortion buckling resistance reduction factor χ_d, which pertains to the buckling of the stiffener in flexure, is derivable from the relative slenderness $\overline{\lambda}_d$:

$$\overline{\lambda_d} \le 0.65 \qquad \chi_d = 1 \quad \text{(III.18)}$$

$$0.65 < \overline{\lambda_d} < 1.38 \qquad \chi_d = 1.47 - 0.732\overline{\lambda_d} \quad \text{(III.19)}$$

$$\overline{\lambda_d} \ge 1.38 \qquad \chi_d = \frac{0.66}{\overline{\lambda_d}} \quad \text{(III.20)}$$

Where:

$$\overline{\lambda_d} = \sqrt{\frac{f_{yb}}{\sigma_{cr,s}}} \quad \text{(III.21)}$$

In the third step, various iterations can be explored to enhance the accuracy of the reduction factor for the buckling of the stiffener.

If $\chi_d < 1$, the calculation of the effective section can be refined iteratively, starting the iteration with the modified values of ρ obtained using the formulas in EN 1993-1-3 (European Committee for Standardization, 2006) with:

$$\sigma_{com,Ed,i} = \frac{f_{yb}}{\gamma_{M0}} \quad \text{so that:} \quad \overline{\lambda_{p,red}} = \overline{\lambda_p}.\sqrt{\chi_d} \quad \text{(III.22)}$$

Effective cross-section of the web:

$$\lambda_{hp} = \frac{h_p / t}{28.4 \times \varepsilon \sqrt{k_\sigma}} \quad \text{(III.23)}$$

$$h_{peff} = \rho . h_p \tag{III.24}$$

$$h_e = 0.5 \times h_{peff} \tag{III.25}$$

In order to determine the ultimate load of the C-section, it is essential to calculate the effective width for each compression segment separately. This calculation requires the assumption that the load is solely carried by the effective areas. The effective cross-section of a C-section can be found by utilizing the following formula:

$$A_{eff} = t\left[b_{e1} + b_{e3} + h_{e1} + h_{e2} + \left(b_{e2} + c_{eff\,1} \right) \chi_{d1} + \left(b_{e4} + c_{eff\,2} \right) \chi_{d2} \right] \tag{III.26}$$

III.6 RESISTANCE OF CROSS-SECTIONS

III.6.1 Axial compression

The design compressive strength of a cross-section $N_{c,Rd}$ must be determined as follows:

- If its effective section A_{eff} is less than its cross-section A_g :

$$N_{c,Rd} = \frac{f_{yb} A_{eff}}{\gamma_{M1}} \tag{III.27}$$

- If its effective section A_{eff} is equal to its cross-section A_g :

$$N_{c,Rd} = \frac{f_{ya} A_g}{\gamma_{M0}} \tag{III.28}$$

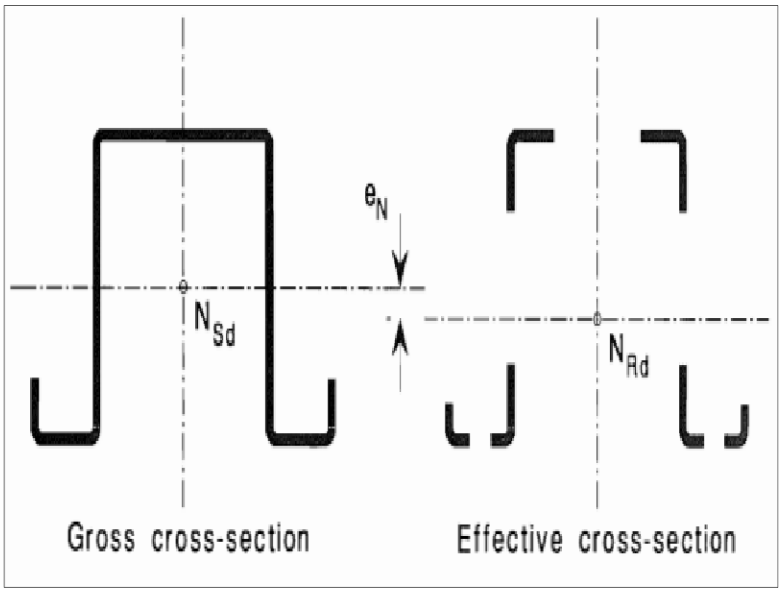

Figure III.5. Effective cross-section of form hat under compression (European Committee for Standardization, 2006).

III.7 RIVETING ASSEMBLY OF ELEMENTS

Rivets, permanent fastening elements widely used in various fields such as aviation, transportation, construction, boilers, bridges, ships, automotive, appliances, electronics, etc., have replaced bolts due to their lower cost. In addition to their fastening function, rivets can also serve as rotation axes (as in folding garden furniture), electrical contacts, stops, etc (Mohamad et al., 2007).

III.7.1 Principle of riveting

A rivet consists of a cylindrical rod called a "shank," which is equipped with a "head" at one end (Figure III.6). The shape of the head varies depending on the type of rivet (MANSOURI, 2022).

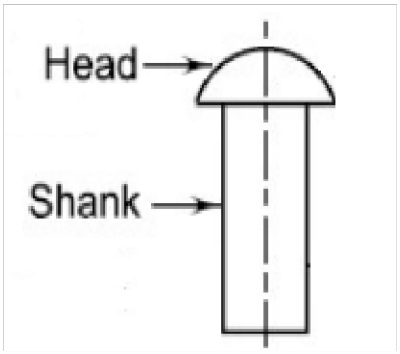

Figure III.6. The components of a rivet (Li et al., 2021).

To assemble using riveting, it's necessary to start by drilling holes, either through conventional drilling, punching, or punching and reaming, with a diameter slightly larger than that of the shank. Then, the rivets are inserted, and a rivet set is used to form the rivet head (Figure III.7) (MANSOURI, 2022).

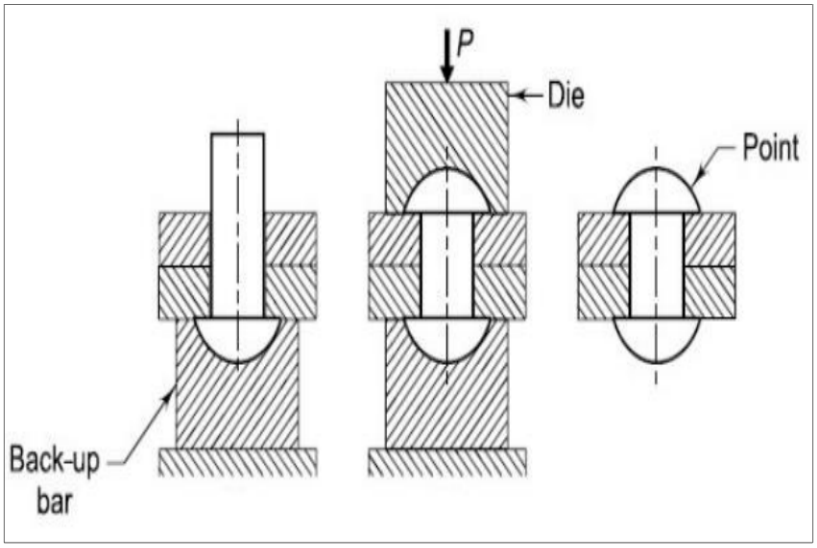

Figure III.7. A riveting assembly (Li et al., 2021).

III.7.2 Rivet section, length, and drilling diameter

When it comes to determining the diameter (in millimeters) of the rivet in relation to the thickness (in millimeters) of the sheets, practitioners typically apply the following formula:

$$d = \frac{45.H}{(15 + H)} \tag{III.29}$$

III.7.3 Assembly of rivets using cold setting (d<10 mm)

The rivet is secured by compressing the material to create locking elements, namely the rivet head and the rivet. This type of assembly is referred to as a locking element assembly.

III.7.4 Arrangement of rivets

There are two configurations of rivets: common rivets, arranged in a chain, and watertight rivets, arranged in a staggered pattern, as illustrated in the Figure III.8. In a strength rivet, the pitch, also known as spacing, is greater than in a watertight rivet (MANSOURI, 2022).

III.7.4.1 Chain arrangement

In this arrangement, the rivets are organized and aligned at regular intervals (Figure III.8.a, and III.8.b).

III.7.4.2 Staggered arrangement

In this scenario, the rivets are arranged alternately in each column, and sometimes, there is no apparent pattern in their placement, meaning they are distributed randomly (Figure III.8.c).

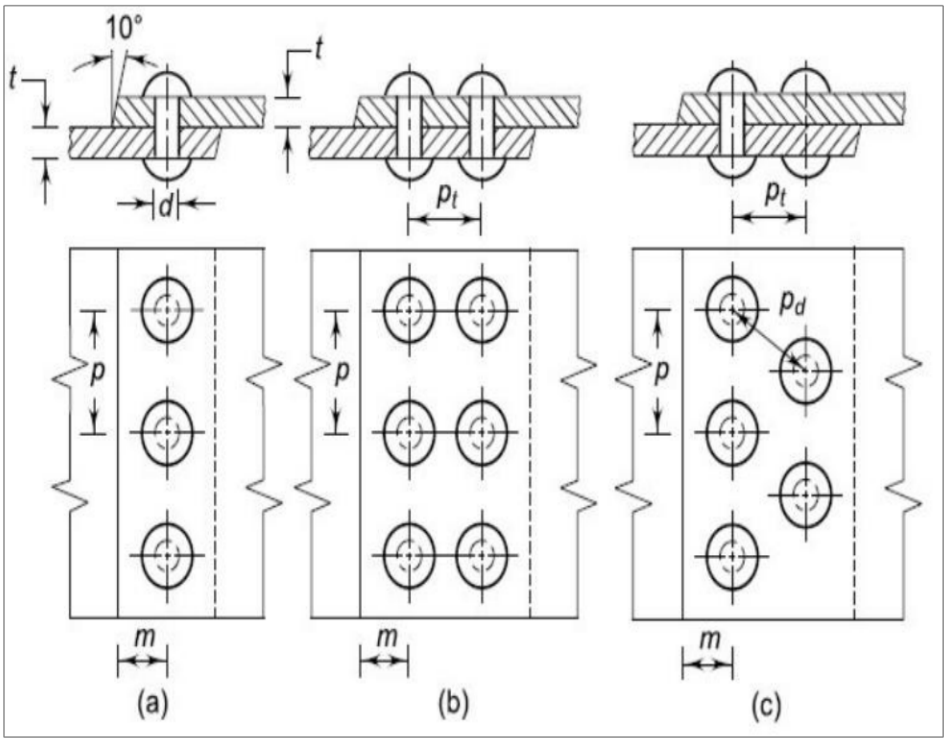

Figure III.8. Arrangement of rivets: (a) Single riveted lap joint; (b) Double riveted lap joint (chain pattern); (c) Double riveted lap joint (zig-zag pattern) (A A H Al-Filfily and A A Muhmmed, 2022; Bhandari, 2010).

III.7.5 Positioning of rivets

These various distances must fall within ranges of minimum and maximum values that vary depending on mechanical requirements, construction methods, and corrosion risks (Bhandari, 2010). The placement of the rivets is calculated based on EN 1993-1-8 (EN 1993-1-8, 2005).

- ✓ ***Pitch (p)***

The measurement of the rivet pitch is determined by the gap between the center of one rivet and the center of the neighboring rivet in the identical row. Generally, the value of p is equal to three times the shank diameter, denoted as d (Figure III.8).

- ✓ ***Margin (m)***

The margin refers to the space from the plate's edge to the centerline of rivets in the closest row, typically denoted as m = 1,5d (Figure III.8).

- ✓ ***Transverse pitch (p_t)***

The transverse pitch, also referred to as back pitch or row pitch, denotes the measurement between two successive rows of rivets within a single plate. Generally, the transverse pitch is calculated as p_t=0,8p for chain riveting and p_t=0,6p for zig-zag riveting, as illustrated in Figure III.8.

- ✓ ***Diagonal pitch (p_d)***

The diagonal pitch refers to the measurement from the center of a rivet to the center of the neighboring rivet in the adjacent row (see Figure III.8).

III.8 WELDING ASSEMBLY OF ELEMENTS

Welding is a well-known metal joining process valued for its reliability, efficiency, and practicality, widely used across various sectors such as the nuclear industry, aerospace, automotive, transportation, and offshore. Despite its numerous advantages, this process does have its limitations, particularly regarding welding defects that can compromise the desired properties of the joint. Thermal cycles play a significant role in the formation of residual stresses, deformations, steel microstructure, and hardness. Due to localized heating during the welding process, controlling thermal cycles is crucial and often essential (Attarha and Sattari-Far, 2011).

The use of welding technology in the fabrication of large structures offers numerous advantages compared to mechanical assembly methods, including enhanced structural performance, weight reduction, design flexibility, and cost savings, among others (Liang and Deng, 2018).

III.8.1 Butt welds

The butt welding process (Figure III.9), which is the primary form of resistance welding, allows, as its name suggests, joining the ends of bars or profiles with the same cross-section, or pieces previously prepared to fit this case. This technique enables welding across the entire thickness of the joined surfaces in a butt or T-joint assembly. Typically, it's necessary to prepare the edges

of the surfaces before welding. However, in some situations where the surface thickness is less than 5mm, this preparation may be omitted (Niou et al., 2016).

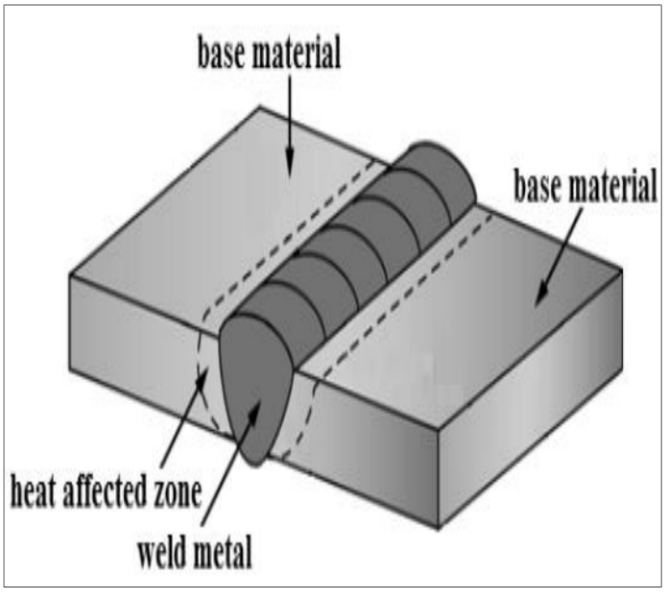

Figure III.9. Presentation of a butt weld (Arsić et al., 2013).

III.8.2 Fundamental welding formulas

The formulas provided by Eurocode 3 Part 1-8 (EN 1993-1-8, 2005) state that the components of the average stress related to the weld throat section must satisfy the following conditions:

$$\sqrt{\sigma_{\perp}^2 + 3\left(\tau_{\perp}^2 + \tau_{//}^2\right)} \leq \frac{f_u}{\beta_w \gamma_{Mw}} \qquad \text{And} \qquad \sigma_{\perp} \leq \frac{0.9 f_u}{\gamma_{Mw}} \qquad \text{(III.30)}$$

With:

$\sigma_{\perp}$: Perpendicular component to the section.

$\tau_{\perp}$: Component in the plane of the section perpendicular to the longitudinal axis of the weld bead.

$\tau_{//}$: Component in the plane of the section parallel to the longitudinal axis of the weld bead.

β_w: Correlation factor dependent on the steel used provided by:

$\beta_w = 0,8$ in the case of S235 steel (f_u=360MPa)

$\beta_w = 0,85$ in the case of S275 steel (f_u=430MPa)

$\beta_w = 0,9$ in the case of S355 steel (f_u=510MPa)

γ_{Mw}: Partial safety factors vary depending on the characteristics of the steels.

γ_{Mw} = 1,25 for steel with yield strength S235.

γ_{Mw} = 1,30 for steel with yield strength S275.

γ_{Mw} = 1,35 for steel with yield strength S355.

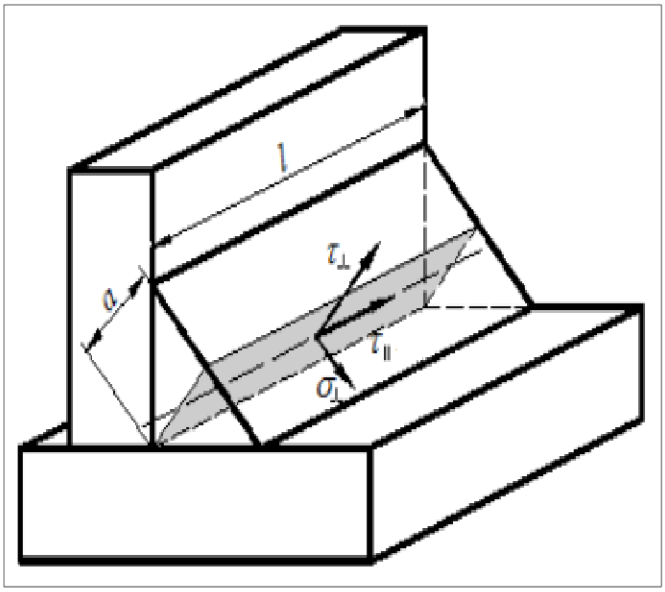

Figure III.10. The representation of a weld bead (Cichański and Tomaszewski, 2015).

III.9 EUROCODE 4: DESIGN OF COMPOSITE STEEL AND CONCRETE STRUCTURES

Eurocode 4 Part 1-1 is employed for evaluating components and hybrid structures utilized in building construction and infrastructure. It adheres to safety and performance standards for structures, along with the principles and calculation procedures outlined in EN 1990 - Basis of Structural Design (Gulvanessian, 2002).

It focuses solely on the strength, functionality, durability, and fire resistance of hybrid structures, excluding other criteria such as thermal or acoustic insulation.

III.10 VERIFICATION OF THE BUCKLING RESISTANCE OF CF-CFS BUILT-UP COLUMNS

If the calculated axial force N_{sd} is appropriate for each buckling plane, the composite column exhibits adequate buckling resistance, as formulated below:

$$N_{sd} \leq \chi N_{Pl,Rd} \quad \text{(III.31)}$$

With:

χ: The reduction factor associated with the examined buckling plane is determined using the reduced slenderness $\bar{\lambda}$ and by referring to the appropriate European buckling curve.

The computation of the reduction coefficient χ for buckling is executed as outlined below:

$$\chi = \frac{1}{\phi + \sqrt{\phi^2 + \bar{\lambda}^2}} \quad \text{(III.32)}$$

Where:

$$\phi = 0,5\left[1 + \alpha\left(\bar{\lambda} - 0,2\right) + \bar{\lambda}^2\right] \quad \text{(III.33)}$$

The expression for the reduced slenderness $\bar{\lambda}$ of the composite column for the bending plane under consideration is given by:

$$\bar{\lambda} = \sqrt{\frac{N_{Pl,R}}{N_{cr}}} \quad \text{(III.34)}$$

The determination of the critical elastic load N_{cr} for a composite column involves the utilization of Euler's formula:

$$N_{cr} = \frac{\pi^2 (EI)_e}{l_f^2} \quad \text{(III.35)}$$

When dealing with temporary loads, the effective elastic flexural stiffness $(El)_e$ of the cross-sectional area of a composite column can be calculated in the following manner:

$$(EI)_e = E_s I_s + 0,8 E_{cd} I_c \quad \text{(III.36)}$$

$$E_{cd} = \frac{E_{cm}}{\gamma_c} \quad \text{(III.37)}$$

The compressive axial load resistance capacity of a section is calculated by combining the plastic resistances of its constituent elements, according to the following formulas:

For sections encased with concrete:

$$N_{Pl,Rd} = A_{eff}\frac{f_y}{\gamma_{M1}} + 0,85A_c\frac{f_c}{\gamma_c} \quad \text{(III.38)}$$

For sections filled with concrete:

$$N_{Pl,Rd} = A_{eff}\frac{f_y}{\gamma_{M1}} + A_c\frac{f_c}{\gamma_c} \quad \text{(III.39)}$$

The effective cross-sectional areas of steel A_{eff} and concrete A_c are taken into account. The confinement effect of concrete within a hollow profile, regardless of its shape, results in an increase in its strength. This increase is considered by substituting the conventional value of $0,85f_c$ with f_c.

Table III.4 provides the European curves applicable to composite columns according to EN 1994-1-1 (Eurocode 4, 2004):

Table III.4. Buckling curves and member imperfections for composite columns.

Cross-section	Limits	Axis of Buckling	Buckling curve	Member imperfection
concrete encased section 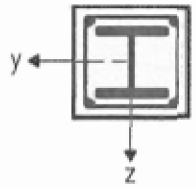		y-y	b	L/200
		z-z	c	L/150
partially concrete encased section 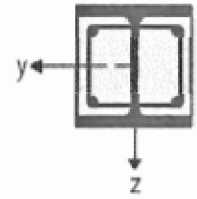		y-y	b	L/200
		z-z	c	L/150

circular and rectangular hollow steel section 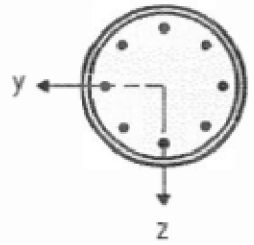	$\rho_s \leq 3\%$	any	a	L/300
	$3\% < \rho_s \leq 6\%$	any	b	L/200
circular hollow steel sections with additional I-section 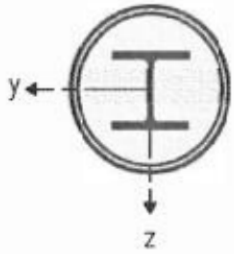		y-y	b	L/200
		z-z	b	L/200
partially concrete encased section with crossed I-sections 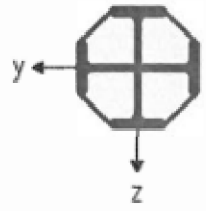		any	b	L/200

III.11 CONCLUSION

Calculation codes, among which the European code (Eurocode) is most frequently used, are utilized to comprehend the phenomenon of instability in cold-formed components. As is currently the case with most calculation systems for thin-walled CFS profiles, the calculation methodology for such profiles is based on the effective width theory. For cold-formed profiles in the Eurocode, the hot-rolled profile computation method is applied; nevertheless, this necessitates figuring out the effective section, which is not an easy task.

When designing, assembling, and using cold-formed posts, it is essential to consider these regulations appropriately to ensure their optimal performance and minimize the risks of failure

or instability. It is crucial to verify regulatory aspects to ensure that products and processes comply with current standards and laws. Numerical analysis and experimental testing are key assets in validating regulatory requirements.

CHAPTER IV

Numerical study of cold-formed steel built-up columns

IV.1 INTRODUCTION

This recent years, the use of finite element modeling has significantly increased, especially in representing cold-formed built-up columns, whether they are empty or filled with concrete. This surge in popularity can be attributed to the availability of commercial software like ABAQUS and ANSYS, along with various other computational codes. The finite element analysis method enables a direct modeling of the composite action between steel and concrete components. Furthermore, it allows for a more precise consideration of factors such as local and global imperfections, as well as boundary conditions.

The finite element analysis method is gaining popularity as it provides the opportunity to incorporate composite action, provided that a concrete, rational, and precise model describing the behavior of concrete under passive confinement is available.

This chapter presents a numerical modeling based on the finite element method, applying it specifically to cold-formed assembled elements, unfilled and concrete-filled. Each column consists of two C-profiles made of cold-formed steel, which come in different lengths and sections. The goal was once to spotlight the conduct and development of the outcomes obtained during our simulations.

IV.2 PRESENTATION OF THE ABAQUS COMPUTATIONAL CODE

ABAQUS is a versatile commercial computational code, distinguished by its broad range of applications spanning thermomechanics, acoustics, and fluid mechanics. We utilized version 6.14, which consists of three distinct modules that we briefly introduce below:

IV.2.1 ABAQUS CAE

This module is designed to define and visualize various simulations. At the beginning of the modeling process, problems are described using geometric entities, for which it is necessary to specify physical properties, as well as different calculation steps such as contacts, loads, initial conditions, and boundary conditions. The subsequent phase involves discretization, during which the various entities, according to their respective definitions, are meshed or not with the definition of elements. The final phase, facilitating the calculations, requires the synthesis of an analysis file that will be called upon by one of the two other calculation modules (STANDARD or EXPLICIT).

IV.2.2 ABAQUS STANDARD

This module embodies the implicit calculation code designed for quasi-static analyses, whether linear or non-linear, thermal, acoustic, and more. The calculation algorithm relies on iterations aimed at achieving the overall equilibrium of the system at each time increment.

IV.2.3 ABAQUS EXPLICIT

The explicit module is frequently employed for dynamic analyses. Unlike implicit code, the explicit algorithm is non-iterative. It relies on a large number of very short increments determined by the propagation speed of an elastic wave C_d. The concept of wave propagation has the advantage of limiting the resolution to the elements affected by the wave, resulting in efficiency compared to implicit code (which primarily solves the system at each increment). This characteristic grants it the ability to perform rapid calculations. Nevertheless, the explicit module faces two major challenges, namely, the stability of calculations and vibrational modes.

IV.2.4 Introduction to various types of elements in ABAQUS

Like any computational software, ABAQUS provides a variety of element types distinguished by their interpolation properties, symmetry, and physical characteristics. The software offers three-dimensional (3D) elements, two-dimensional (2D) elements, linear elements (1D), and connectors. The selection among these different dimensions depends on the nature of the problem to be simulated, allowing consideration of geometric symmetries, loads, boundary conditions, and material properties (Systemes, 2014).

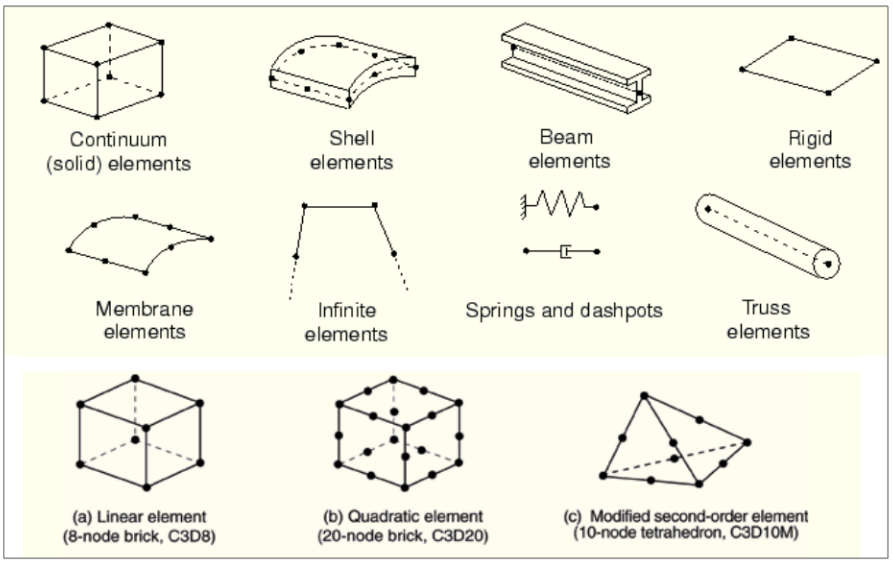

Figure IV.1. Different types of elements available in the ABAQUS library (Hibbitt et al., 2014).

IV.3 GEOMETRIC SPECIFICATIONS FOR BUILT-UP COLUMNS

Our research focuses on investigating the behavior of cold-formed built-up columns under varying slenderness conditions. We examine three configurations of assembled cold-formed columns. The first configuration involves a back-to-back arrangement (Figure IV.2.a), where two C-sections are joined at the web using double row flat-head rivets, with a transversal pitch of 35mm. However, the longitudinal pitch between the rivets is 50mm as illustrated in Figure IV.2.d. The second configuration features a face-to-face arrangement with connections made through conventional welding (Figure IV.2.b). The rivets utilized have a diameter of 6mm and are of nuance S235, possessing a tensile strength at rupture of 400MPa. In the box configuration, rivets are positioned in the upper and lower flanges at 50mm spacing in a single row (Figure IV.2.c). This configuration offers several advantages, including stiffening the flanges of the assembled element and eliminating the need for concrete formwork during pouring.

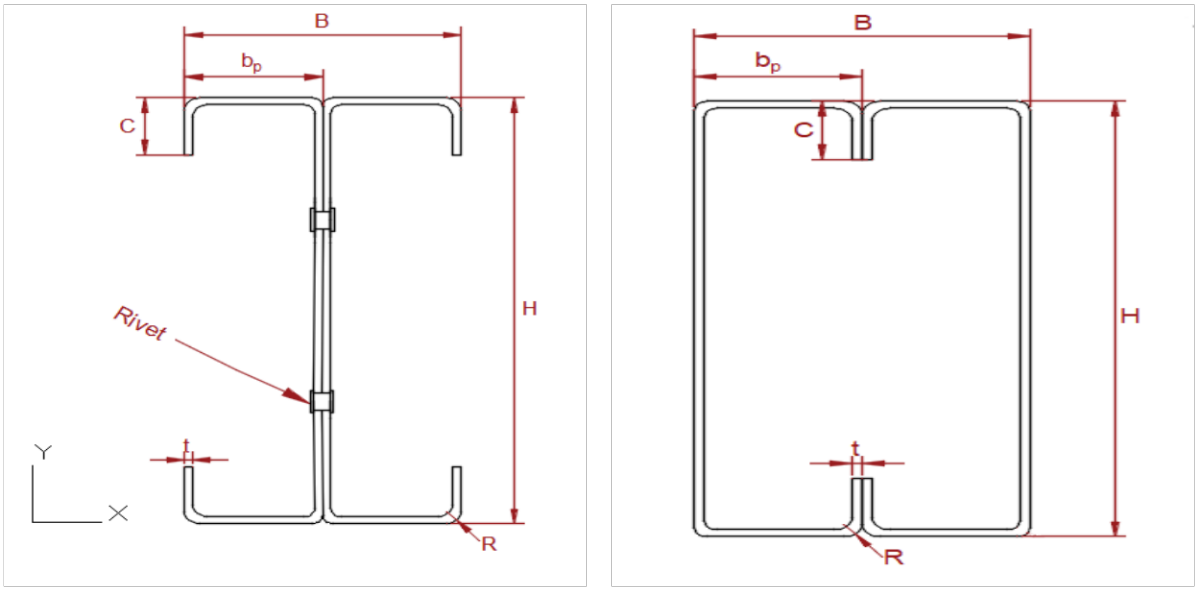

(a) (b)

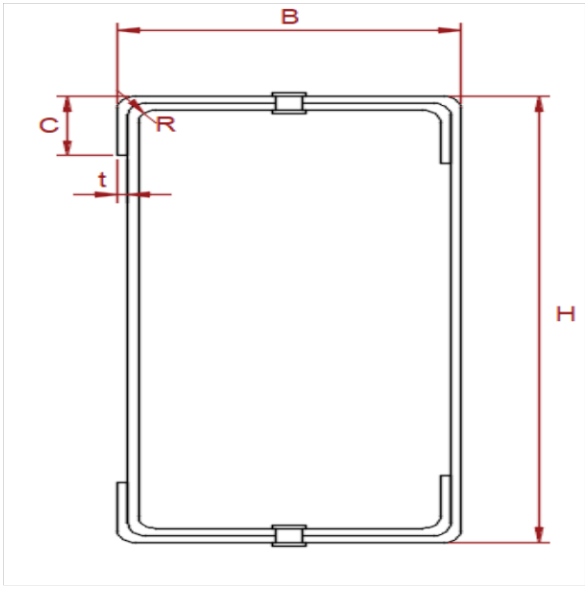

(c)

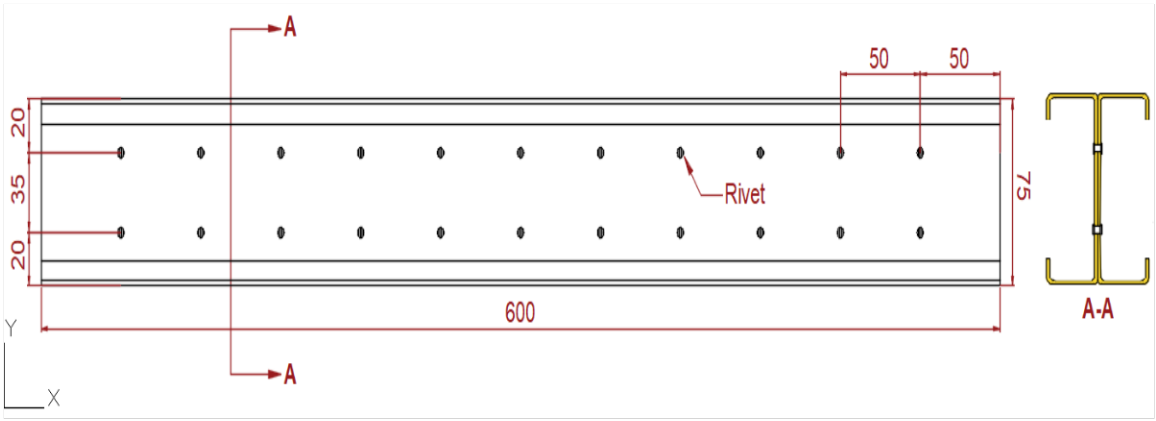

(d)

Figure IV.2. Cross-section of the studied models: (a) Back-to-back; (b) Face-to-face; (c) Box; (d) Longitudinal view of back-to-back model.

The three models depicted in Figure IV.2 are filled with concrete of strength class C25/30, as illustrated in Figure IV.3. The dimensions are selected in accordance with the regulations and constraints outlined in Eurocode 3 Part 1-3. All geometrical properties of both unfilled and concrete-filled models are detailed in Table IV.1.

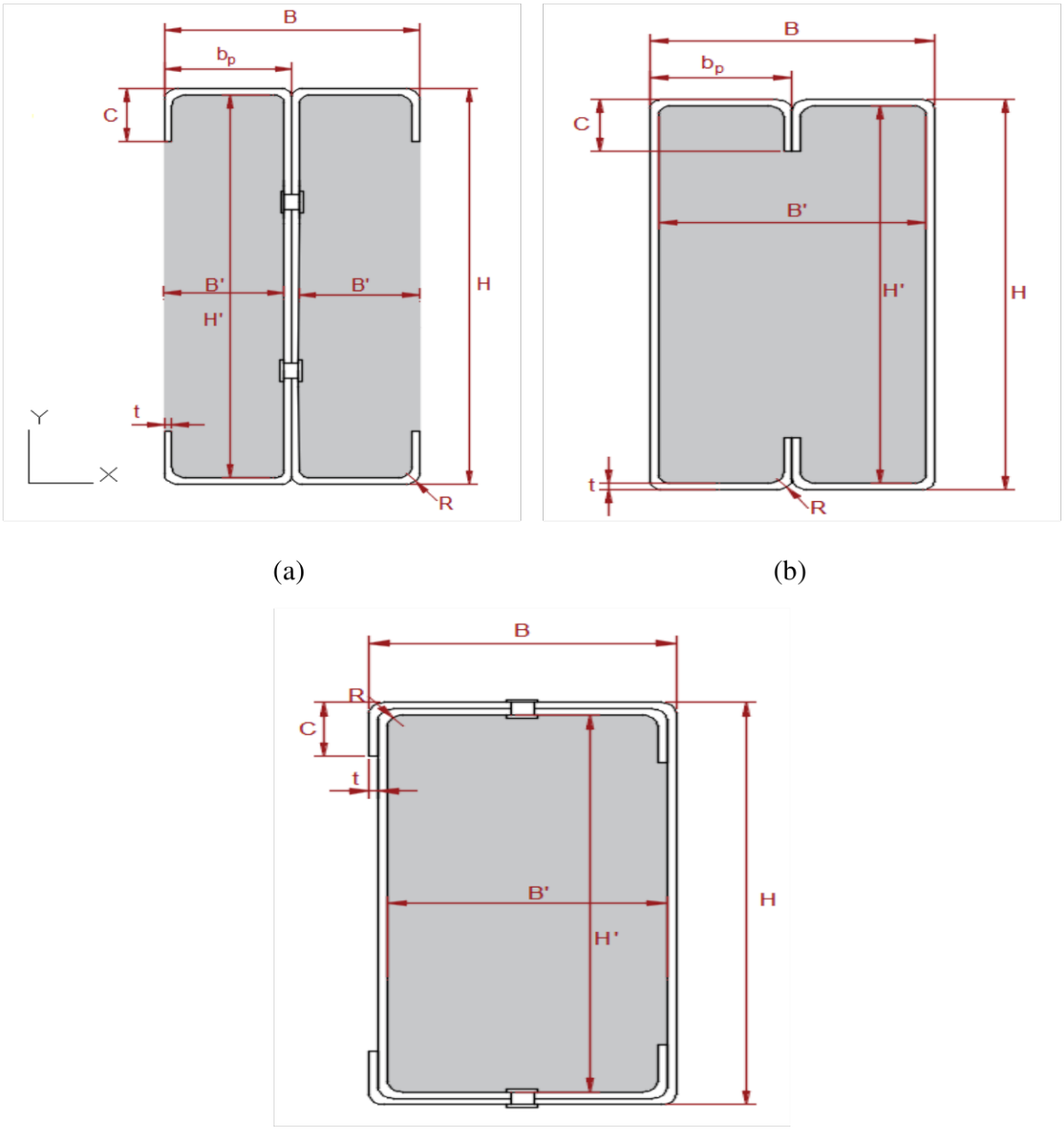

Figure IV.3. Cross-section of concrete-filled models: (a) Back-to-back partially encased with concrete; (b) Face-to-face filled with concrete; (c) Box filled with concrete.

Table IV.1. Geometrical properties of the studied cross-sections.

Sections	B (mm)	b_p (mm)	H (mm)	C (mm)	R (mm)	t (mm)	B' (mm)	H' (mm)
Back-to-back	40	20	75	10	2,1	1,2	18,8	72,6
Face-to-face	40	20	75	10	2,1	1,2	37,6	72,6
Box	40	-	75	10	2,1	1,2	36,4	70,2

IV.4 NUMERICAL STUDY OF BUILT-UP COLD-FORMED STEEL COLUMNS UNFILLED AND FILLED WITH CONCRETE

The finite element analysis principle entails dividing a structure into a finite number of elements with defined sizes and degrees of freedom (Anas et al., 2021; Morkhade et al., 2018). A nonlinear finite element analysis was carried out using ABAQUS software, which was selected due to its excellent handling of nonlinear issues (Hedayati and Vahedi, 2017; Kouider et al., 2021). This numerical simulation comprises several key steps, including model design, material behavior assignment, boundary conditions, interaction, load application, and mesh type selection (Hadidane et al., 2022). Figures IV.4 and IV.5, respectively, show numerical modeling of CFS columns with 1,2mm thickness and different configurations such as back-to-back, face-to-face, and box, both empty and concrete-filled. Taking into account variations in column lengths (600mm, 1200mm, 1800mm, and 2000mm), these columns are compressed.

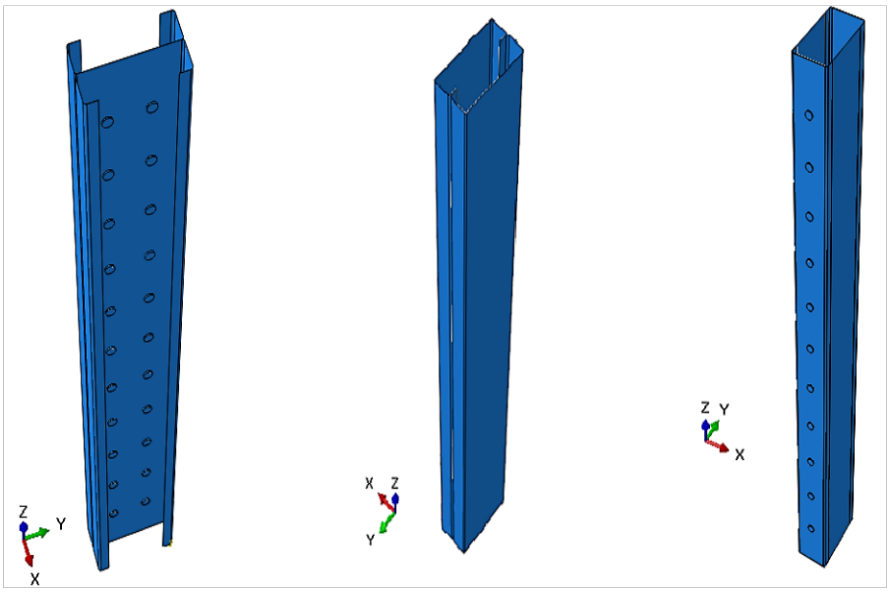

(a) (b) (c)

Figure IV.4. Numerical models of the empty C-columns: (a) Back-to-back; (b) Face-to-face; (c) Box.

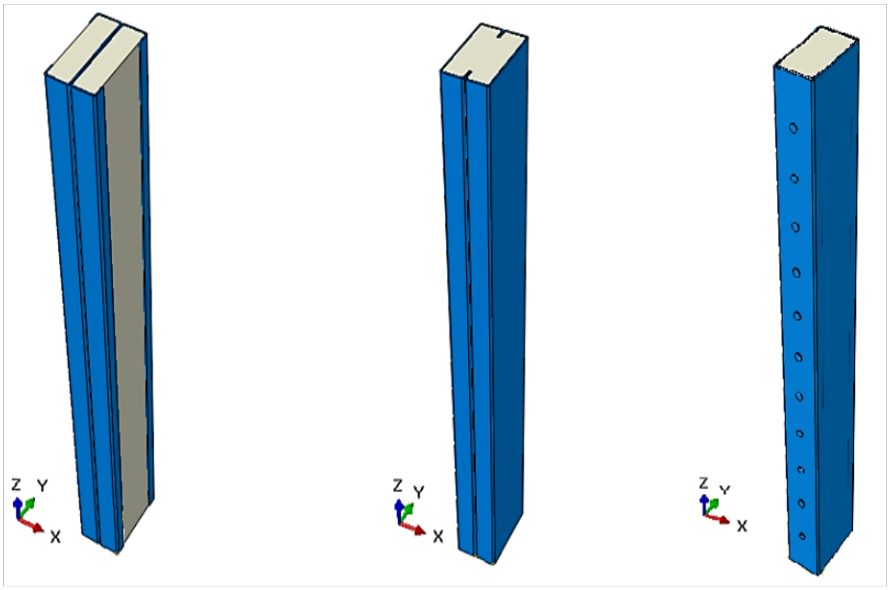

(a) (b) (c)

Figure IV.5. Numerical models of concrete-filled C-columns: (a) Back-to-back partially encased with concrete; (b) Face-to-face filled with concrete; (c) Box filled with concrete.

The steel utilized for the concept of the columns is CR250, demonstrating a perfectly elastic-plastic behavior, as illustrated in Figure IV.6, with ε_y is the yield strain of the steel and ε_u is the ultimate strain of the steel.

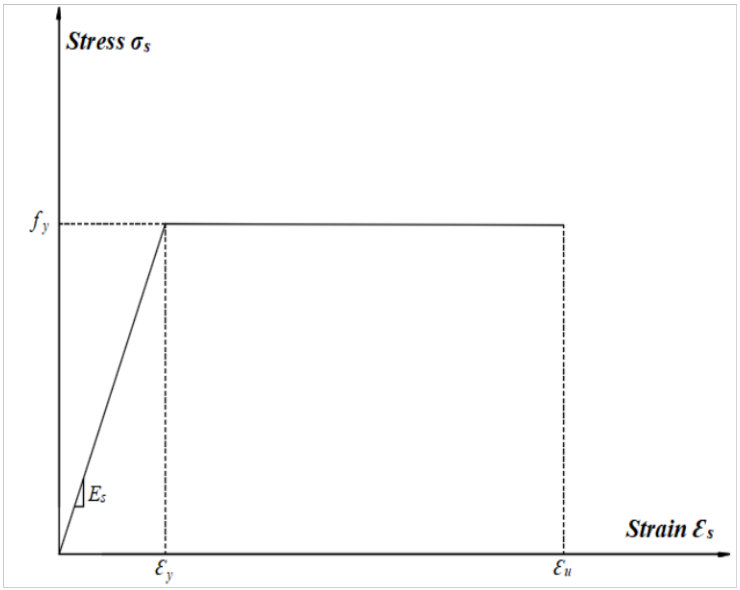

Figure IV.6. Stress-strain curve of the steel.

Table IV.2 provides a detailed overview of the mechanical properties of the materials under consideration, specifically concrete and steel. In this table, the symbols f_y and f_u represent the

yield and tensile strengths of the steel, while f_c denotes the compressive strength of the concrete. EN 1993-1-3 (European Committee for Standardization, 2006) states that the steel grade is established using the rules found in it. Conversely, EN 1994-1-1 (Eurocode 4, 2004) recommendations are where the concrete's strength class (C25/30) is derived.

Table IV.2. Mechanical properties of the elements used.

Element	Density ρ (kg/m^3)	Elastic modulus E (MPa)	Poisson's ratio ν	Yield strength f_y (MPa)	Tensile strength f_u (MPa)	Compressive strength f_c (MPa)
Steel	7850	210000	0,3	250	330	-
Concrete	2400	23500	0,2	-	-	25

IV.5 BOUNDARY CONDITIONS AND LOADING

The boundary conditions and loading for the columns under study are depicted in Figure IV.7. It can be observed that the upper rigid plate, in contact with the top of the column, has been fixed in two translation directions (U_x and U_y). Conversely, the bottom rigid plate, which touches the end of the column, has been fixed in three translation directions (U_x, U_y, and U_z). This specific arrangement allows for the U_z direction to remain unfixed, thereby facilitating the application of a 10mm imposed displacement.

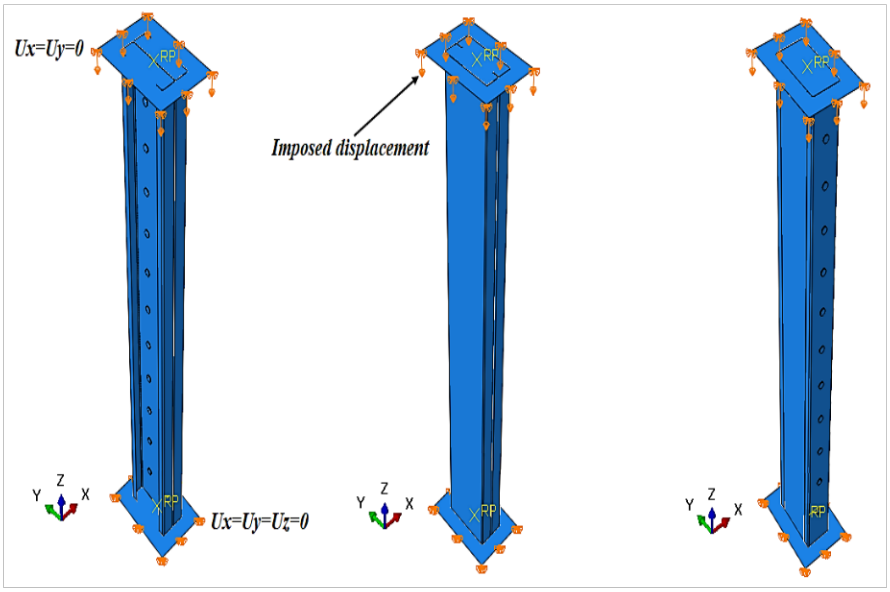

Figure IV.7. Loading and boundary conditions of the columns.

IV.6 MESHING AND INTERACTION CONTACT

Contact interaction delineates the pressure, adhesion (normal), and friction (tangential) stresses arising from the contact between deformable objects at shared points or surfaces. In our study, we employed a surface-to-surface interface contact approach to investigate this phenomenon. In Figure IV.8.a, we observed that the interaction between the C-columns and the rivets involved the use of the friction option, with a penalty value of 0.3 for tangential behavior and "hard contact" for normal behavior. Conversely, in the case of the steel-concrete interaction (Figure IV.8.b), we utilized friction with a penalty value of 0,25 for tangential behavior (Ellobody and Young, 2006), while maintaining "hard contact" for normal behavior. To facilitate the interaction between the rigid plates and the ends and tops of the columns (Figure IV.8.c), we employed the 'Tie' option. Additionally, for the interaction between the rigid plates and the concrete at both ends (Figure IV.8.d), we specified 'Rough' for tangential behavior and 'hard contact' for normal behavior (Dai and Lam, 2010).

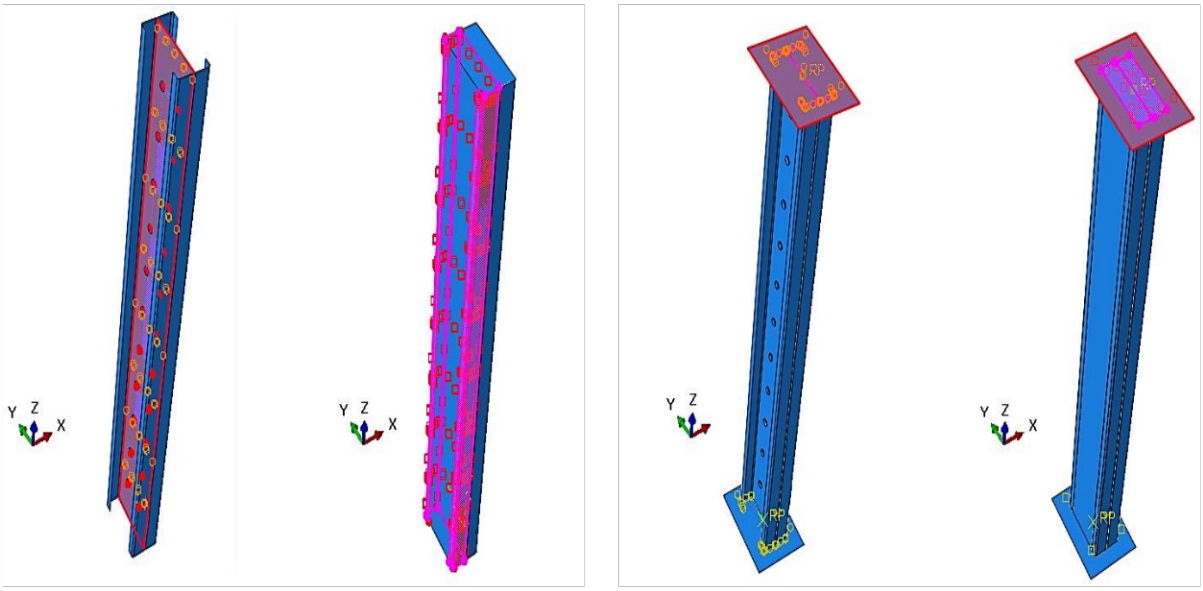

(a) (b) (c) (d)

Figure IV.8. Interaction contact of the studied models: (a) C-profiles-rivets interaction; (b) Steel-concrete interaction; (c) Plate-steel interaction; (d) Plate-concrete interaction.

In relation to the finite element meshing of the models (Figure IV.9), an R3D4 mesh type was employed for the rigid plates. According to the ABAQUS library (Duval et al., 2014), this mesh consists of a 4-node 3D bilinear brittle quadrilateral element. The choice was made to utilize the 8-node linear brick solid element type C3D8R for the columns and concrete, providing three

degrees of freedom at each node. Furthermore, the rivets were modeled using the C3D10 element type, a 10-node quadratic tetrahedron. We carried out a sensitivity evaluation to discover the perfect mesh measurement for acquiring convergence to a correct solution. The chosen mesh sizes were 1mm for the rivets and 10mm for the other components, including cold-formed columns, concrete, and plates.

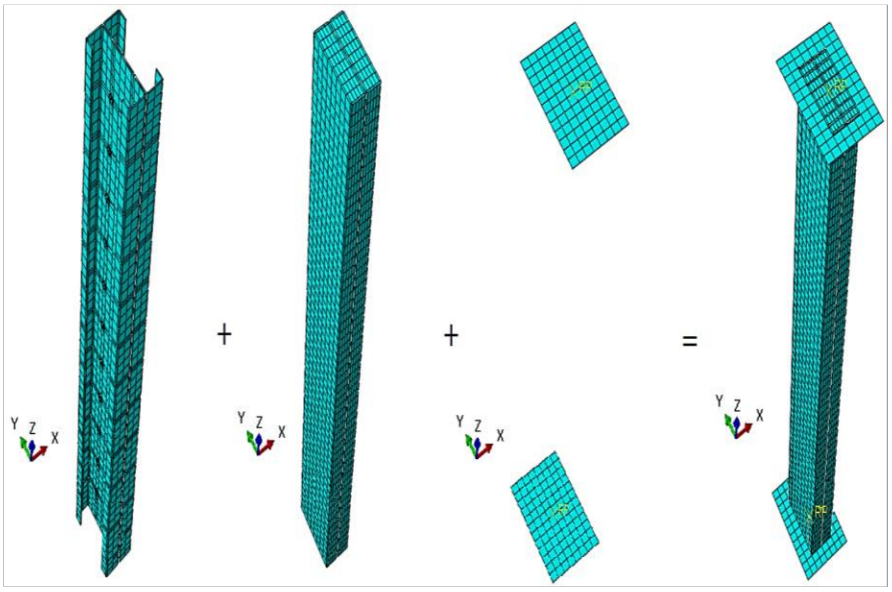

Figure IV.9. Meshing of the assembled C-section columns.

IV.7 FAILURE MODES OF COLD-FORMED STEEL ASSEMBLED COLUMNS

The importance of distortional buckling is on the rise, and the analysis of local buckling is becoming more complicated due to the increasing complexity of cold-formed steel section shapes. Sectional buckling modes, which encompass local and distortional buckling, have the potential to interact with global buckling and with one another.

Figure IV.10 illustrates the failure modes of cold-formed steel unfilled back-to-back C-columns at various lengths (600mm, 1200mm, 1800mm, and 2000mm). It is worth noting that all columns undergo local buckling due to their relatively thin thickness, manifested by rotational deformation without translation along the internal bending lines.

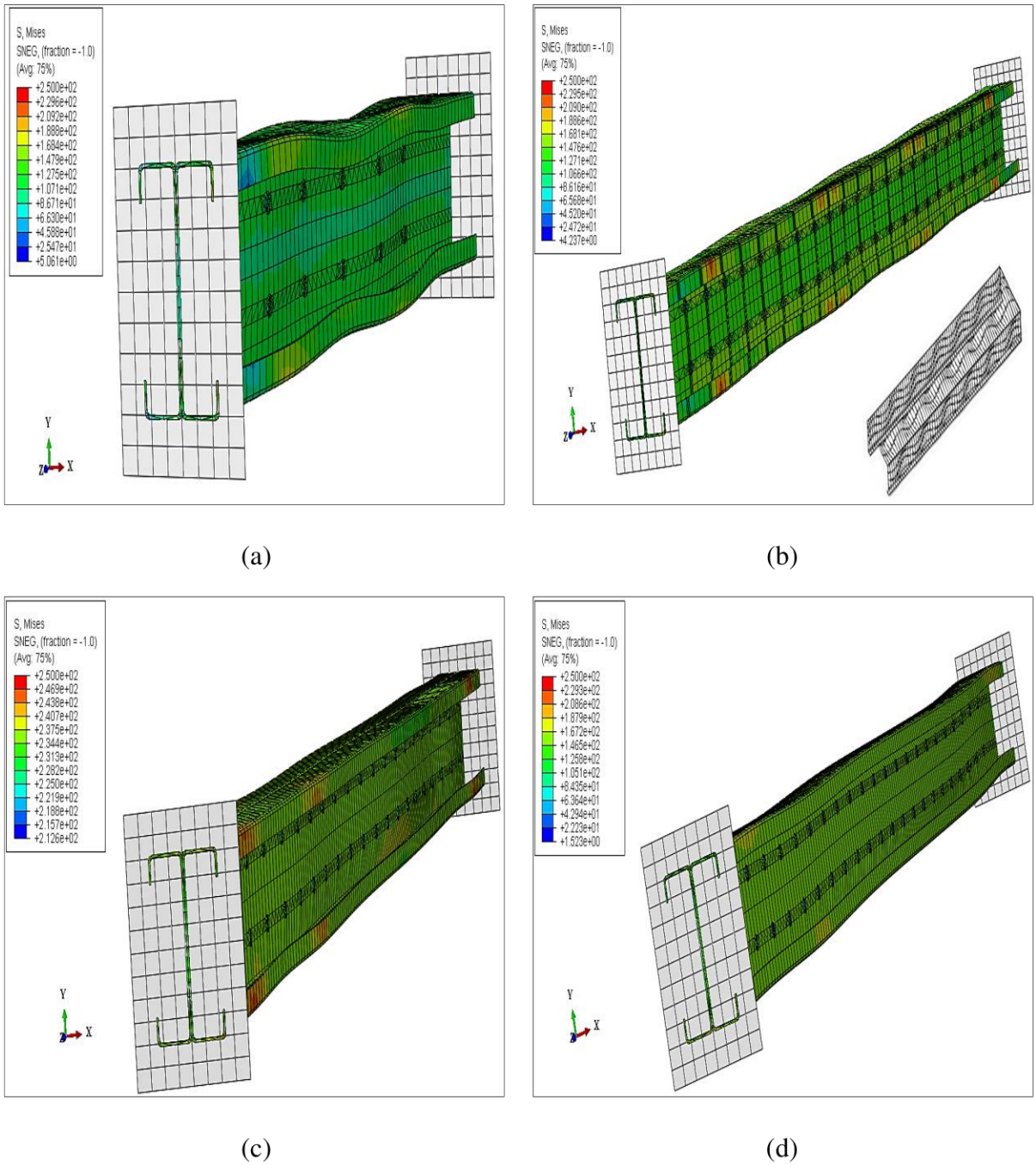

Figure IV.10. Failure modes of back-to-back empty columns with different lengths: (a) L=600mm; (b) L=1200mm; (c) L=1800mm; (d) L=2000mm.

The failure mode observed in the cold-formed steel back-to-back assembled C-columns, which were partially encased with concrete at different lengths, demonstrates distinct behavior depending on the column size. The 600mm and 1200mm columns exhibit a failure mode characterized by distortional behavior and disbonding between the steel and concrete contact surfaces. This is further illustrated by the buckling of the flanges towards the exterior, as

depicted in Figures IV.11.a and IV.11.b. Conversely, the 1800mm and 2000mm columns display buckling indicative of global instability, as shown in Figures IV.11.c and IV.11.d.

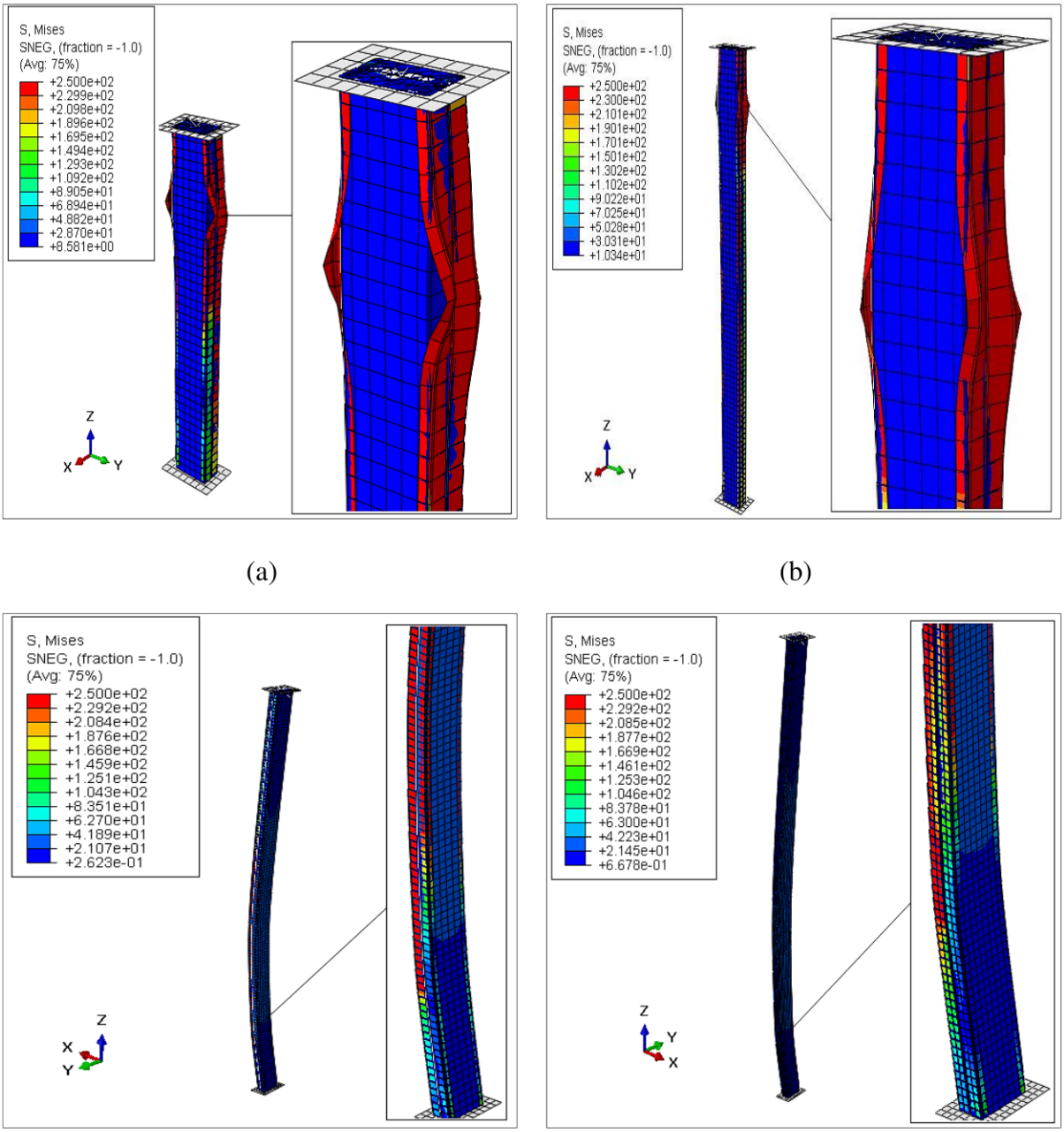

Figure IV.11. Failure modes of back-to-back partially encased with concrete columns at various lengths: (a) L=600mm; (b) L=1200mm; (c) L=1800mm; (d) L=2000mm.

Compressive deformations don't always play a decisive role in vertical structural elements. On the other hand, buckling is a form of instability specific to slender compressed elements, occurring at a certain load and depending on the relationship between the cross-section and

length of the element in consideration. While studying the failure modes of face-to-face unfilled built-up columns with various lengths, we observed a local buckling instability for the columns with 600mm, 1200mm, and 1800mm in length (Figures IV.12.a, IV.12.b, and IV.12.c). Whereas a global and local buckling were noticed for the column with a length of 2000mm (Figure IV.12.d).

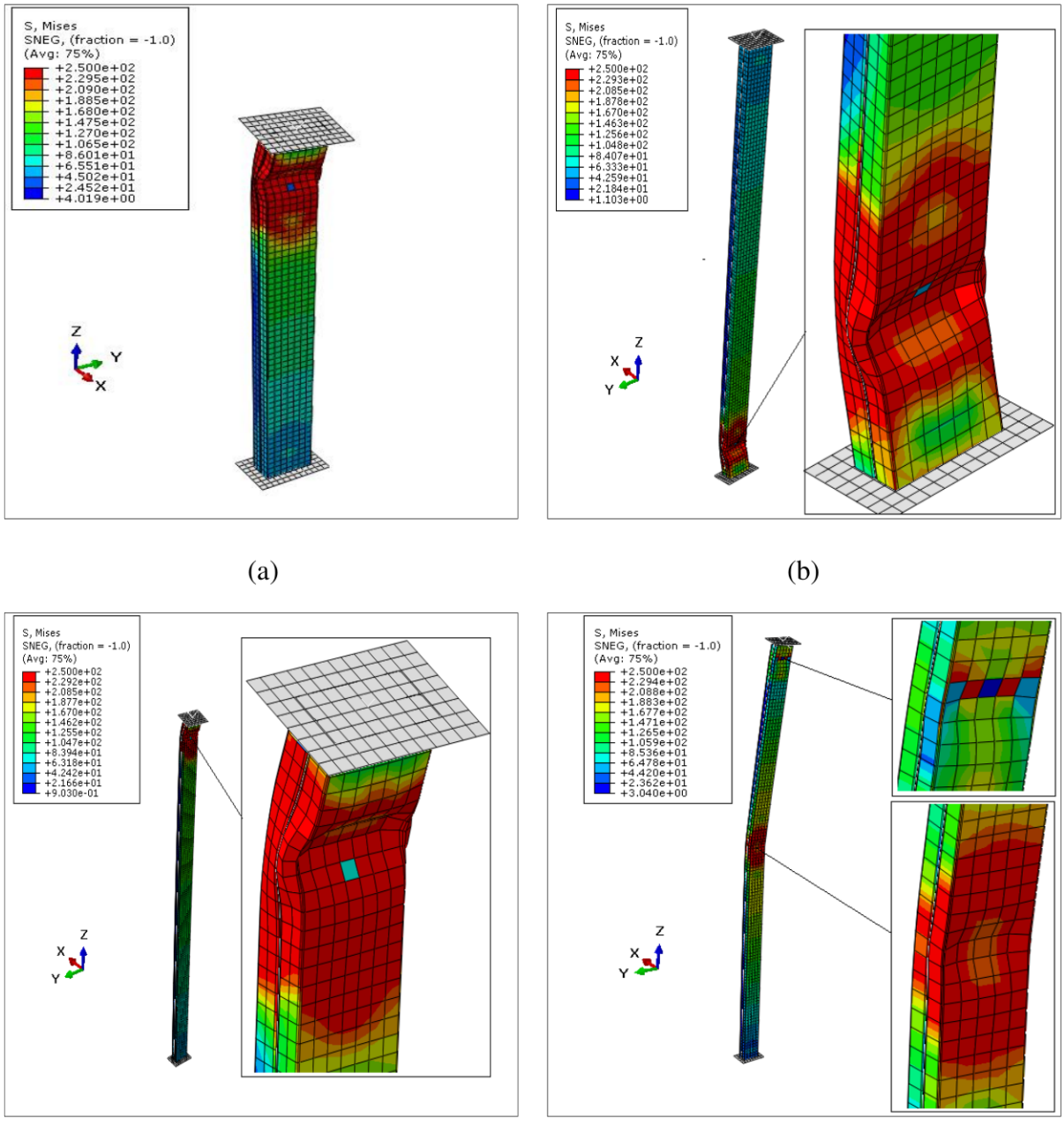

Figure IV.12. Failure modes of face-to-face unfilled columns with different lengths: (a) L=600mm; (b) L=1200mm; (c) L=1800mm; (d) L=2000mm.

The face-to-face C-profile configuration offers significant advantages, particularly with the addition of concrete. Figure IV.13 illustrates the failure modes of face-to-face concrete-filled built-up columns with varying lengths (600mm, 1200mm, 1800mm, and 2000mm). Columns measuring 600mm, 1200mm, and 1800mm in length exhibit local buckling instability (Figures IV.13.a, IV.13.b, and IV.13.c), while those with length 2000mm fail due to global and local instability (Figure IV.13.d). In practical application, this configuration eliminates the need for formwork and ensures the complete containment of concrete, safeguarding its external surface against external forces or aggression.

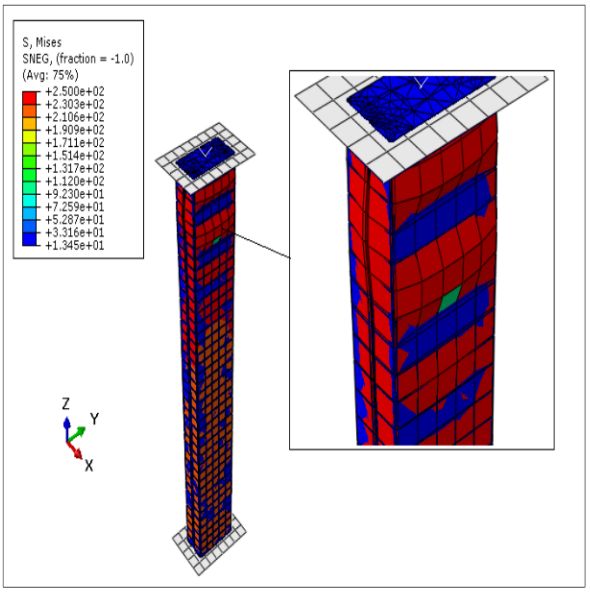

(a)

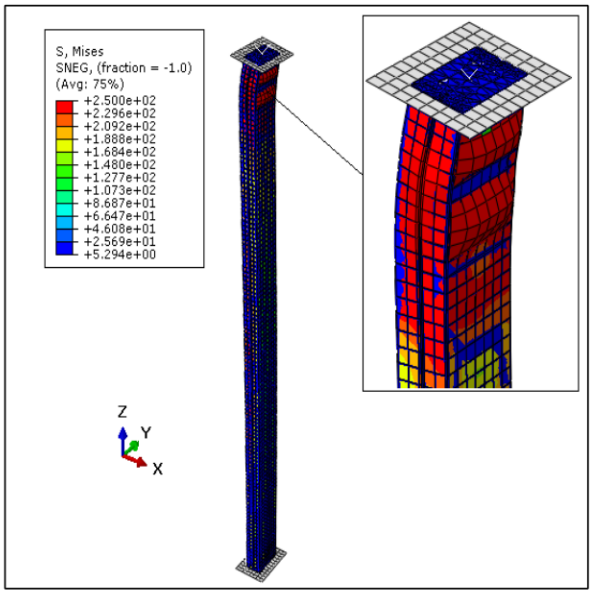

(b)

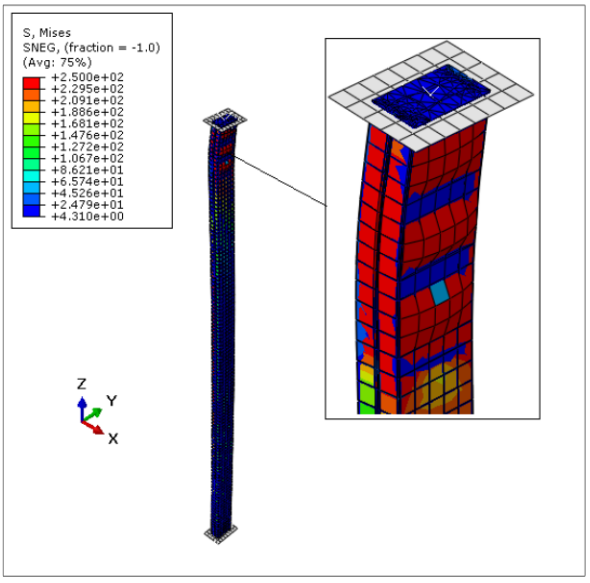

(c)

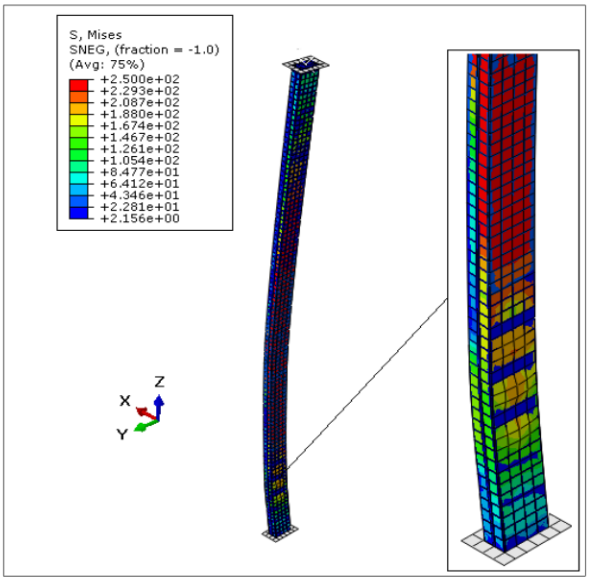

(d)

Figure IV.13. Failure modes of face-to-face concrete-filled columns at various lengths: (a) L=600mm; (b) L=1200mm; (c) L=1800mm; (d) L=2000mm.

We observe from the failure modes of built-up C-section box unfilled columns with different lengths, that the columns with 600mm, 1200mm, and 1800mm in length indicates a local buckling instability in the bottom of the column (Figures IV.14.a, IV.14.b, and IV.14.c). Meanwhile, the column of 2000mm showed a global buckling (Figure IV.14.d).

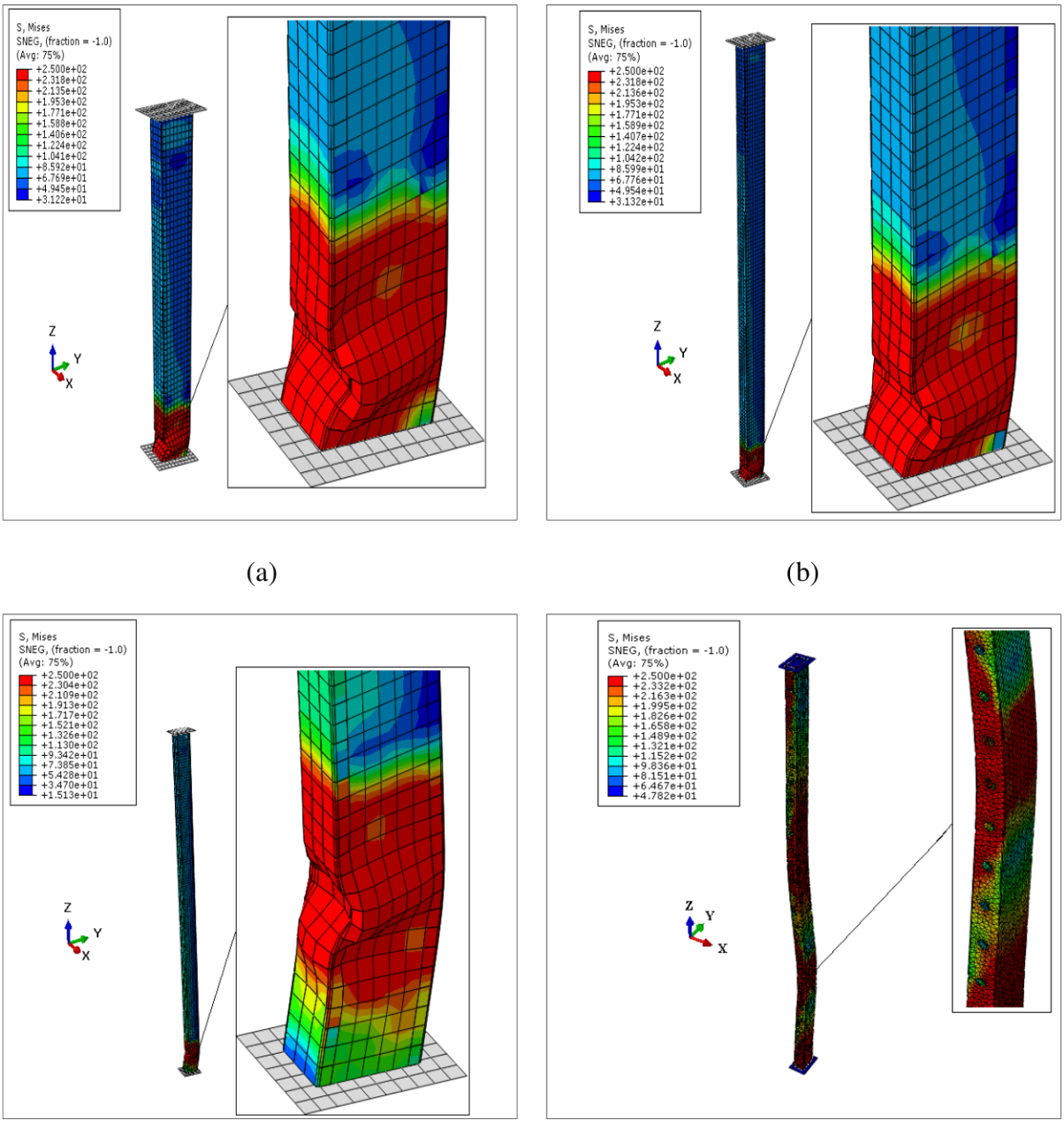

Figure IV.14. Failure modes of box C-section columns unfilled with concrete including different lengths: (a) L=600mm; (b) L=1200mm; (c) L=1800mm; (d) L=2000mm.

As for the failure modes of built-up C-section box filled with concrete columns with different lengths, the columns measuring 600mm, 1200mm, and 1800mm in length failed by local and global buckling (Figures IV.15.a and IV.15.b), and global buckling (Figure IV.15.c) respectively. There is an improvement in the failure mode of the concrete-filled box model with a length of 2000mm (Figure IV.15.d) compared to the unfilled one, which exhibited global buckling instability (Figure IV.14.d).

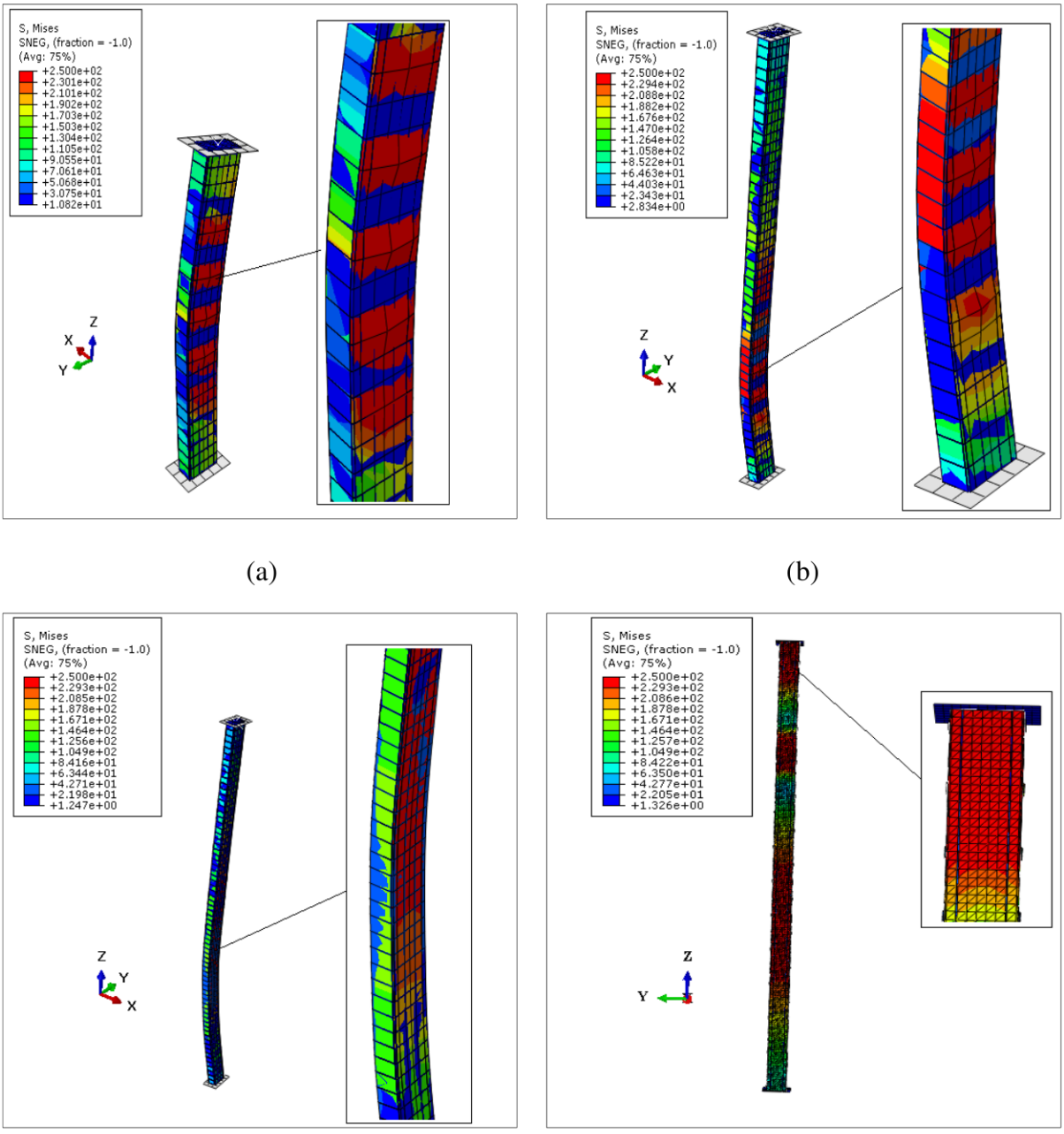

Figure IV.15. Failure modes of box C-section columns filled with concrete including various lengths: (a) L=600mm; (b) L=1200mm; (c) L=1800mm; (d) L=2000mm.

IV.8 RESULTS AND DISCUSSIONS OF THE STUDIED MODELS

The understanding of the fundamental behavior of cold-formed structural assembled elements remains somewhat limited, and assessing their stability presents a challenging task. Our investigation focuses on the load-strain state in the center of the unfilled back-to-back built-up columns at varying slenderness ratios. Our findings suggest that columns measuring 600mm, 1200mm, and 2000mm exhibit similar elastic responses up to a load of 80kN. However, beyond this threshold, plastic deformation becomes apparent, leading to elastic instabilities as corroborated by various studies, including those conducted by Krishanu Roy et al. (Roy et al., 2018). Notably, the 1800mm column exhibits negative compression deformations up to an 80kN load, while the 1200mm length column demonstrates a maximum plastic deformation of approximately $5{,}03\times10^{-3}$ (Figure IV.16.a).

In the face-to-face built-up model scenario, examination of the load-strain state at the midpoint demonstrates that the introduction of additional length can induce instability during the initial elastic phase. This emphasizes how the importance of explicitly addressing both local and global buckling effects (Beulah Gnana Ananthi and Ashvini, 2019). The shorter model exhibited a stiffness profile marked by significant plastic deformation, approximately $87{,}88\times10^{-3}$, indicative of steel yielding behavior (Figure IV.16.b).

The load-strain behavior within the box columns' midpoint, depicted in Figure IV.16.c, displays consistent linear responses across various slenderness ratios. However, a significant transition to plastic deformation, approximately $18{,}04\times10^{-3}$ in magnitude, is evident in the 1200mm length column, mirroring the behavior observed in the back-to-back built-up columns. Interestingly, a substantial 72,12% reduction in deformation is observed in the back-to-back model compared to the box model. Furthermore, it is noteworthy that the box columns exhibit a 30% increase in failure load compared to both the back-to-back and face-to-face models.

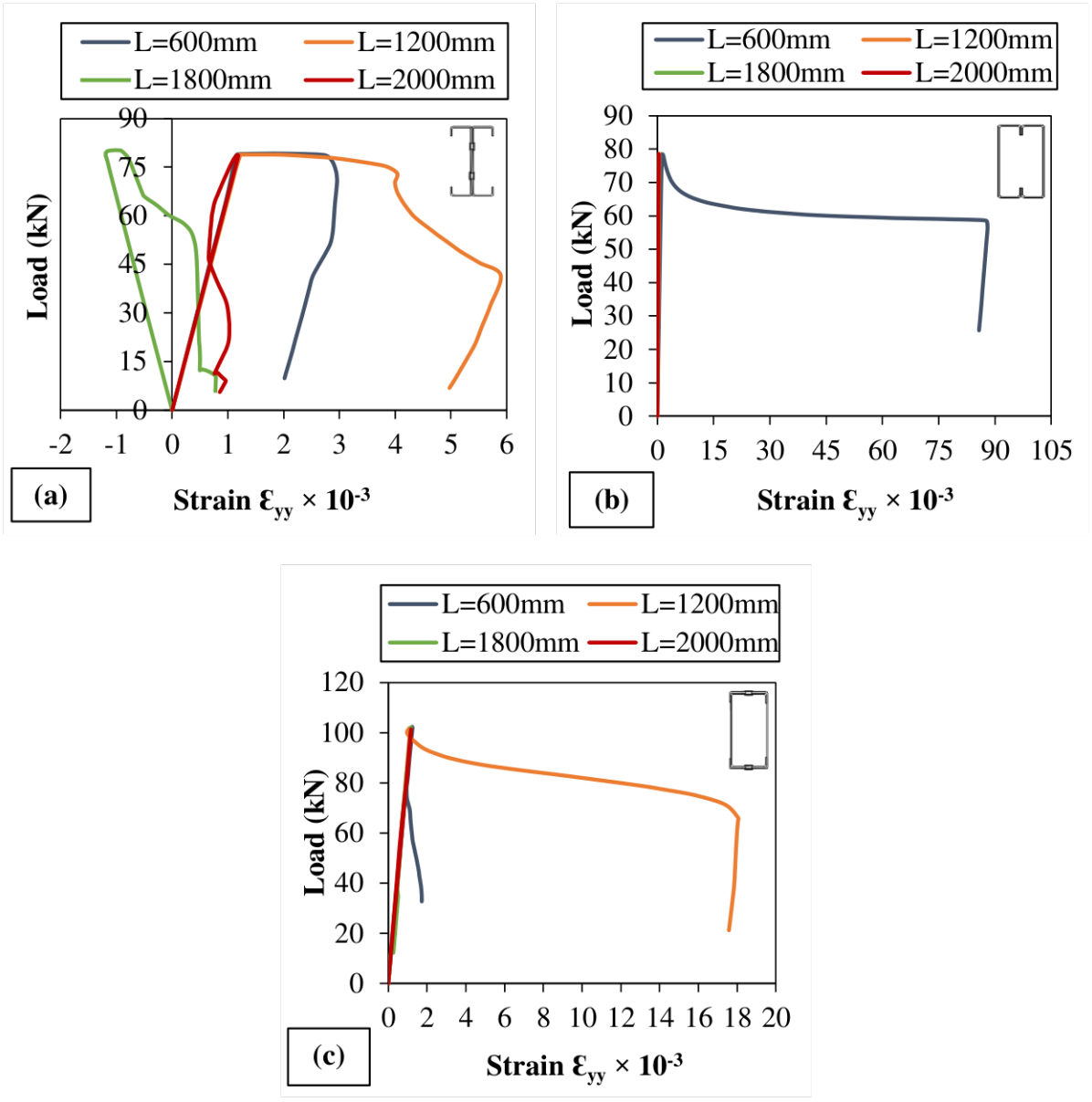

Figure IV.16. Load-strain curves of the assembled cold-formed steel unfilled columns: (a) Back-to-back; (b) Face-to-face; (c) Box.

When examining the columns post-concrete filling, particularly focusing on the load-strain behavior at the midsection of the cold-formed columns connected in a back-to-back configuration at varying lengths (Figure IV.17.a), a notable decrease in deformations was noted. This reduction was coupled with a twofold increase in strength compared to the unfilled model under a load of P=152kN. This improvement in performance can be credited to the synergistic interaction between the concrete core, confined by the outer shells, resulting in heightened stiffness and strength (Rahnavard et al., 2022b; Zeghiche and Chaoui, 2005).

We observe that the behavior in the central region of the column, whether in a face-to-face configuration, filled or unfilled, exhibits a moderate influence that remains within a 40% range. This is apparent from the similarity in the shapes of the load-strain curves in both scenarios, as illustrated in Figures IV.16.b and IV.17.b. Depending on the slenderness, the columns demonstrate instability characterized by outward local buckling in the web portion. The face-to-face model demonstrates a 19% increase in plasticity bearing compared to the back-to-back model, as shown in Figure IV.17.b.

When in contrast to the different configurations—namely, back-to-back and face-to-face—filled with concrete box configuration model shows a 16% increase in rigidity. Interestingly, among columns with different lengths, the ones that are 600mm, 1200mm, and 1800mm show elastoplastic behavior first, then instabilities. By comparison, the column with a length of 2000mm removes instability at the initial elasticity level (Figure IV.17.c).

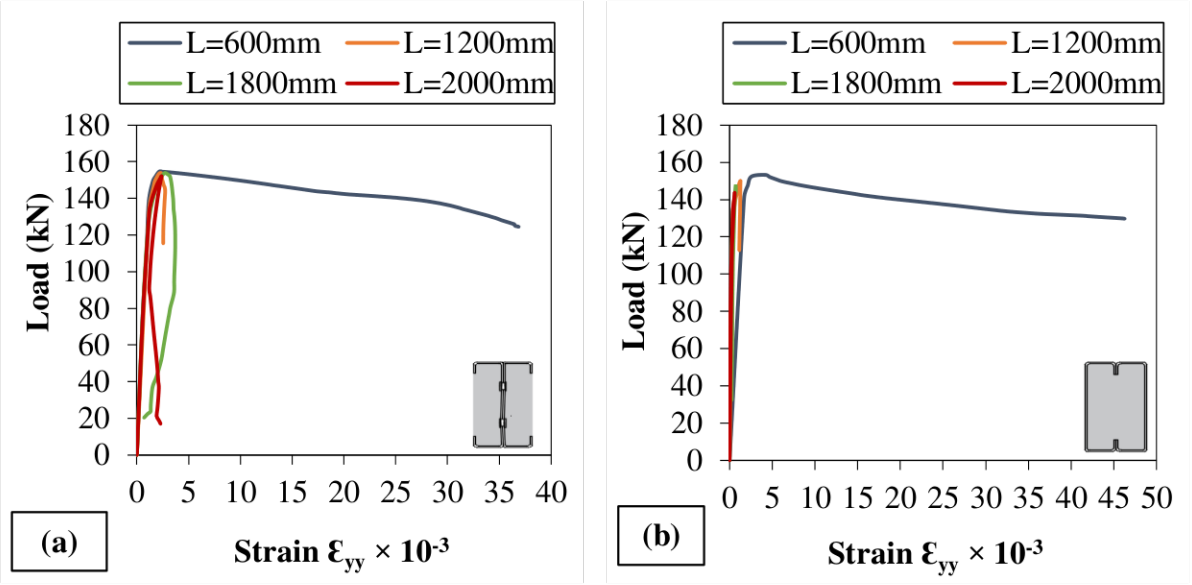

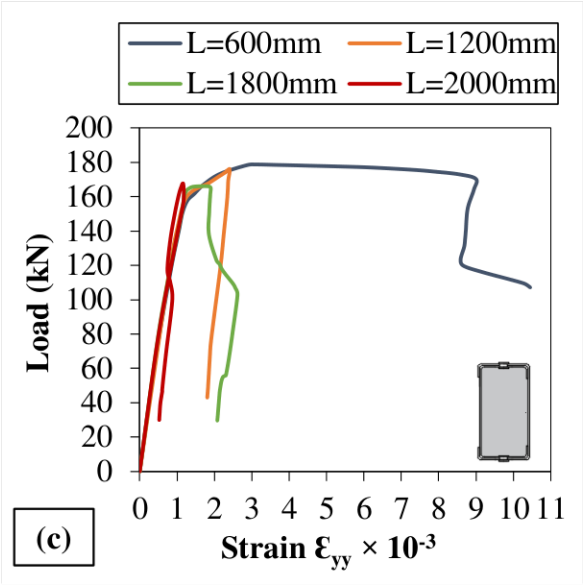

Figure IV.17. Load-strain curves of the assembled cold-formed steel concrete-filled columns: (a) Back-to-back partially encased with concrete; (b) Face-to-face filled with concrete; (c) Box filled with concrete.

The columns display distinct behaviors based on their slenderness, with high-slenderness columns prone to buckling within the elastic range, while those with intermediate slenderness are notably susceptible to imperfections. Upon conducting a comparative analysis of cold-formed built-up columns in various 2000mm length configurations, it becomes apparent that these models undergo elastic instabilities. In the case of unfilled columns (Figure IV.18.a), the maximum lateral displacement occurs at the mid-length (1000mm), resulting in global buckling in the face-to-face configuration and at 550mm in the box configuration. Meanwhile, the back-to-back configuration columns experience local buckling at lengths of 450mm and 1200mm.

In contrast, columns that are filled with concrete (Figure IV.18.b) demonstrate varying characteristics. Global buckling takes place at 800mm for face-to-face columns subjected to positive displacement (tension) and back-to-back columns experiencing negative displacement (compression). Yet as Figure IV.15.d makes abundantly evident, the addition of concrete to the box configuration results in a notable improvement that substantially reduces lateral displacement (a reduction of roughly 92% compared to the unfilled model). In addition, the face-to-face arrangement of the concrete-filled model exhibits a decrease of 28,37% in lateral displacement in comparison to the empty model.

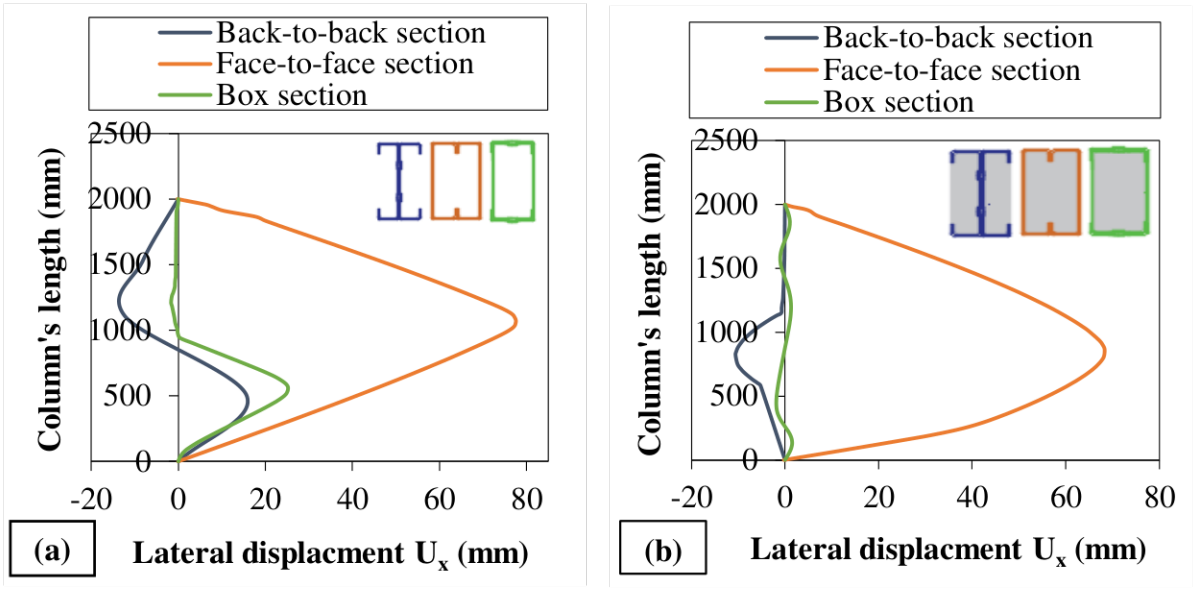

Figure IV.18. Lateral displacement U_x according to the column's length: (a) Unfilled with concrete; (b) Filled with concrete.

Table IV.3 summarizes all the analytical results based on EN 1993-1-3 and EN 1994-1-1, alongside the numerical results for both unfilled and concrete-filled steel columns, including their instability modes. The results showed very good agreement, with a slight difference of no more than 8%. This slight variance is primarily attributable to the consideration of interaction effects between surfaces within the numerical simulations. The ultimate loads in the face-to-face and back-to-back models are very similar, while the ultimate loads in the box model show a significant increase of around 16% for the concrete-filled model and 30% for the unfilled one.

Table IV.3. Comparison between analytical and numerical results of the studied models.

Column	Length (mm)	Unfilled				Concrete-filled			
		Analytical load (kN)	Numerical load (kN)	Discrepancy (%)	Failure mode	Analytical load (kN)	Numerical load (kN)	Discrepancy (%)	Failure mode
Back-to-back	600	76,86	79,24	3	Local buckling	148,42	154,61	4	Distortional instability + disbonding between the contact surfaces of steel and concrete
	1200	75,72	78,88	4	Local buckling	144,64	153,87	6	Distortional instability +

									disbonding between the contact surfaces of steel and concrete
	1800	75,42	80,24	6	Local buckling	143,90	153,90	6,5	Overall buckling
	2000	73,20	78,71	7	Local buckling	141,55	152,20	7	Overall buckling
Face-to-face	600	74,15	78,51	5,5	Local buckling	150,16	153,23	2	Local buckling
	1200	73,87	78,59	6	Local buckling	144,12	150,12	4	Local buckling
	1800	73,31	78,41	6,5	Local buckling	140,39	147,78	5	Local buckling
	2000	72,59	78,48	7,5	Overall + local buckling	135,11	143,73	6	Overall + local buckling
Box	600	98,20	102,29	4	Local buckling	173,37	178,73	3	Local + overall buckling
	1200	96,84	101,94	5	Local buckling	167,47	176,29	5	Local + overall buckling
	1800	95,94	102,07	6	Local buckling	154,43	166,05	7	Overall buckling
	2000	94,35	101,45	7	Overall buckling	154,65	167,73	7,80	-

Figure IV.19 illustrates a comparative analysis of both analytical and numerical findings through graphical histograms, focusing on unfilled and concrete-filled cold-formed columns of varying lengths and configurations: back-to-back (Figure IV.19.a), face-to-face (Figure IV.19.b), and box (Figure IV.19.c). The data reveal a significant correlation between the analytical and numerical results across different lengths for both types of columns, with discrepancies remaining minimal, not exceeding 8%. The critical load for the back-to-back (Figure IV.19.a) and face-to-face (Figure IV.19.b) configurations of unfilled columns is found to be closely aligned with that of the box configuration (Figure IV.19.c), which exhibits an

increase of approximately 30% due to the enhanced stiffness provided by the flanges, thereby significantly contributing to the overall resistance. In contrast, concrete-filled columns demonstrate nearly double the ultimate load compared to their unfilled counterparts, reflecting a 48% increase. This enhancement is primarily attributed to the synergistic interaction between steel and concrete, which improves confinement effects and, consequently, the strength and rigidity of the columns.

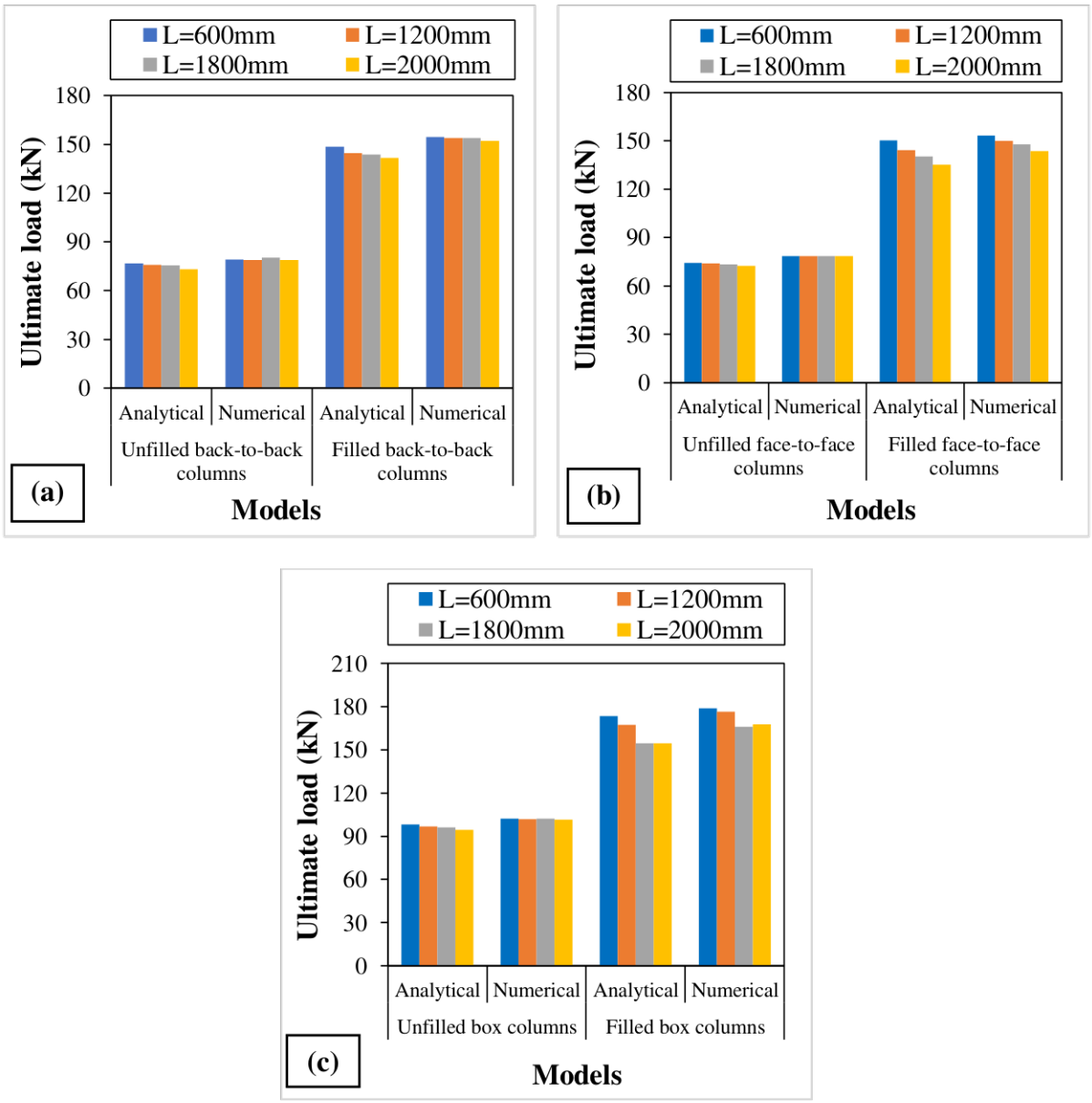

Figure IV.19. Comparison between analytical and numerical results of the studied models at different lengths: (a) Back-to-back; (b) Face-to-face; (c) Box.

IV.9 CONCLUSION

The numerical study of cold-formed built-up columns represents a valuable tool for evaluating their structural behavior under various loads and conditions. Through the use of specialized software such as ABAQUS, finite element models provide an in-depth analysis of the mechanical performance and stress resistance of cold-formed assembled columns. This approach enables a detailed understanding of deformation modes, critical stresses, and potential failure areas, facilitating the optimization of design and enhancement of structural safety.

Validating numerical results through experiments is essential to ensure the credibility and real-world applicability of models. The integration of simulation and experimentation forms a vital component of research and technological development, leading to significant advancements across multiple domains.

CHAPTER V

Experimental study and validation

V.1 INTRODUCTION

The necessity to fortify metal constructions arises as a result of their intensive or prolonged incorrect utilization, which leads to dysfunctions at various levels. This encompasses chemical attacks on steels, such as corrosion, which considerably diminishes the load-bearing capacity of elements and joints in metal structures in general. Depending on the shape of the reinforced element's section, assembly conditions, and the type of loading before and after reinforcement. To simulate all these uncertainties, an experimental approach has been undertaken.

Experimental tests are controlled experiments aimed at testing a hypothesis or verifying the validity of a theory. These tests are frequently conducted under controlled conditions to isolate relevant variables and minimize disruptive factors. Typically, an experimental trial follows a specific protocol that includes formulating the hypothesis to be tested, designing the experiment, collecting data, statistically analyzing the results, and formulating conclusions. The goal is to generate precise and reproducible results that can contribute to the advancement of knowledge in a specific field.

This chapter presents a research study conducted at the Civil Engineering Laboratory of Badji Mokhtar University in Annaba. The primary aim of this study was to evaluate the effectiveness of cold-formed C-section profiles in different arrangements, such as back-to-back, face-to-face, and box configurations.

V.2 DESCRIPTION AND SPECIFICATIONS OF SPECIMENS

A compression test protocol was developed to assess the strength of built-up cold-formed steel columns unfilled and filled with concrete. For the back-to-back model, we used two rows of rivets, each row consisting of 4 rivets with a diameter of 4mm (Figures V.1.b and V.1.d). In the box-section model, we employed a single row of 4 rivets with a diameter of 4mm in both the top and bottom flanges (Figure V.1.a). The face-to-face configuration was achieved by connecting the profiles with standard electric arc welds, using 4 weld beads, each 1,5cm wide (Figure V.1.c).

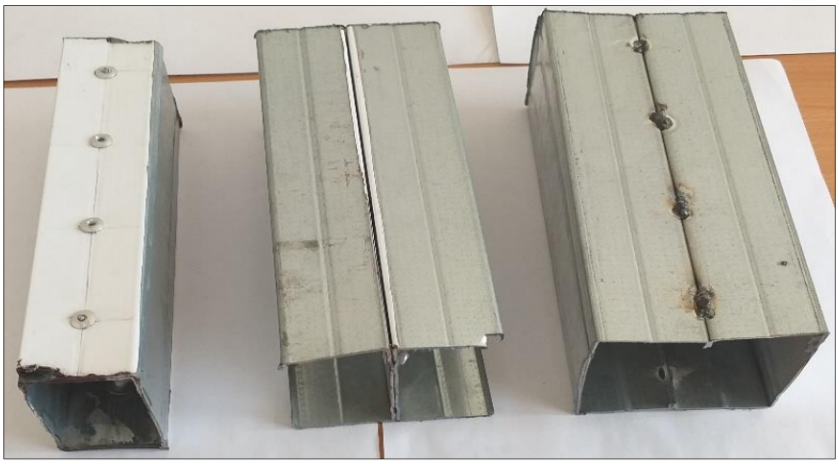

(a) (b) (c)

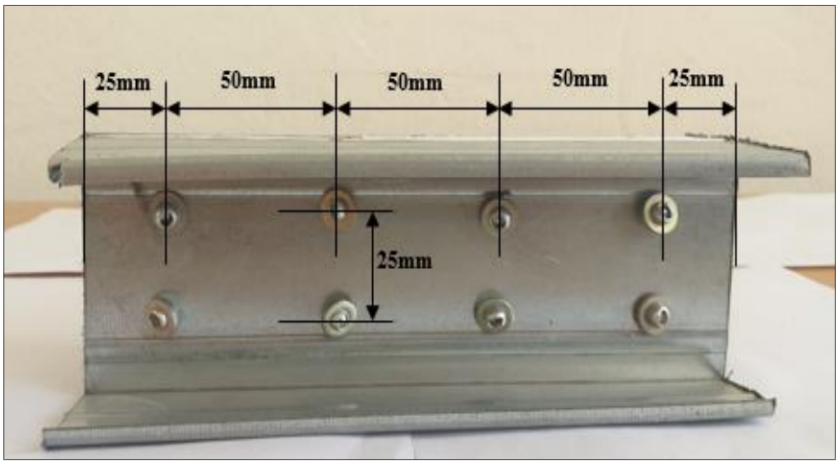

(d)

Figure V.1. Cold-formed steel built-up unfilled columns: (a) Box; (b) Back-to-back; (c) Face-to-face; (d) Back-to-back longitudinal view.

As part of this experimentation, we subjected six specimens with a length of 200mm to simple compression tests. Among these specimens, some were left empty while others were filled with high-strength ordinary concrete (Figure V.2). This approach enables a comparison of the strength and compression behavior properties of the profiles, both in their unfilled state and when filled with concrete.

(a) (b) (c)

Figure V.2. Cold-formed steel built-up filled with concrete columns: (a) Box; (b) Face-to-face; (c) Back-to-back.

Furthermore, we examined two specimens with a length of 580mm configured in a back-to-back arrangement with two rows of rivets, each row consisting of 11 rivets with a diameter of 4mm (Figure V.3.c). These specimens were also subjected to compression tests, both in their empty state and after being filled with concrete (Figures V.3.a and V.3.b).

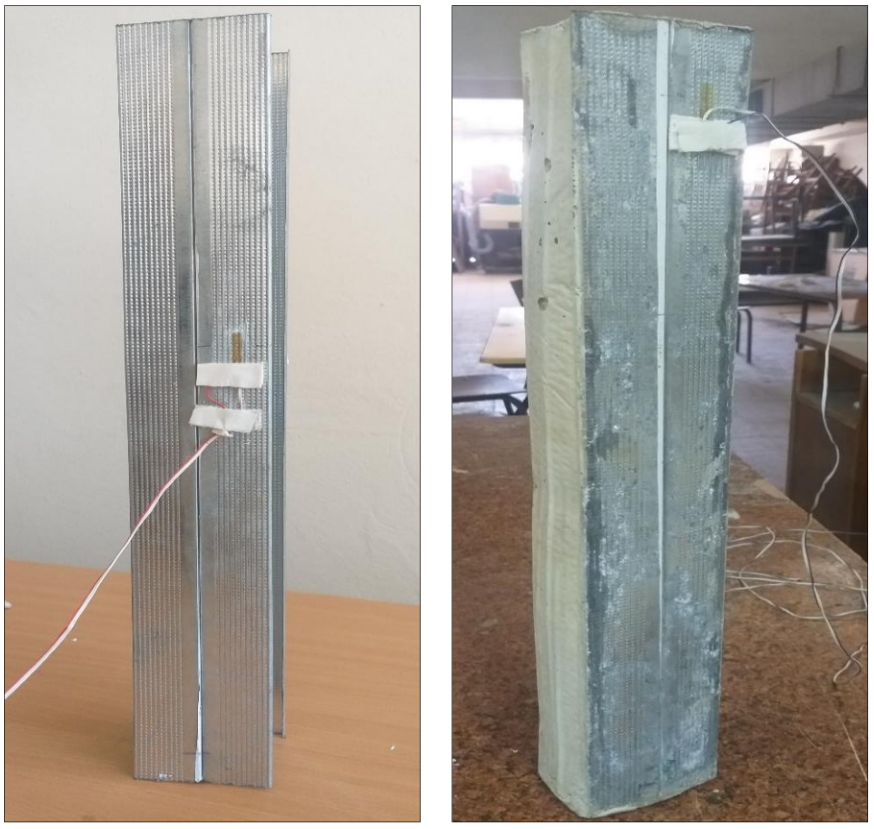

(a) (b)

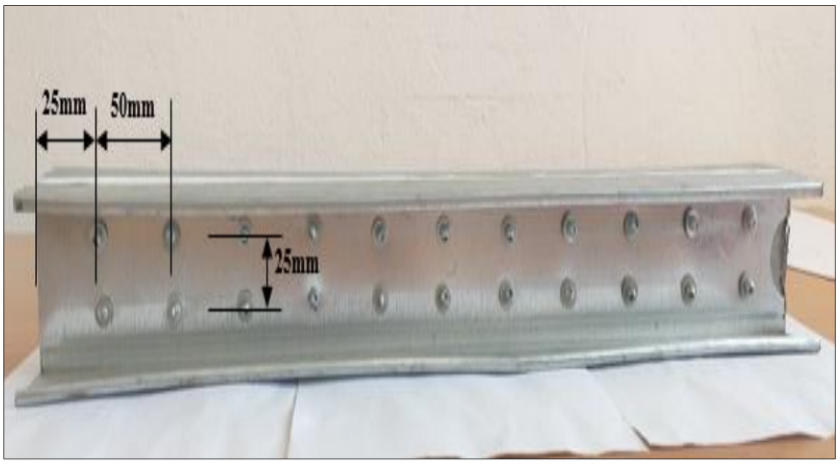

(c)

Figure V.3. Cold-formed steel built-up back-to-back columns: (a) Unfilled with concrete; (b) Filled with concrete; (c) Longitudinal view.

Table V.1 presents the geometric properties of the tested models, following the recommendations and limitations outlined in EN 1993-1-3 (European Committee for Standardization, 2006):

Table V.1. Geometrical properties of cold-formed steel built-up experimental C-sections.

Dimensions	**Sections**		
	Back-to-back (mm)	**Face-to-face (mm)**	**Box (mm)**
B	80	80	40
b_p	40	40	40
H	70	70	70
C	5	5	5
R	1,15	1,15	1,15
t	0,7	0,7	0,7

V.3 TENSILE TEST

The tensile tests conducted in accordance with ASTM A-370 standard (ASTM Committee, 2020), were performed to determine the mechanical properties of the steel used in the experimental study. Seven specimens were prepared for the tensile test, and their geometric characteristics are summarized in Table V.2 and Figure V.4.

The tensile test was conducted until the specimens ruptured (Figure V.5), and the results are depicted in stress-strain curves shown in the Figure V.6. The measurement of the Young's modulus yielded a value of 200787MPa, with an elastic stress of approximately 350MPa.

Table V.2. Geometric characteristics of the specimens.

Specimen	G (mm)	W (mm)	R (mm)	L (mm)	A (mm)	B (mm)	C (mm)
1	25	6,25	6	100	32	32	10
2	25	6,25	6	100	32	32	10
3	25	6,25	6	100	32	32	10
4	25	6,25	6	100	32	32	10
5	25	6,25	6	100	32	32	10
6	25	6,25	6	100	32	32	10
7	25	6,25	6	100	32	32	10

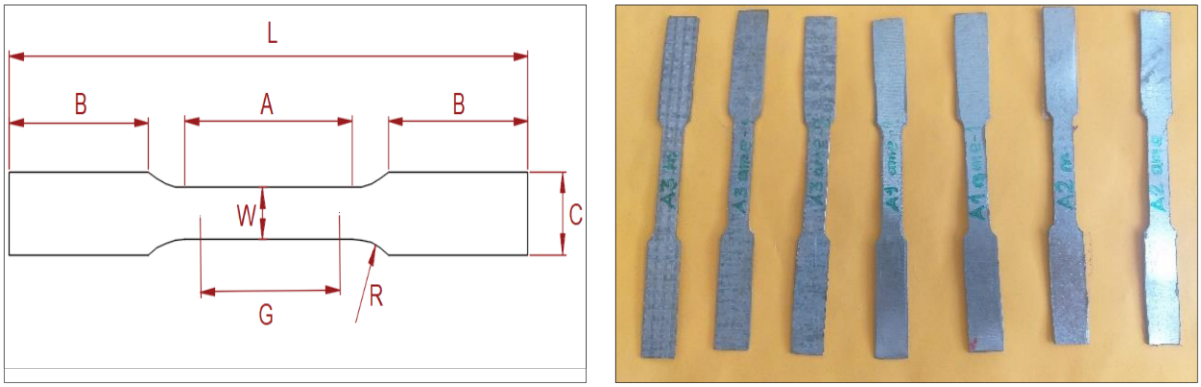

Figure V.4. The specimens prepared for the tensile test.

(a) (b)

Figure V.5. Tensile test: (a) Tensile testing machine; (b) The specimens tested after failure.

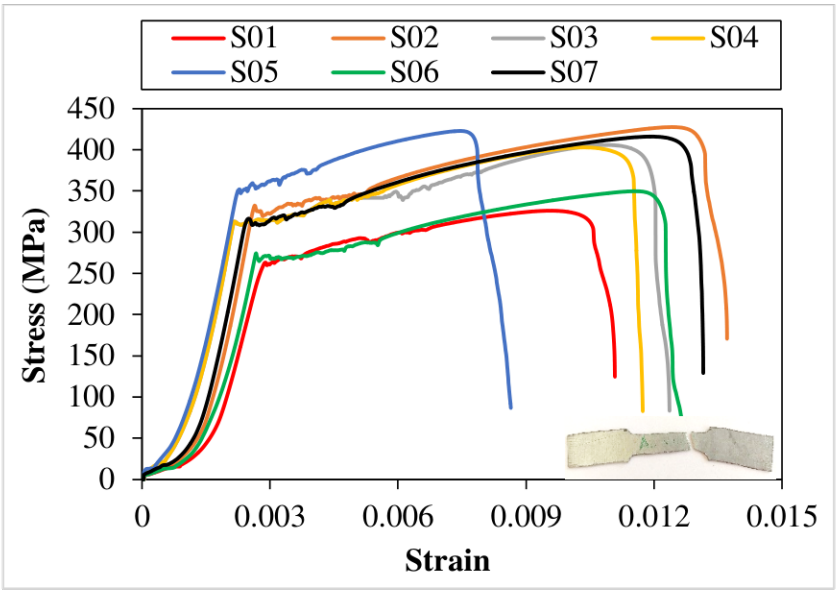

Figure V.6. Evolution of stress as a function of strain for the specimens.

V.4 COMPRESSION TEST

The compression test represents an indispensable method for evaluating the strength of concrete. Optimal quantities of the components used in the concrete are determined through particle size analyses and the Dreux-Gorisse formulation method (Dreux and Festa, 1998). The components were mixed using a concrete mixer and then poured into nine cubic-shaped molds with dimensions of 100mm×100mm. The resulting samples were subjected to compression testing in the laboratory of the Department of Civil Engineering at Badji Mokhtar University in Annaba, at 7, 14, and 28 days, respectively. The concrete used exhibited a satisfactory strength of 25MPa (Figure V.7).

Figure V.7. Compression machine and specimens tested for crushing.

V.5 INSTRUMENTS USED AND TESTING PROCEDURES

This experimental study aims to analyze the mechanical performance of built-up cold-formed columns with various configurations, focusing on load-strain and load-lateral displacement relationships. Lateral displacements are measured using displacement comparators (Figure V.9.a). Strain gauges, with a gauge factor of 2,07, are positioned to capture deformations in the most stressed areas (Figure V.8). The strain gauges were carefully bonded and connected to 10-channel strain gauge bridges for deformation readings (Figure V.9.b).

Figure V.8. The placement of the strain gauges.

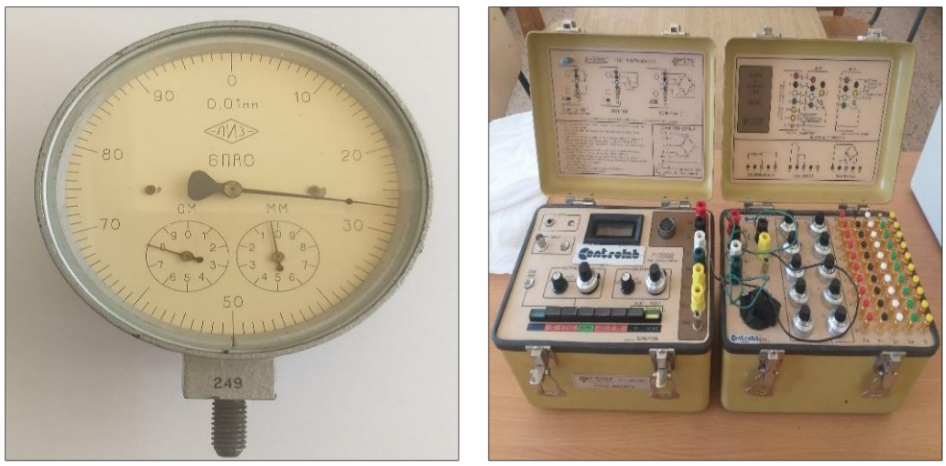

(a) (b)

Figure V.9. Measurement equipment: (a) Displacement comparators; (b) Strain gauge bridges.

The prepared specimens, both hollow and concrete-filled, are fixed at both ends and subjected to simple compression. A «BeraTest» machine with a capacity of 1500kN is used, providing numerical recording of the results. Strains and lateral displacements are recorded as the applied

load increases (Figure V.10). The compression test is conducted in accordance with ASTM E9-09 standards (ASTM, 2009). The specimens are tested to failure.

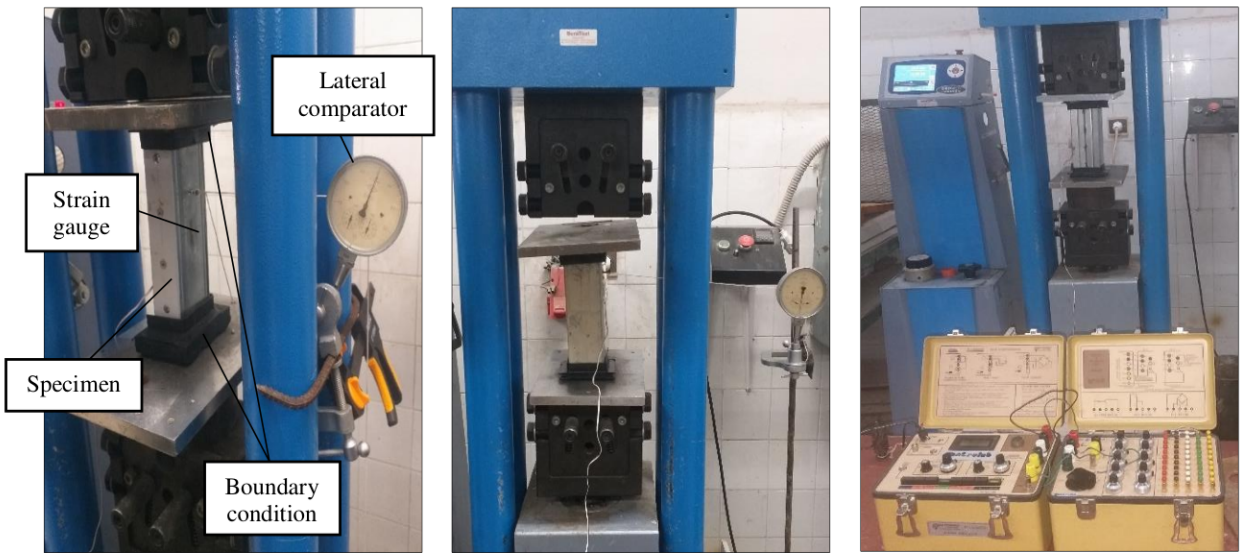

Figure V.10. The columns tested under compression.

V.6 VALIDATION OF RESULTS

V.6.1 Failure modes

The numerical and experimental failure modes of a 200mm in length cold-formed built-up back-to-back unfilled column (BE) are illustrated in the Figure V.11. There is a correspondence between the numerical and experimental failure modes. The observed instability is of a local and distortional type, considered sectional buckling modes. No failure at the rivets is observed when the ultimate strength is reached. Distortional buckling is localized in the flanges, whereas local buckling occurs in the web, caused by uneven internal stresses.

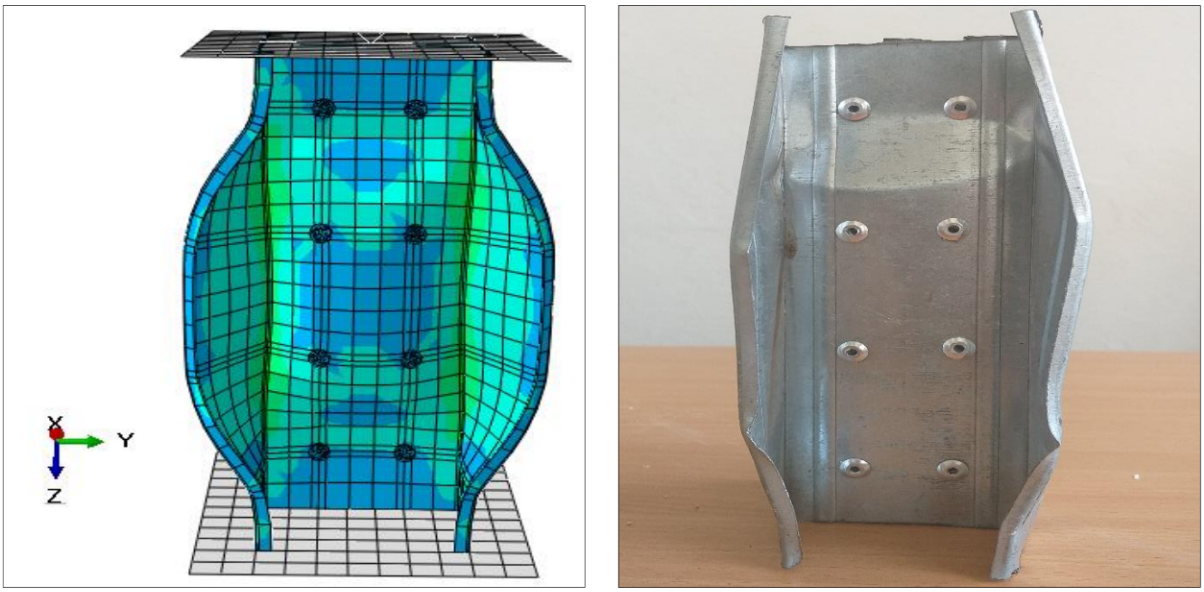

(a) (b)

Figure V.11. Failure modes of cold-formed steel built-up back-to-back unfilled column: (a) Numerical; (b) Experimental.

For the cold-formed steel assembled back-to-back column filled with concrete (BF) with a length of 200mm, we observed an experimental failure mode similar to the numerical one, characterized by local buckling at the flanges concentrated at one-third of the column's span (Figure V.12). During testing, the load was applied cyclically. In the first loading cycle, a relatively subtle external buckling was accommodated by the steel section and concrete (Figures V.12.a and V.12.b). As the load was increased to the failure point of the specimen, a separation between the concrete surface and the steel in the column specimen was noted, along with concrete crushing (Figure V.12.c).

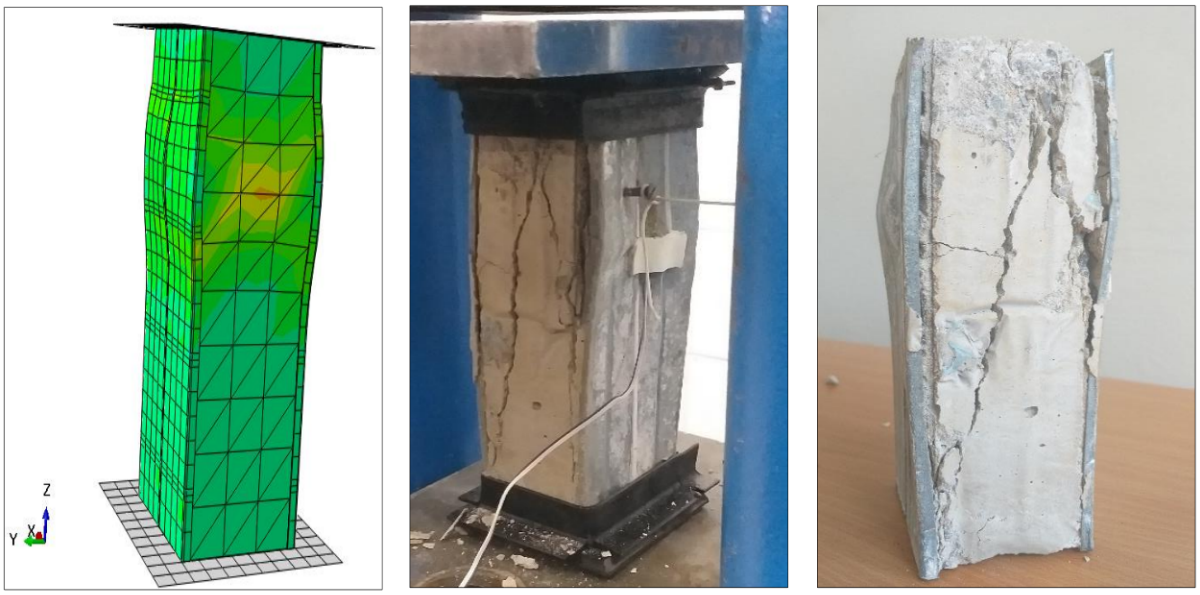

(a) (b) (c)

Figure V.12. Failure mode of cold-formed steel built-up back-to-back filled with concrete column: (a) Numerical; (b) First experimental loading; (c) Loading until failure.

During numerical analysis and testing, the cold-formed built-up face-to-face unfilled model (FE) with a length of 200mm, exhibited continuous local buckling characterized by sinusoidal waves, as shown in the Figure V.13. The welds used for assembly remained intact until the failure of the column specimen, as evidenced by the perfect bonding in the assembled sections at the end of the test.

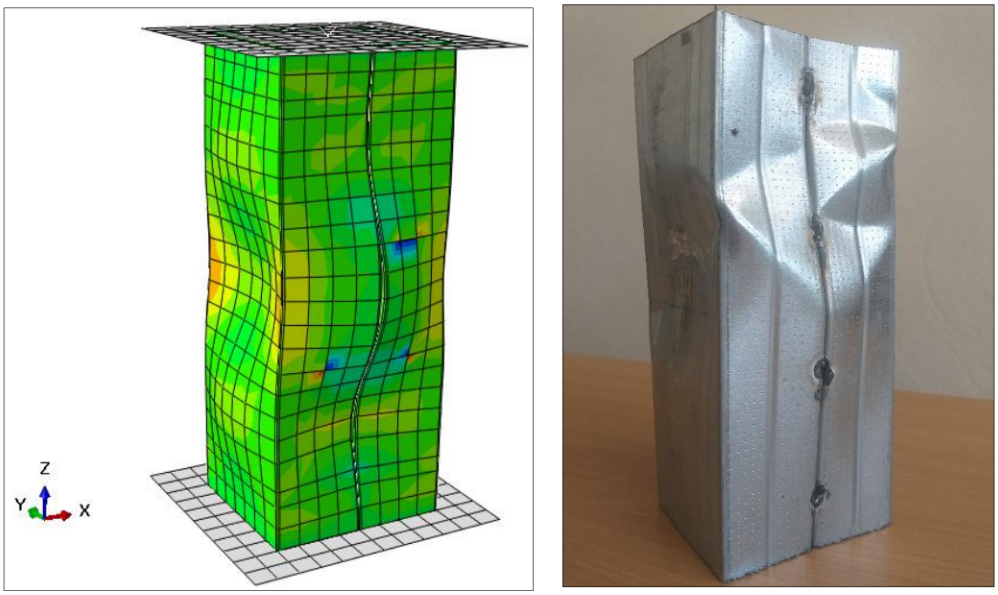

(a) (b)

Figure V.13. Failure mode of cold-formed steel built-up face-to-face unfilled column: (a) Numerical; (b) Experimental.

The failure mode of the built-up face-to-face cold-formed concrete-filled model (FF) with a length of 200mm, also reveals local buckling at the middle of the column, along with a significant separation of the steel, resulting in weld failure. The lateral pressure exerted by the concrete (confinement force) acts on the internal walls of the cold-formed section (Tomii and SAKINO, 1979). The concrete filling provides increased rigidity, which was observed during the test (Figure V.14).

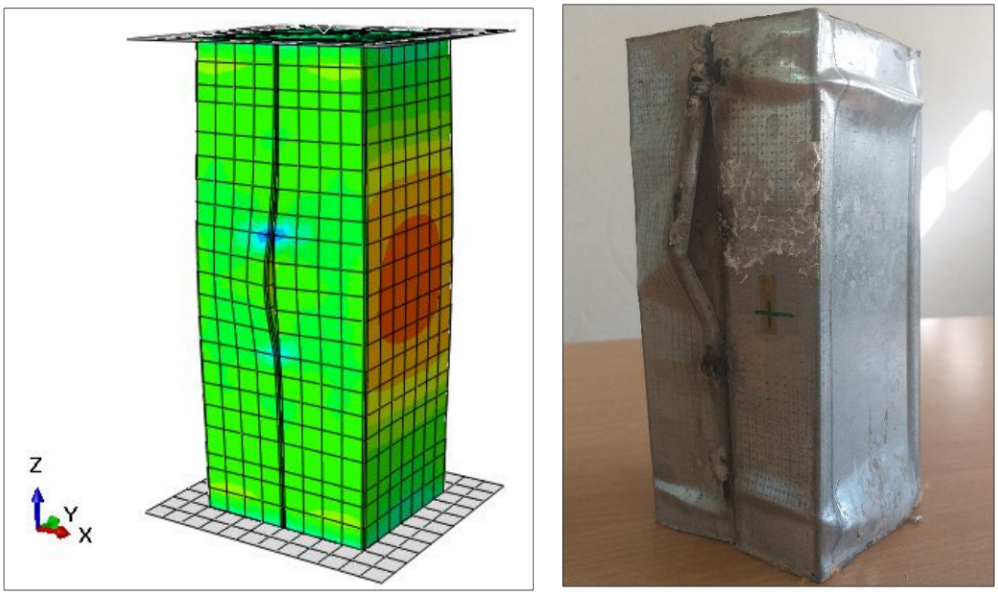

(a) (b)

Figure V.14. Failure mode of cold-formed steel built-up face-to-face filled with concrete column: (a) Numerical; (b) Experimental.

Figure V.15 illustrates a comparison between the numerical and experimental failure modes of the cold-formed, empty assembled box section column (BOE) with a length of 200mm. A continuous local buckling in the form of a sinusoidal wave, i.e., a smooth and regular curve of walls rising and falling periodically, is observed. The deformation propagates continuously along the affected column specimen, without interruptions or marked discontinuities. The rivets demonstrated remarkable strength up until the failure of the column specimen.

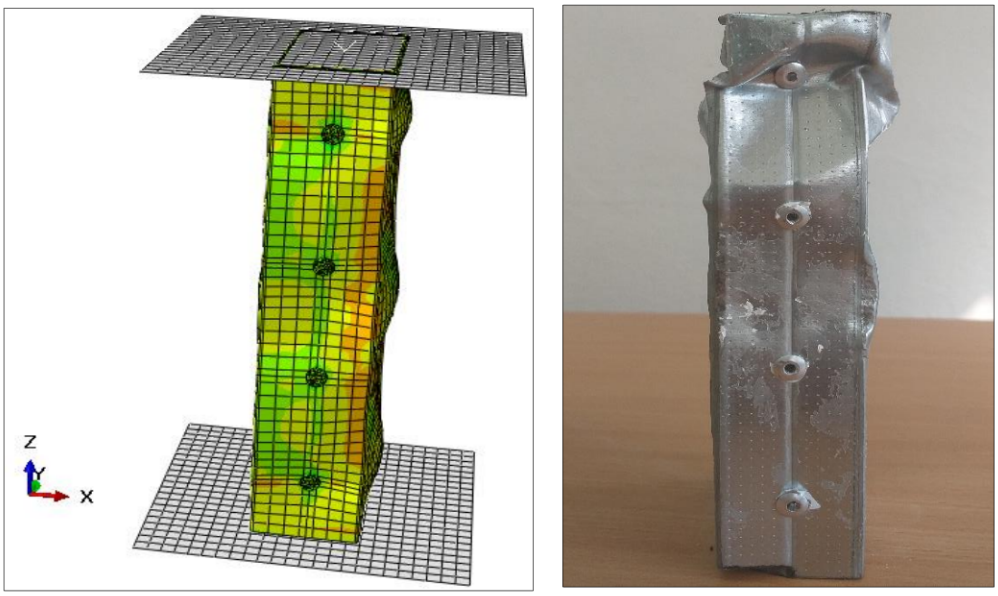

(a) (b)

Figure V.15. Failure mode of cold-formed steel built-up box section unfilled column: (a) Numerical; (b) Experimental.

For the concrete-filled cold-formed assembled box column (BOF) with a length of 200mm, there is an observed increase in the specimen's column resistance during testing, along with an improvement in failure mode compared to the unfilled model. Local buckling at the lower end of the column results in internal concrete pressures (confinement effect) in both numerical and experimental models (Figure V.16). The rivets demonstrated remarkable strength until the failure of the tested models.

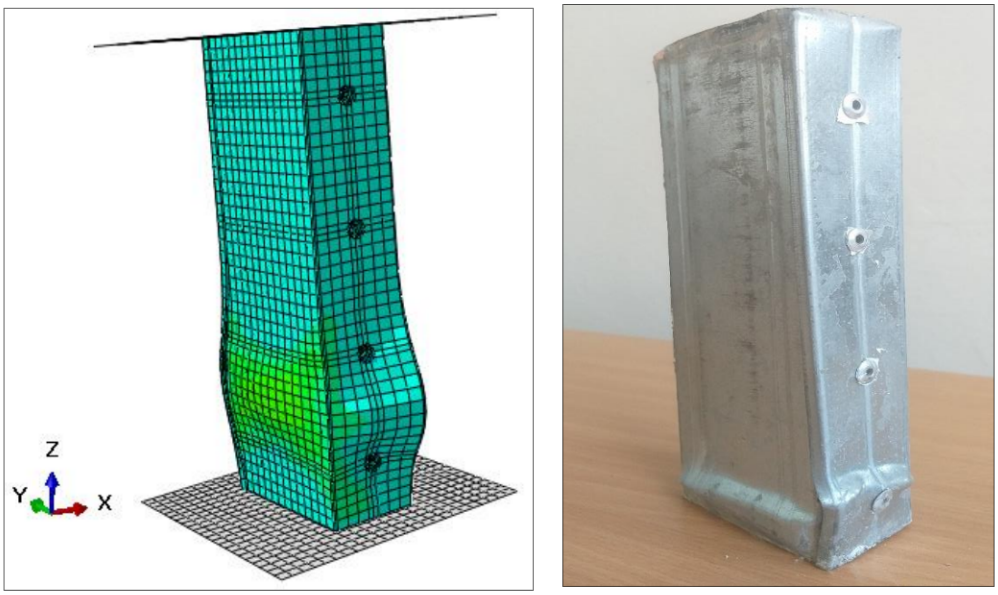

(a) (b)

Figure V.16. Failure mode of concrete-filled cold-formed steel built-up box column: (a) Numerical; (b) Experimental.

By increasing the column length to 580mm, the Figure V.17 presents a comparison between the numerical and experimental failure modes of the cold-formed steel built-up back-to-back empty column (BE). A discernible continuous distortional local buckling with sinusoidal waves is observed. The local mode is concentrated at the web, characterized by a relatively short buckling wavelength of the section, while the distortional mode is characterized by relative movement of the plate junction lines (DJAFOUR, 2015).

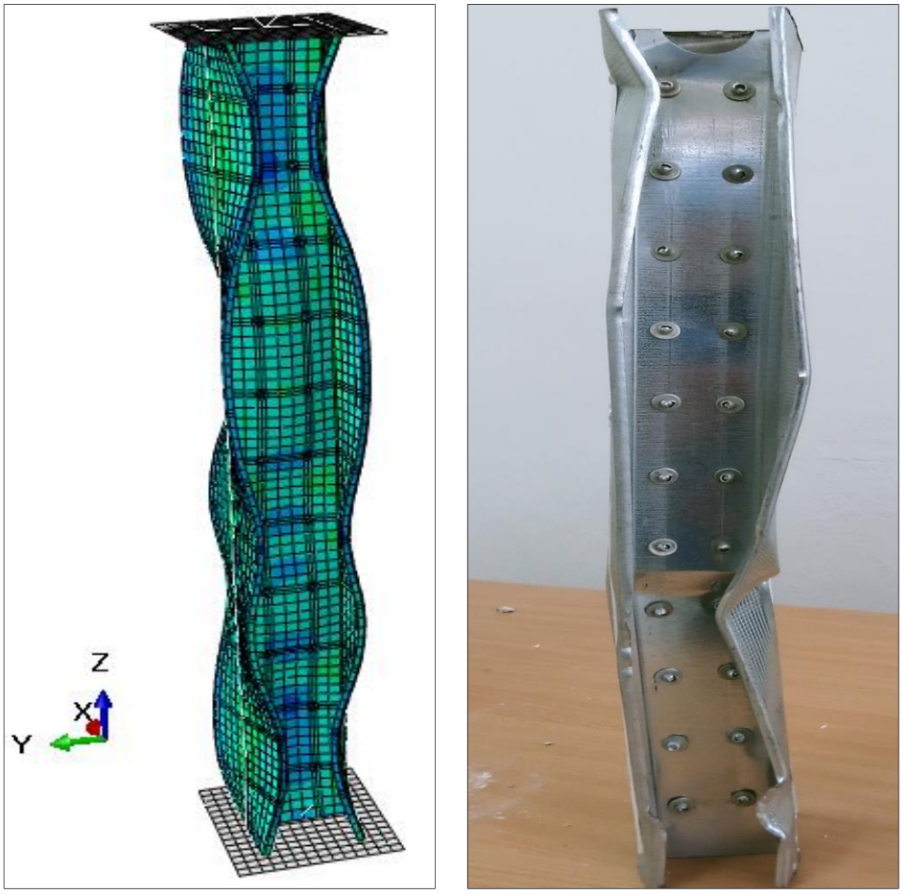

(a) (b)

Figure V.17. Failure mode of cold-formed steel assembled back-to-back unfilled column: (a) Numerical; (b) Experimental.

There is a very good correlation between the experimental and numerical failure modes of the concrete-filled cold-formed steel assembled back-to-back models (BF) with a length of 580mm.

Localized detachment is observed at the upper end between the concrete surface and the steel in the column specimen. Distortional instability is noted in the upper part of the column. During testing, the load increases progressively until failure. A very good resistance of the tested model was observed (Figure V.18).

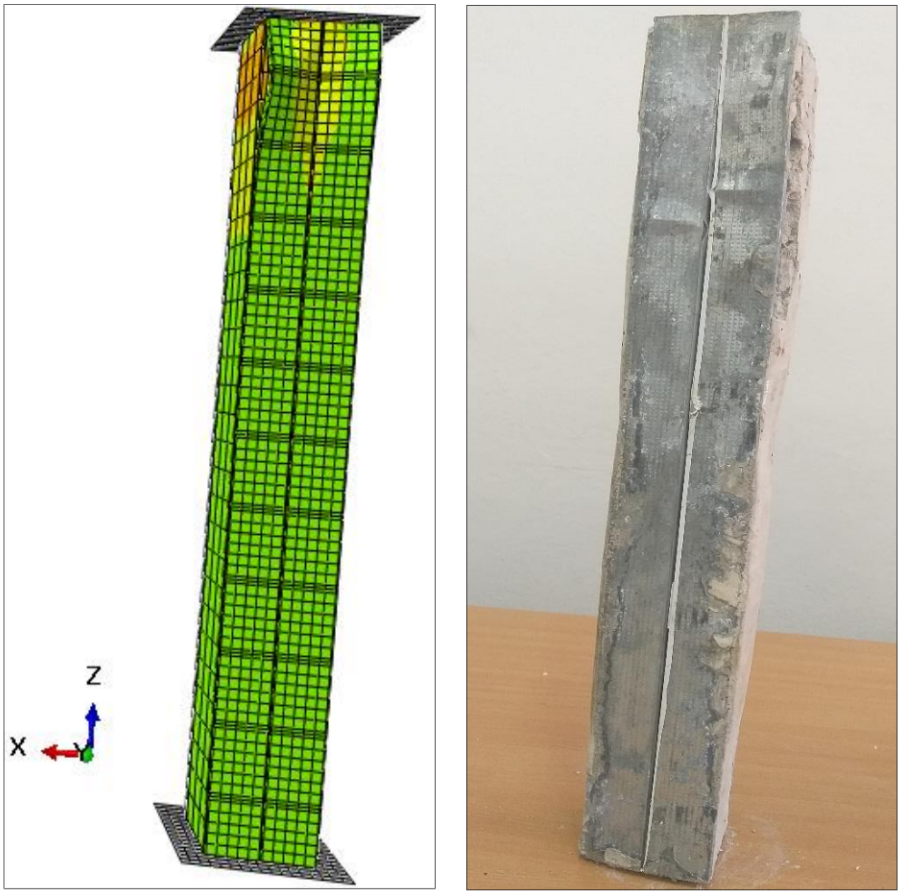

(a) (b)

Figure V.18. Failure mode of concrete-filled cold-formed steel assembled back-to-back column: (a) Numerical; (b) Experimental.

V.6.2 Interpretation of the results

Cold-formed steel profiles (CFS) are extensively utilized in the structural system of both residential and non-residential constructions. The widespread use of thin-walled structures can be attributed to several significant advantages, such as their rapid assembly. Additionally, they are economical and environmentally friendly due to their high recyclability. The addition of concrete to cold-formed steel profiles results in a remarkably high compressive strength.

Figure V.19 presents the numerical curves of the load-strain state in the most stressed areas of the studied models (back-to-back, face-to-face, and box) with a length of 200mm.

Figure V.19.a demonstrates an elasto-plastic behavior in all the three unfilled columns. The face-to-face configuration model (FEA FE) exhibits significant plastic flow, which can prevent premature failure caused by local buckling effects compared to the other models. Local buckling is observed in the back-to-back (FEA BE) and box (FEA BOE) configuration models. The process of designing cold-formed sections is primarily based on determining the critical elastic loads of these failure modes. All three empty models show a similar failure load of approximately 79kN. The open back-to-back model, comprising several walls free along one longitudinal edge, is at risk of critical elastic buckling (Bambach, 2006).

Figure V.19.b illustrates the behavior laws of the studied configurations when filled with concrete. The back-to-back model (FEA BF) exhibits elastic buckling instability, as shown in the failure mode observed in the Figure V.12.a, with separation between the steel and the concrete due to stress concentration that induced buckling. After reaching the maximum load, both the face-to-face (FEA FF) and box (FEA BOF) concrete-filled models show a progressive decrease in applied load (peak) with increasing strain. The critical loads of the back-to-back (FEA BF) and face-to-face (FEA FF) models are nearly the same at 213kN, whereas for the box model (FEA BOF), it's 193kN, representing a difference of approximately 10,36%.

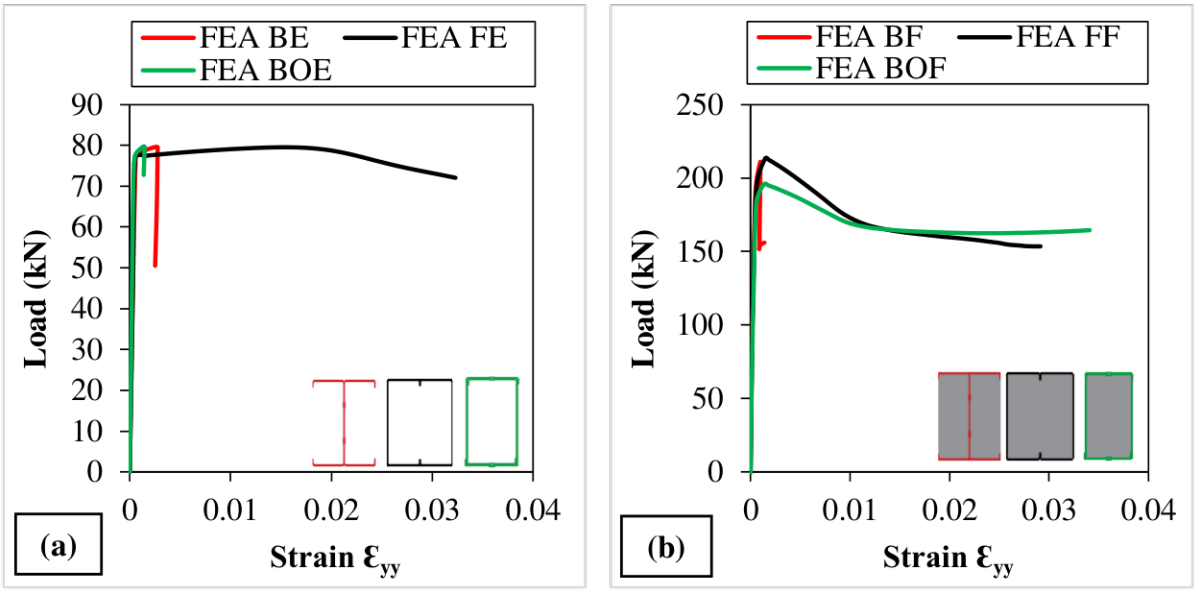

Figure V.19. Numerical load-strain state of cold-formed steel built-up columns: (a) Unfilled with concrete; (b) Filled with concrete.

The numerical curves of the load- lateral displacement U_y state for the empty models with a length of 200mm, as shown in Figure V.20.a, exhibit an elasto-plastic behavior in all three curves. These curves reveal a decrease in the applied load with an increase in lateral displacement after reaching the maximum load. The back-to-back empty model (FEA BE) shows a significant lateral displacement of 18mm, indicating instabilities, as illustrated in the failure mode (Figure V.11.a). Open sections are more prone to instabilities than closed sections.

An elasto-plastic behavior is also observed in the filled columns with different configurations (back-to-back, face-to-face, and box). Back-to-back encased with concrete column (FEA BF) shows a reduction in lateral displacement of approximately 47,10% and 60,84% compared to the face-to-face (FEA FF) and box (FEA BOF) filled with concrete columns, respectively (Figure V.20.b). This decrease is due to the absence of the confinement effect in the back-to-back filled column, unlike the other columns (FEA FF and FEA BOF), which benefit from a confinement force.

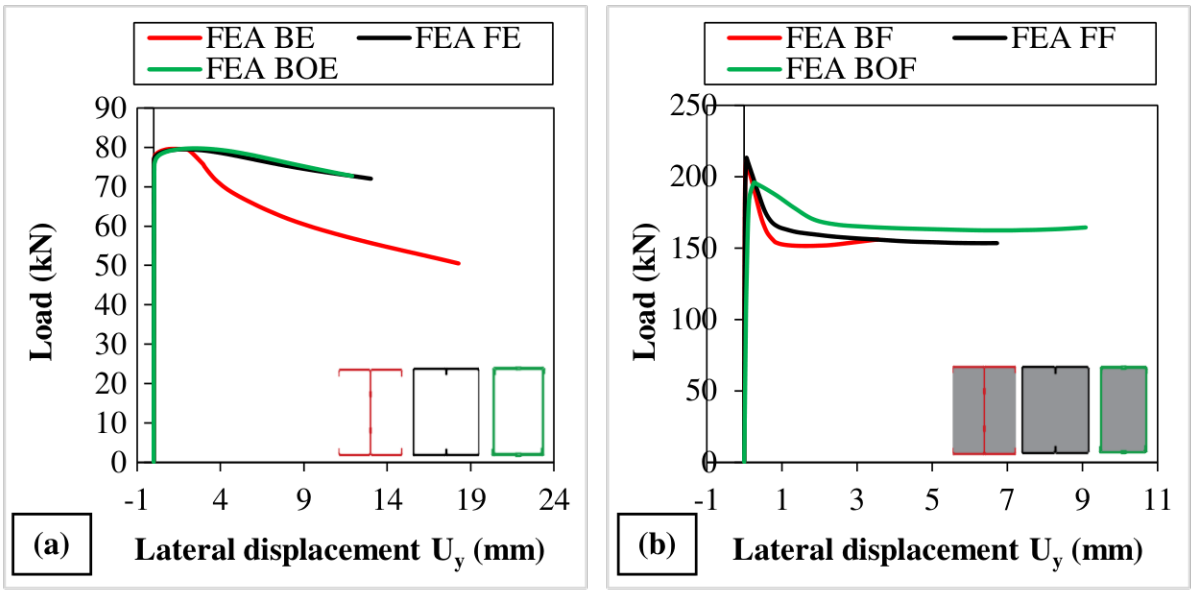

Figure V.20. Numerical load-lateral displacement state of cold-formed steel built-up columns: (a) Unfilled with concrete; (b) Filled with concrete.

By increasing the column length to 580mm, Figure V.21 presents the load-strain and load-lateral displacement curves obtained with ABAQUS for back-to-back assembled models. The load-strain state of the studied models, illustrated in Figure V.21.a, shows an improvement in the ultimate load of the encased with concrete column (FEA BF) by approximately 55,55% compared to the unfilled column (FEA BE). The empty model exhibits linear behavior up to the maximum load of about 79kN, followed by a sudden failure characterized by local

distortional buckling, as shown in Figure V.17.a. In contrast, the concrete-filled model, after reaching the maximum load, shows a gradual decrease in the applied load (the peak) with increasing deformation.

In the load-lateral displacement state, illustrated in Figure V.21.b, an improvement in the lateral displacement of the filled column by approximately 43,82% compared to the empty one is observed. This improvement is due to the concrete encasement, which forms a remarkable bond with the steel, thereby reducing instabilities. For the back-to-back encased model (FEA BF), it is observed that at a lateral displacement value of 6mm, the load decreases to a value of 87,66kN. This reduction in load is due to the detachment between the concrete surface and the steel, as clearly demonstrated in the failure mode (Figure V.18.a).

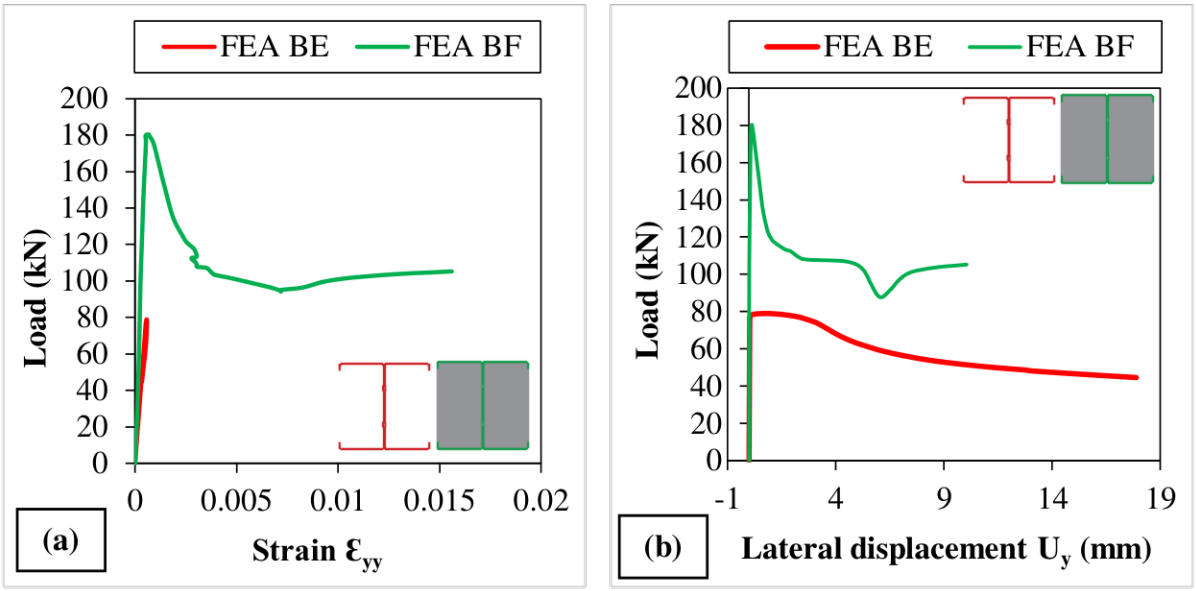

Figure V.21. Numerical curves of cold-formed steel built-up back-to-back columns: (a) Load-strain; (b) Load-lateral displacement.

A comparative analysis between the numerical and experimental load-strain curves of the studied columns with a length of 200mm was performed (Figure V.22). A good correlation between the numerical and experimental ultimate loads was observed, with a divergence not exceeding 5% in all models.

The experimental and numerical curves of the back-to-back unfilled columns (TEST BE and FEA BE) and the back-to-back concrete-encased columns (TEST BF and FEA BF), as shown in Figure V.22.a, are almost coinciding in the elastic region. A significant increase in the critical load of the filled columns by approximately 62,18% compared to the empty columns is

observed. Upon reaching the ultimate load, the experimental back-to-back concrete-encased specimen (TEST BF) shows detachment between the steel and concrete, accompanied by cracking in the concrete. This indicates that the steel bears the majority of the load, resulting in deformation of the column flanges, as clearly illustrated in Figures V.12.b and V.12.c. After reaching the peak load (210kN), the numerical back-to-back concrete-encased model (FEA BF) demonstrate a decrease in load to a value of 152kN with a constant deformation of 0,0009. The load then remains constant while the deformation continues to increase, indicating that the material continues to deform.

For the face-to-face columns, both empty and concrete-filled (Figure V.22.b), a linear behavior is observed in the range [0-83]kN for the empty models (FEA FE and TEST FE) and [0-220]kN for the concrete-filled models (FEA FF and TEST FF). Beyond these loads, instabilities start to appear. Additionally, in the concrete-filled face-to-face model (FF), detachment of the steel is observed due to weld rupture (Figure V.14). The numerical curves exhibit a significant yield plateau, while the experimental curves were stopped once the load decreased to the target value. There is an increase of approximately 4,64% in the ultimate load of the face-to-face concrete-filled model compared to the back-to-back concrete-encased model.

A reduction in the failure load of approximately 5,58% and 6,86% was observed for the assembled box section concrete-filled column compared to the back-to-back and face-to-face filled with concrete columns, respectively. The numerical concrete-filled box model (FEA BOF) presents a linear behavior up to a failure load of 198kN, after which the load begins to decrease to a value of 166kN, indicating the onset of column deformation and the emergence of instabilities. Subsequently, the load remains constant while the deformation continues to increase (Figure V.22.c). This increased deformation indicates that the column continues to deform and resist due to the interaction between the inner surfaces of the steel and concrete, demonstrating superior structural performance compared to their hollow counterparts (Chen et al., 2023). The rivets exhibit notable strength, as illustrated in Figure V.16, acting like shear studs that ensure a strong connection between the steel and concrete, leading to improved performance and stability of the filled column.

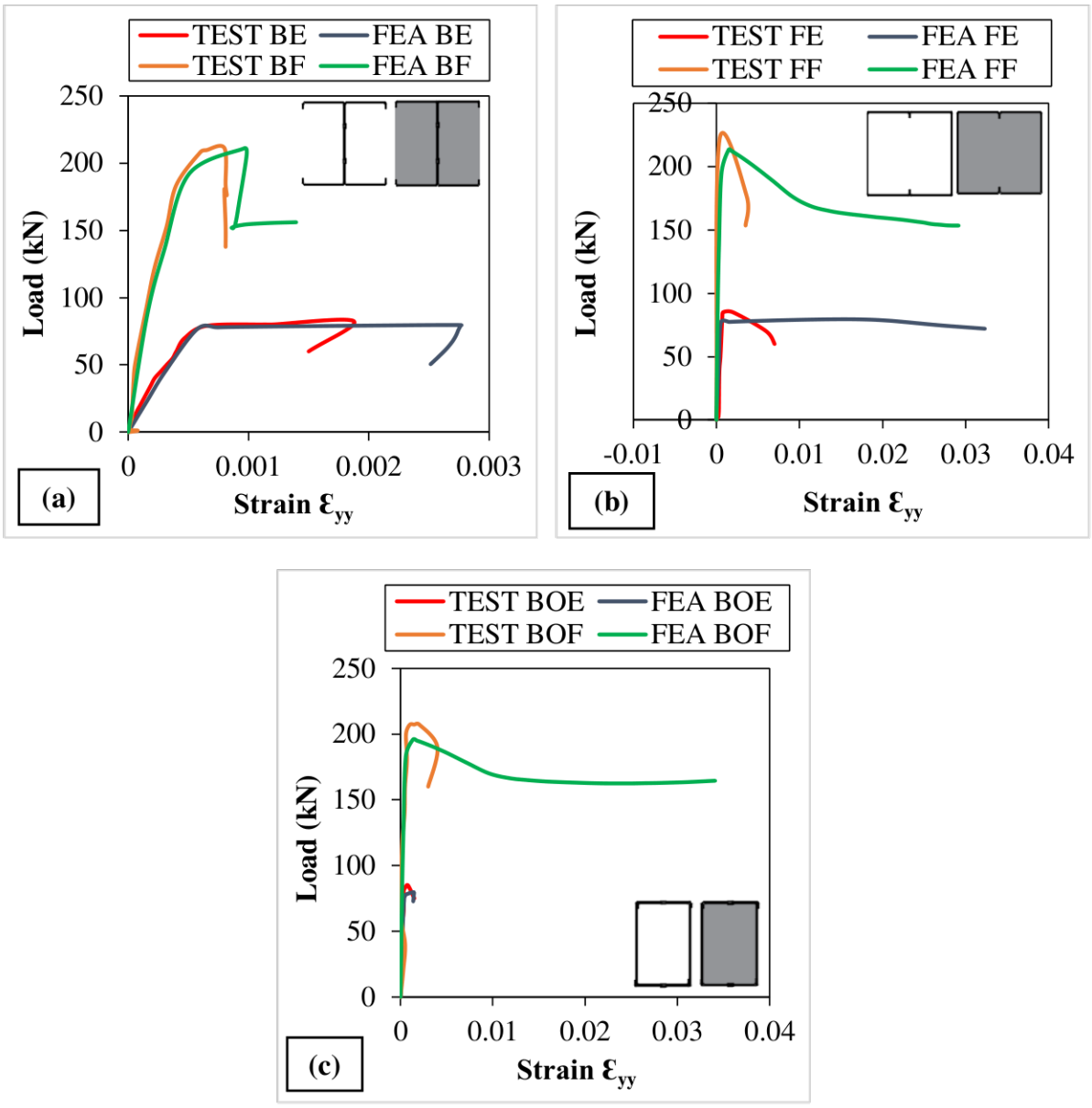

Figure V.22. Comparative curves of the load-strain state of the studied models: (a) Back-to-back; (b) Face-to-face; (c) Box.

Figure V.23 illustrates the load-lateral displacement U_y state for the numerical models and experimental specimens (back-to-back, face-to-face, and box) with a length of 200mm. During the experimental test, displacement comparators are placed in the most stressed areas to measure variations in lateral displacement. Built-up back-to-back encased with concrete columns, FEA BF and TEST BF, demonstrate a significant reduction in lateral displacement of approximately 77,77% and 83,18% compared to the unfilled columns, FEA BE and TEST BE, respectively (Figure V.23.a). This reduction is attributed to the remarkable combination of steel and concrete, which enhances instability.

The numerical and experimental curves for assembled face-to-face model unfilled and filled with concrete overlap in the elastic region, as shown in Figure V.23.b. A moderate enhancement in lateral displacement of approximately 48,31% and 40,66% is observed when comparing the numerical models and experimental tests, respectively. The confined concrete generates a lateral pressure force exerted on the inner walls of the steel section, leading to weld rupture and significant detachment of the steel, as clearly illustrated in Figure V.14.b.

A modest improvement due to the confinement effects on lateral displacement of approximately 33,68% was observed between the empty and filled models in the box section column (Figure V.23.c). The hollow numerical and experimental columns (FEA BOE and TEST BOE) exhibit linear behavior in the range [0-82]kN, accompanied by a significant yield plateau for the FEA BOE model. This indicates that the column continues to resist and deform, as presented in Figure V.15 by a continuous, noticeable local buckling in a sinusoidal form.

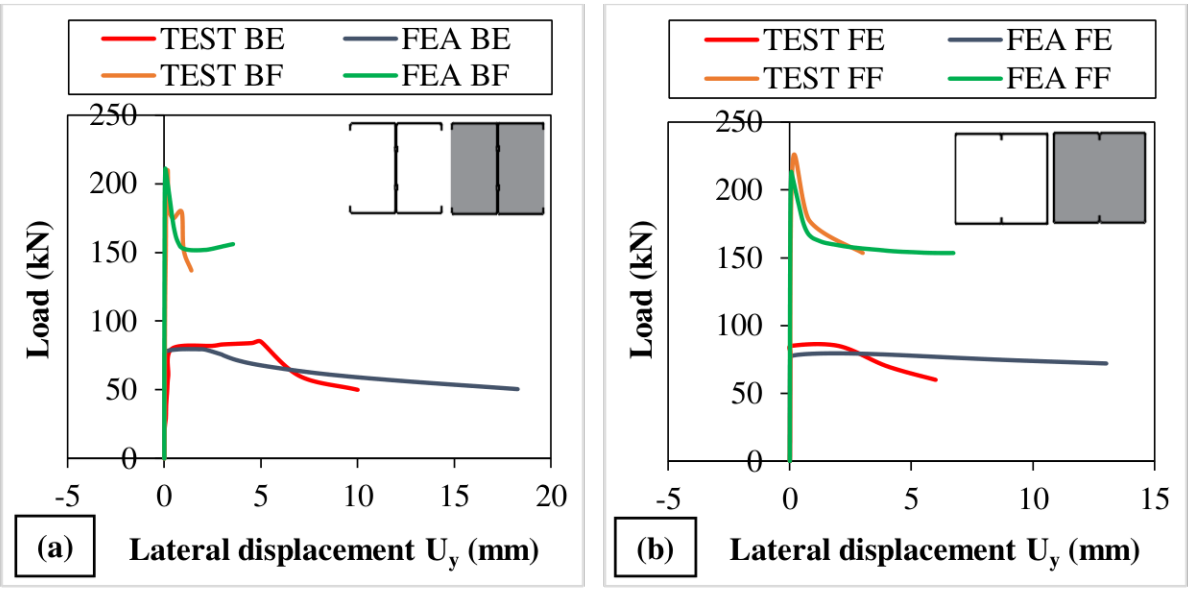

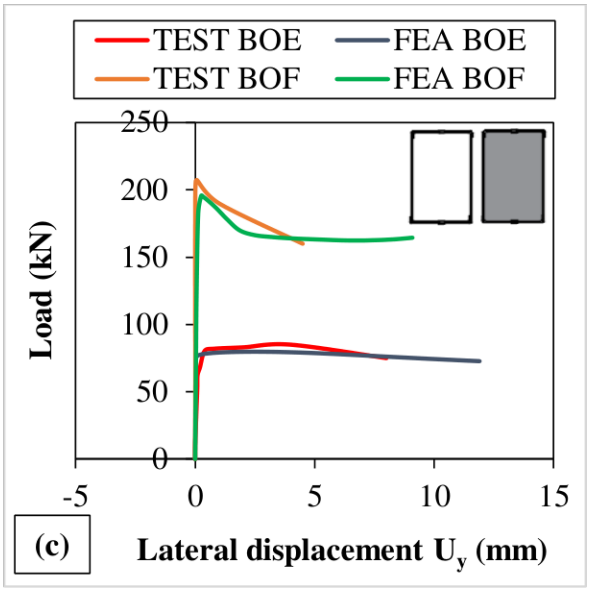

Figure V.23. Comparative curves of the load-lateral displacement state of the studied models: (a) Back-to-back; (b) Face-to-face; (c) Box.

By increasing the length of the back-to-back configured post to 580mm, a 65,52% increase in slenderness was achieved. The load-strain state of the assembled back-to-back posts, as shown in Figure V.24.a, exhibits a notable agreement between the numerical and experimental curves. The unfilled numerical model (FEA BE) displays elastic behavior followed by a sudden failure, indicating a direct failure of the column. This means that the slender column (back-to-back) tends to fail at a lower load, and its cross-section does not enter the permanent deformation phase. In contrast, the filled numerical model (FEA BF) shows elastoplastic behavior up to a maximum strain value of 0,015, demonstrating a very significant improvement in ductility.

An enhancement in the lateral displacement of the concrete-encased post compared to the empty post is observed in both numerical and experimental cases (Figure V.24.b). This indicates that the behavior of slender columns is influenced by buckling phenomena, as illustrated in Figure V.17, where the column can lose stability under axial loads (Yang et al., 2024). Therefore, it is often necessary to use reinforcement techniques, such as adding concrete, to maintain their structural integrity and ensure stability. Additionally, a slight reduction in the critical load, by approximately 10%, is noted for the back-to-back encased model with a length of 580mm compared to the back-to-back encased model with a length of 200mm.

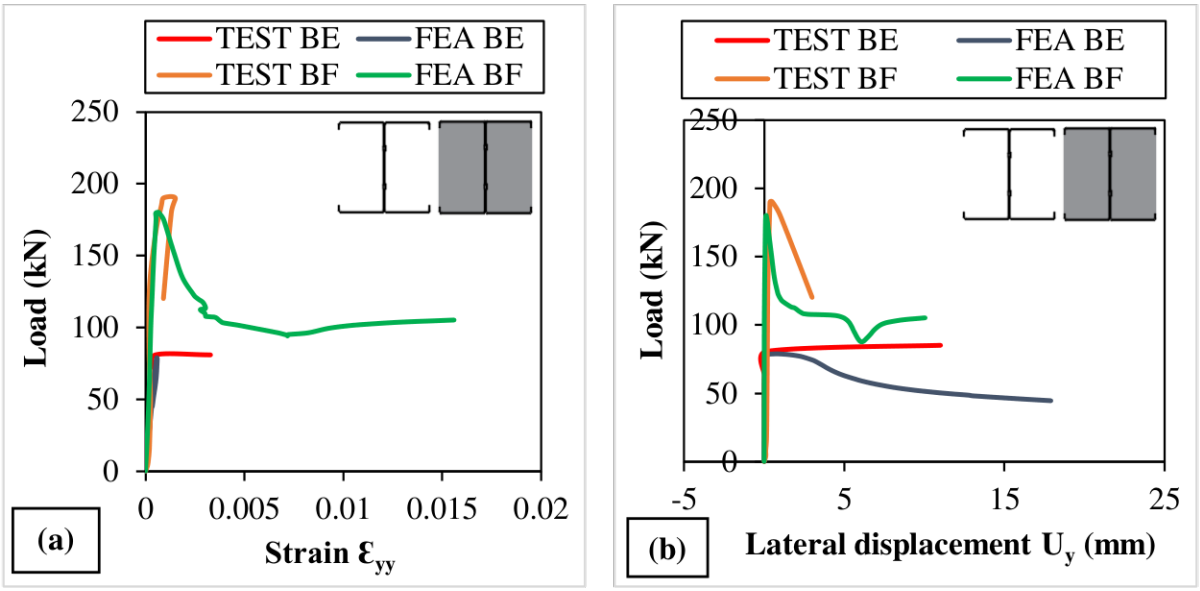

Figure V.24. Comparative curves of cold-formed steel built-up back-to-back columns: (a) Load-strain; (b) Load-lateral displacement.

The experimental test results are summarized in Table V.3, which also includes the numerical results for both unfilled and concrete-filled built-up columns, along with the corresponding modes of instability for each. The findings revealed excellent agreement between the numerical and experimental critical loads, with a variance of no more than 5%.

Table V.3. Numerical and experimental results of the studied columns.

Model	Length (mm)	Unfilled				Concrete-filled			
		Numerical load (kN)	Experimental load (kN)	Discrepancy (%)	Failure mode	Numerical load (kN)	Experimental load (kN)	Discrepancy (%)	Failure mode
Back-to-back	200	79,59	82,5	3,5	Local and distortional buckling	210,43	211,14	0,3	Local buckling + separation between the concrete surface and the steel
	580	78,75	81	2,7	Local and distortional buckling	182,35	190	4	Distortional instability + localized detachment at the upper

									end between the concrete surface and the steel
Face-to-face	200	79,51	83,20	4,4	Local buckling	213,32	220,93	3,4	Local buckling + significant separation of the steel
Box	200	79,74	82	2,7	Local buckling	198,69	207,40	4,2	Local buckling

We noted a strong correlation between the numerical and experimental results with only a slight difference not exceeding 5%. Compared to the unfilled columns, the failure loads in concrete-filled columns represent a significant increase of about 60%. Concrete-filled built-up face-to-face column demonstrates significantly higher strength compared to the other columns, with a failure load of 220kN (Figure V.25).

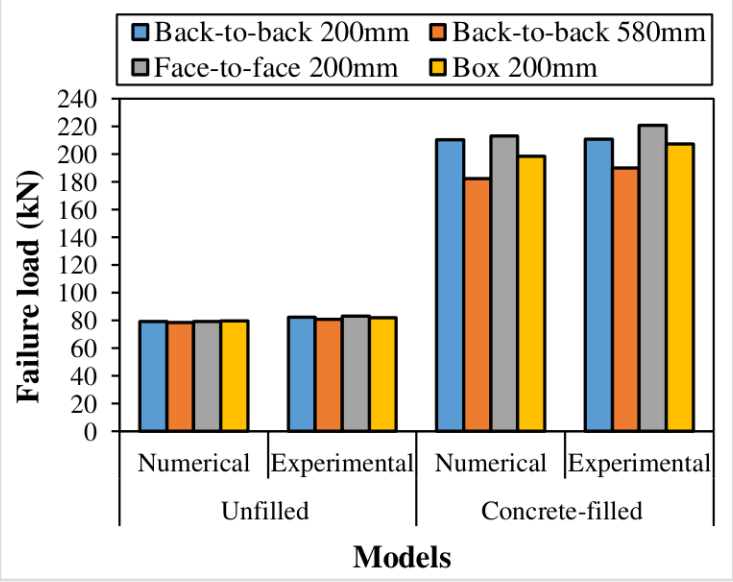

Figure V.25. Comparison between the numerical and experimental failure loads of the studied models.

V.7 CONCLUSION

The geometric and mechanical characterization play a crucial role for providing geometric data during the identification of the numerical model on one hand. On the other hand, it functions to

validate the accuracy of the numerical model that the numerical computation program has verified. It should also be noted that this numerical simulation must introduce and take into account all the effects that the structural elements underwent during their manufacturing and testing.

This chapter outlines the experimental setup used for conducting the tests, as well as the procedure to follow. The numerical results were validated by experimental findings, which showed a very good correlation. We can conclude that our carefully developed experimental models have successfully demonstrated that built-up cold-formed columns exhibit various types of instability, including local, and distortional buckling. It is evident that the addition of concrete plays a significant role in minimizing these instabilities, as clearly illustrated in the failure modes Figures, and in enhancing the strength by approximately 60%, as well shown in the curves.

GENERAL CONCLUSION AND RECOMMENDATIONS

GENERAL CONCLUSION

Research on cold-formed steel built-up columns is of particular significance due to their increasing use in civil constructions. The behavior of concrete-filled cold-formed steel built-up columns under axial compression demonstrates remarkable and predictable stability. The steel, serving as the primary structural support, mainly bears the compressive load, while the concrete provides effective confinement, thereby enhancing overall strength and improving ductility. This synergy results in superior strength and a greater ability to improve performance against instabilities.

This thesis presents a numerical and experimental study of cold-formed steel C-section assembled columns in various configurations, including back-to-back, face-to-face, and box. These columns were tested both unfilled and filled with high-strength concrete under compression. Concrete confinement was considered, particularly for the face-to-face and box configurations. The analytically calculated critical load values, based on EN 1993-1-3 and EN 1994-1-1 standards, were compared with the numerical results obtained. This research has led to the following conclusions:

- ✓ For unfilled columns with a length of 2000mm, the maximum lateral displacement occurred at the midpoint in the face-to-face configuration, and at 550mm in the box configuration. Local buckling was observed in the back-to-back configuration columns at lengths of 450mm and 1200mm.
- ✓ It is noteworthy that the unfilled box columns exhibited an approximately 30% increase in failure load compared to the back-to-back and face-to-face models.
- ✓ Among the studied models, the concrete-filled box configuration demonstrated optimal performance in minimizing imperfections resulting from elastic instabilities compared to the other models.
- ✓ Adding concrete inside the built-up cold-formed steel columns significantly increased their structural strength, providing greater load capacity and enhanced compression resistance. This combination of cold-formed steel and concrete improved their overall performance.
- ✓ Assembled face-to-face configured columns, whether filled with concrete or not, demonstrated a moderate influence, remaining within a range of 40%.
- ✓ With the focus on measuring lateral displacement, the results show that the suggested models offer a trustworthy and effective way to evaluate the stability of doubly

constructed columns with various configurations. Cold-formed steel built-up models are able to accurately represent many forms of instability, such as distortional, local, and global buckling.

- ✓ Unlike the unfilled assembled columns, the concrete-filled built-up columns exhibited a significant reduce in deformations and a twofold increase in load-bearing capacity.
- ✓ The results showed a remarkable correlation between the numerical and experimental outcomes, with discrepancies not exceeding 5%.
- ✓ Concrete-filled built-up face-to-face column (FF) demonstrates significantly higher strength compared to the other columns, with a failure load of 220kN.
- ✓ Slender open-section columns are more susceptible to instabilities, such as local and distortional buckling, compared to short columns. Therefore, it is often necessary to employ reinforcement techniques, such as concrete encasement, to maintain their structural integrity and ensure stability.
- ✓ Based on the experimental test, it's concluded that rivet assembly is more effective than welding. This is especially evident when the columns are filled with concrete, as the rivets act as studs, ensuring a strong connection between the steel and the concrete. This has led to an improvement in the performance and stability of the concrete-filled box column.
- ✓ Closed-section columns (face-to-face and box) exhibit a moderate improvement in lateral displacement, approximately 37%. This modest enhancement is due to the confinement effect, which generates lateral force on the inner walls of the steel section. This force leads to the rupture of welds with a notable separation of the steel, which was clearly observed during the experimental testing of concrete-filled built-up face-to-face column.

RECOMMENDATIONS

Taking into account various aspects of modeling cold-formed steel built-up columns, whether unfilled or filled with concrete, we can formulate the following recommendations:

- ✓ Further research will be conducted to assess the influence of other factors, such as the b/t ratio of built-up sections with different slenderness ratios, on the load-bearing capacity of assembled columns.

- ✓ Exploring additional types of loading, such as combined bending, could enhance our understanding and offer further insights into the behavior of the structures under investigation.
- ✓ Deepening this research by exploring the use of other filling materials, such as lightweight concrete and self-compacting concrete, could shed valuable insights on the performance of the studied columns and open new perspectives for their design and application.

REFERENCES

A A H Al-Filfily, A A Muhmmed, 2022. EFFECT OF DIFFERENT RIVETING SHAPE ON STRENGTH OF BONDED JOINT OF ALUMINUM POLYMER USING FEM. https://doi.org/10.13140/RG.2.2.18423.80802

ABNT, 2010. Brazilian Standard on Design of Cold-formed Steel Structures. Brazilian Standards Association, Rio de Janeiro.

ACI Committee, 1999. Building code requirements for structural concrete:(ACI 318-99); and commentary (ACI 318R-99). American Concrete Institute.

AISI, 2001. North American specification for the design of cold-formed steel structural members. American Iron and Steel Institute, Washington, D.C.

AISI-S100-04, 2004. North American Specification for the Design of Cold-formed Steel Structural Members (NAS) + Respective Commentary. American Iron and Steel Institute, Washington, D.C.

AISI-S100-07, 2007. North American Specification for the Design of Cold-Formed Steel Structural Members. American Iron and Steel Institute, Washington, D.C.

AISI-S100-12, 2012. North American Specification for the Design of Cold-Formed Steel Structural Members. American Iron and Steel Institute, Washington, D.C 473.

Alex, J., Iyappan, G., 2016. Experimental study on flexural behaviour of cold formed steel section. Int J Res Sci Engg Tech 40, 219–222.

Anas, S.M., Alam, M., Umair, M., 2021. Experimental and numerical investigations on performance of reinforced concrete slabs under explosive-induced air-blast loading: A state-of-the-art review. Structures 31, 428–461. https://doi.org/10.1016/j.istruc.2021.01.102

Arsić, M., Lazić, V., Arsic, D., Savić, Z., Živče, Š., 2013. Effect of Enhanced Mechanical Properties of Weld Metal and Heat Affected Zone on the Strength of the Welded Joint 15, 6.

ASTM, A., 2009. E9-09. Standard test methods of compression testing of metallic materials at room temperature.

ASTM Committee, 2020. Standard test methods and definitions for mechanical testing of steel products ASTM A 370-20. ASTM International.

Attarha, M.J., Sattari-Far, I., 2011. Study on welding temperature distribution in thin welded plates through experimental measurements and finite element simulation. Journal of Materials Processing Technology 211, 688–694. https://doi.org/10.1016/j.jmatprotec.2010.12.003

Bambach, M.R., 2006. Local buckling and post-local buckling redistribution of stress in slender plates and sections. Thin-Walled Structures 44, 1118–1128. https://doi.org/10.1016/j.tws.2006.10.005

Ban, H., Shi, G., 2018. A review of research on high-strength steel structures. Proceedings of the Institution of Civil Engineers - Structures and Buildings 171, 625–641. https://doi.org/10.1680/jstbu.16.00197

Becque, J., 2019. Optimization of cold-formed steel products: achievements, challenges and opportunities. ce papers 3, 211–218. https://doi.org/10.1002/cepa.1048

Beulah Gnana Ananthi, G., Ashvini, B., 2019. Experimental theoretical and numerical studies on cold-formed steel stub channel columns with stiffeners. Asian J Civ Eng 20, 171–185. https://doi.org/10.1007/s42107-018-0096-2

Bhandari, V., 2010. Design of machine elements. Tata McGraw-Hill Education.

BOULMAALI-HACENE CHAOUCHE, Y., 2023. ELEMENTS FINIS POUR L'ANALYSE LINEAIRE ET NON LINEAIRE DES PLAQUES ET COQUES MINCES ET EPAISSES APPLICATION AUX ELEMENTS TUBULAIRES EN ACIER REMPLIS DE BETON (Thèse de Doctorat en Sciences en Génie civil). Université de badji Mokhtar - Annaba, Annaba.

CEN, E., 2005. 1-1-Eurocode 3: Design of steel structures-Part 1-1: General rules and rules for buildings. European Committee for Standardization, Brussels.

Chen, H., Brockenbrough, R., Haws, R., 2010. Overview of Recent Changes and Additions to AISI Standards 15.

Chen, J., He, Y., Jin, W.-L., 2010. Stub column tests of thin-walled complex section with intermediate stiffeners. Thin-Walled Structures 48, 423–429. https://doi.org/10.1016/j.tws.2010.01.008

Chen, M.-T., Zhang, T., Young, B., 2023. Behavior of concrete-filled cold-formed steel built-up section stub columns. Thin-Walled Structures 187, 110692. https://doi.org/10.1016/j.tws.2023.110692

Cichański, A., Tomaszewski, T., 2015. NUMERICAL VERIFICATION OF QUASI-STATIC STRENGTH OF THE HORIZONTAL BICYCLE WELDED FRAME 7.

Cold-formed steel structures, 2nd ed. ed, 2005. . Standards Australia ; Standards New Zealand, Sydney, N.S.W., Wellington [N.Z.].

Craveiro, H.D., Rahnavard, R., Laím, L., Simões, R.A., Santiago, A., 2022. Buckling behavior of closed built-up cold-formed steel columns under compression. Thin-Walled Structures 179, 109493. https://doi.org/10.1016/j.tws.2022.109493

Dai, X., Lam, D., 2010. Numerical modelling of the axial compressive behaviour of short concrete-filled elliptical steel columns. Journal of Constructional Steel Research 66, 931–942. https://doi.org/10.1016/j.jcsr.2010.02.003

Dar, A.R., 2021. Bending response of cold-formed steel built-up beams with overlapped flanges in stiffened channels. Innov. Infrastruct. Solut. 6, 175. https://doi.org/10.1007/s41062-021-00546-5

De Wilde, J., 2007. Model tests on the vortex induced motions of the air can of a free standing riser system in current. Presented at the Proceedings of the Deep Offshore Technology Conference, pp. 1–10.

Dhatt, G., Lefrançois, E., Touzot, G., 2012. Finite element method. John Wiley & Sons.

DJAFOUR, N., 2015. Proposition d'une méthode de classification des modes d'instabilité des colonnes en acier formées à froid. Université Abou Bekr BELKAID – Tlemcen 149.

Djelil, M., 2019. Décomposition modale des phénomènes d'instabilité des profils en acier formés à froid par la méthode des splines bandes finies. Université Abou-Bekr BELKAID – Tlemcen. https://doi.org/10.13140/RG.2.2.14682.08647

Dreux, G., Festa, J., 1998. New guide of concrete and its constituents. Paris: Edition Eyrolles 416.

Dubina, D., 2001. The ECBL approach for interactive buckling of thin-walled steel members. Steel and Composite Structures, An International Journal 1, 75–96.

Dubina, D., 1996. Coupled instabilities in bar members–general report. Presented at the Proceedings of the Second International Conference on Coupled Instabilities in Metal Structures, Belgium, pp. 119–132.

Dubina, D., Ungureanu, V., Landolfo, R., 2012. Design of cold-formed steel structures. Presented at the Eurocode, pp. 1–3.

Duval, A., Al-akhras, H., Maurin, F., Elguedj, T., Duval, A., Al-akhras, H., Maurin, F., Elguedj, T., 2014. Abaqus/CAE 6.14 user's manual. Dassault Systémes Inc.

Ellobody, E., Young, B., 2006. Design and behaviour of concrete-filled cold-formed stainless steel tube columns. Engineering Structures 28, 716–728. https://doi.org/10.1016/j.engstruct.2005.09.023

EN 1993-1-5, 2006. Eurocode 3: Design of steel Structures. Part 1.5: Eurocode 3-Design of steel structures-Part 1-5: Plated structural elements.

EN 1993-1-8, 2005. Eurocode 3: Design of steel structures-Part 1-8: Design of joints. CEN: Brussels, Belgium.

Eurocode 4, 2004. Design of composite steel and concrete structures Part 1.1 General rules and rules for buildings. European Committee for Standardization EN1994-1-1.

European Committee for Standardization, 2006. Eurocode 3: Design of steel structures, Part 1-3: General rules—Supplementary rules for cold-formed members and sheeting. EN 1993-1-3.

European Committee for Standardization, 2004. EN 1992-1-1 Eurocode 2: Design of Concrete Structures—Part 1-1: General Rules and Rules for Buildings.

Fadhel, E., 2014. Effect of Shot Peening on The Buckling Behaviour of Steel CK35 under Combined Loading.

Glauz, R.S., 2023. Strength-based requirements for end connections of built-up cold-formed steel columns. Thin-Walled Structures 182, 110265. https://doi.org/10.1016/j.tws.2022.110265

Gulvanessian, H., 2002. Eurocode 0: BS EN 1990: 2002. Basis of structural design. Thomas Telford, London.

Hadidane, Y., Kouider, N., Benzerara, M., 2022. Flexural behavior of delta and bi-delta cold-formed steel beams: experimental investigation and numerical analysis. Frattura ed Integrità Strutturale 16, 69–88. https://doi.org/10.3221/IGF-ESIS.61.05

Hancock, G.J., Murray, T., Ellifrit, D.S., 2001. Cold-formed steel structures to the AISI specification. CRC Press.

Harrat, O., Hadidane, Y., Anas, S.M., Sor, N.H., Deifalla, A.F., Awoyera, P.O., Gouider, N., 2024. Nonlinear Study on the Mechanical Performance of Built-Up Cold-Formed Steel Concrete-Filled Columns under Compression. Computer Modeling in Engineering \& Sciences 139. https://doi.org/10.32604/cmes.2023.044950

Hedayati, E., Vahedi, M., 2017. Numerical investigation of penetration in ceramic/aluminum targets using smoothed particle hydrodynamics method and presenting a modified analytical model. Computer Modeling in Engineering & Sciences 113, 295–323.

Henriksson, A., Panarelli, J., 2017. Initial bow imperfection for flexural buckling of steel members-Verification and optimisation regarding analysis of columns and beam-columns.

Hibbitt, D., Karlsson, B., Sorensen, P., 2014. ABAQUS user-manual release 6.14. Dassault Systèmes Simulia Corp., Providence, RI.

Hu, H.-T., Huang, C.-S., Wu, M.-H., Wu, Y.-M., 2003. Nonlinear Analysis of Axially Loaded Concrete-Filled Tube Columns with Confinement Effect. J. Struct. Eng. 129, 1322–1329. https://doi.org/10.1061/(ASCE)0733-9445(2003)129:10(1322)

Johnson, R.P., Buckby, R.J., 1975. Composite structures of steel and concrete. Crosby Lockwood Staples London.

Kanthasamy, E., Hussain, J., Thirunavukkarasu, K., Poologanathan, K., Roy, K., Beulah Gnana Ananthi, G., Suntharalingam, T., 2022. Flexural Behaviour of Built-Up Beams Made of Optimised Sections. Buildings 12, 1868. https://doi.org/10.3390/buildings12111868

KEBAILI, B., 2013. Analyse des colonnes mixtes Acier Béton (Thèse de Doctorat en Sciences en Génie civil). Université de badji Mokhtar - Annaba, Annaba.

Kouider, N., Hadidane, Y., Benzerara, M., 2021. Numerical investigation of the cold-formed I-beams bending strength with different web shapes. Frattura ed Integrità Strutturale 16, 153–171. https://doi.org/10.3221/IGF-ESIS.59.12

Laím, L., Rodrigues, J.P.C., Silva, L.S.D., 2013. Experimental and numerical analysis on the structural behaviour of cold-formed steel beams. Thin-Walled Structures 72, 1–13. https://doi.org/10.1016/j.tws.2013.06.008

Li, G., Renaud, G., Liao, M., 2021. Assessing the riveting process and the quality of riveted lap joints in aerospace and other applications, in: Welding and Joining of Aerospace Materials. Elsevier, pp. 383–426. https://doi.org/10.1016/B978-0-12-819140-8.00013-4

Li, G.-Q., Wang, W.-Y., Chen, S.-W., 2009. A simple approach for modeling fire-resistance of steel columns with locally damaged fire protection. Engineering Structures 31, 617–622. https://doi.org/10.1016/j.engstruct.2008.11.004

Li, Z., Schafer, B.W., 2010. Application of the finite strip method in cold-formed steel member design. Journal of Constructional Steel Research 66, 971–980. https://doi.org/10.1016/j.jcsr.2010.04.001

Liang, H., Roy, K., Fang, Z., Lim, J.B.P., 2022. A Critical Review on Optimization of Cold-Formed Steel Members for Better Structural and Thermal Performances. Buildings 12, 34. https://doi.org/10.3390/buildings12010034

Liang, W., Deng, D., 2018. Influences of heat input, welding sequence and external restraint on twisting distortion in an asymmetrical curved stiffened panel. Advances in Engineering Software 115, 439–451. https://doi.org/10.1016/j.advengsoft.2017.11.002

Loughlan, J., 2018. Thin-walled structures: advances in research, design and manufacturing technology.

Mander, J.B., Priestley, M.J.N., Park, R., 1988. Theoretical Stress-Strain Model for Confined Concrete. J. Struct. Eng. 114, 1804–1826. https://doi.org/10.1061/(ASCE)0733-9445(1988)114:8(1804)

MANSOURI, K., 2022. Assemblage des Matériaux. Université Abbes LAGHROUR Khenchela 63.

Mansuri, S., Parmar, K., 2017. Numerical investigation of flexural strength of cold form built-up beams. Int. J. Adv. Res. Sci. Eng 6, 109–116.

Moen, C.D., Schafer, B.W., 2009. Elastic buckling of cold-formed steel columns and beams with holes. Engineering Structures 31, 2812–2824. https://doi.org/10.1016/j.engstruct.2009.07.007

Mohamad, A., Lorrain, B., Karama, M., Puel, B., 2007. Caractérisation des assemblages rivetés et vissés en fatigue. Presented at the CFM 2007-18ème Congrès Français de Mécanique, AFM, Maison de la Mécanique, 39/41 rue Louis Blanc-92400 Courbevoie.

Moradibistouni, M., Vale, B., Isaacs, N., 2021. A life cycle study of insulation in a case study building with a focus on the effect of the national energy profile. Journal of Building Engineering 43, 103178. https://doi.org/10.1016/j.jobe.2021.103178

Morkhade, S.G., Shaikh, S., Kumbhar, A., Shaikh, A., Tiwari, R., 2018. Comparative study of ultimate load for castellated and plain-webbed beams. International Journal of Civil Engineering and Technology 9, 1466–1476.

Nikishkov, G., 2004. Introduction to the finite element method. University of Aizu 1–70.

Niou, S., Azzouz, S., Chaoui, K., Azari, A., 2016. Développement d'une méthode pour caractériser la résistance mécanique circonférentielle d'un joint de tube plastique soudé bout-à-bout. Presented at the 10èmes Journées de Mécanique de l'EMP (JM'10–EMP), p. 7.

North American Specification for the Design of Cold-Formed Steel Structural Members, 2016 Edition, 2016. 505.

Rahnavard, R., Craveiro, H.D., Lopes, M., Simões, R.A., Laím, L., Rebelo, C., 2022a. Concrete-filled cold-formed steel (CF-CFS) built-up columns under compression: Test and design. Thin-Walled Structures 179, 109603. https://doi.org/10.1016/j.tws.2022.109603

Rahnavard, R., Craveiro, H.D., Simões, R.A., Laím, L., Santiago, A., 2022b. Buckling resistance of concrete-filled cold-formed steel (CF-CFS) built-up short columns under compression. Thin-Walled Structures 170, 108638. https://doi.org/10.1016/j.tws.2021.108638

Rahnavard, R., Craveiro, H.D., Simões, R.A., Laím, L., Santiago, A., 2022c. Fire resistance of concrete-filled cold-formed steel (CF-CFS) built-up short columns. Journal of Building Engineering 48, 103854. https://doi.org/10.1016/j.jobe.2021.103854

Rasmussen, K.J.R., Khezri, M., Schafer, B.W., Zhang, H., 2020. The mechanics of built-up cold-formed steel members. Thin-Walled Structures 154, 106756. https://doi.org/10.1016/j.tws.2020.106756

Richart, F.E., Brandtzæg, A., Brown, R.L., 1928. A study of the failure of concrete under combined compressive stresses. University of Illinois at Urbana Champaign, College of Engineering ….

Roy, K., Ting, T.C.H., Lau, H.H., Lim, J.B.P., 2018. Effect of thickness on the behaviour of axially loaded back-to-back cold-formed steel built-up channel sections - Experimental and numerical investigation. Structures 16, 327–346. https://doi.org/10.1016/j.istruc.2018.09.009

Saddek, A., Abdullah, A., Tohamy, S., Ahmed, A., 2018. Performance of Stiffened and Unstiffened Cold-formed Channel Sections in Pure Bending.

Sæther, I., Sand, B., 2012. FEM simulations of reinforced concrete beams attacked by corrosion 19.

Schafer, B.W., 2011. Cold-formed steel structures around the world: A review of recent advances in applications, analysis and design. Steel Construction 4, 141–149. https://doi.org/10.1002/stco.201110019

Schafer, B.W., 2006. Designing cold-formed steel using the direct strength method.

Schafer, B.W., Pekoz, T., 1998. Direct Strength Prediction of Cold-formed Steel Members Using Numerical Elastic Buckling Solutions.

Shanmugam, B., Palanisamy, M., Awoyera, P.O., Chinnasamy, S., Subramaniam, M., 2021. A Study on the Effect of Hollow Tubular Flange Sections on the Behavior of Cold-Formed Steel Built-Up Beams. Advances in Civil Engineering 2021, 1–9. https://doi.org/10.1155/2021/4482887

Somadasa, W., 2006. Flexural behaviour and design of cold-formed steel beams with rectangular hollow flanges (Doctoral thesis). Queensland University of Technology (QUT), Brisbane, Australia.

Sujitha, R., Sunmathi, N., Manikandan, R.K., Arunprasad, J., Rajkumar, S., Sharma, S., Sharma, K., Li, C., Tag Eldin, E.M., 2022. Analytical and Experimental Study on Cold-Formed Steel Built-Up Sections for Bending. Materials 15, 7140. https://doi.org/10.3390/ma15207140

Systemes, D., 2014. Simulia ABAQUS, 6.14. Theory and User's Manuals.

Teoh, K.B., Chua, Y.S., Dai Pang, S., Kong, S.Y., 2023. Experimental investigation of lightweight aggregate concrete-filled cold-formed built-up box section (CFBBS) stub columns under axial compression. Engineering Structures 279.

Timoshenko, S., Gere, J.M., 1961. Theory of elasticity stability. McGraw.

Tomii, M., SAKINO, K., 1979. Experimental studies on concrete filled square steel tubular beam-columns subjected to monotonic shearing force and constant axial force. Transactions of the Architectural Institute of Japan 281, 81–92. https://doi.org/10.3130/aijsaxx.281.0_81

Veríssimo, H., 2008. Dimensionamento de elementos estruturais de aço enformados a frio de acordo com o Eurocódigo 3. Instituto Superior Técnico.

Vilnay, O., Rockey, K.C., 1981. A generalised effective width method for plates loaded in compression. Journal of Constructional Steel Research 1, 3–12. https://doi.org/10.1016/0143-974X(81)90002-X

Von Kármán, T., Sechler, E.E., Donnell, L.H., 1932. The strength of thin plates in compression. Transactions of the American Society of Mechanical Engineers 54, 53–56.

Weng, C.C., Pekoz, T., 1990. Residual Stresses in Cold-Formed Steel Members. J. Struct. Eng. 116, 1611–1625. https://doi.org/10.1061/(ASCE)0733-9445(1990)116:6(1611)

Winter, G., Pian, R., 1946. Crushing strength of thin steel webs. Cornell University.

Xie, Z., Yan, W., Yu, C., Mu, T., Song, L., 2018. Improved shear strength design of cold-formed steel connection with single self-piercing rivet. Thin-Walled Structures 131, 708–717. https://doi.org/10.1016/j.tws.2018.03.025

Yang, J., Luo, K., Wang, W., Shi, Y., Li, H., 2024. Research on the flexural buckling behavior of the cold-formed steel back-to-back built-up columns with Σ-section. Engineering Structures 302, 117404. https://doi.org/10.1016/j.engstruct.2023.117404

Yu, C., 2016. Recent Trends in Cold-formed Steel Construction, Woodhead Publishing series in civil and structural engineering. Woodhead Publishing.

Yu, C., Yan, W., 2011. Effective Width Method for determining distortional buckling strength of cold-formed steel flexural C and Z sections. Thin-Walled Structures 49, 233–238. https://doi.org/10.1016/j.tws.2010.11.006

Yu, W., 2000. Cold-formed steel design, 3rd ed. ed. Wiley, New York.

Yu, W.-W., LaBoube, R.A., Chen, H., 2019. Cold-formed steel design. John Wiley & Sons.

Zeghiche, J., Chaoui, K., 2005. An experimental behaviour of concrete-filled steel tubular columns. Journal of Constructional Steel Research 61, 53–66. https://doi.org/10.1016/j.jcsr.2004.06.006

Zhang, J.-H., Young, B., 2012. Compression tests of cold-formed steel I-shaped open sections with edge and web stiffeners. Thin-Walled Structures 52, 1–11. https://doi.org/10.1016/j.tws.2011.11.006

ANNEX A

A.1 DETERMINATION OF THE CHARACTERISTICS OF THE SECTIONS

$h_p = H - t_{nom} = 75 - 1.24 =$ **73.76mm**

$b_p = B - t_{nom} = 40 - 1.24 =$ **38.76mm**

$C_p = C - \frac{t_{nom}}{2} = 10 - \frac{1.24}{2} =$ **9.38mm**

A.2 VERIFICATION OF GEOMETRIC PROPERTIES

$1mm \leq t_{nom} \leq 4mm \quad \Rightarrow \quad 1mm \leq 1.24mm \leq 4mm \quad \Rightarrow$ **O.K**

$\frac{B}{t} \leq 60 \quad \Rightarrow \quad \frac{40}{1.2} = 33.33 < 60 \quad \Rightarrow$ **O.K**

$\frac{H}{t} \leq 500 \quad \Rightarrow \quad \frac{75}{1.2} = 62.5 < 500 \quad \Rightarrow$ **O.K**

$\frac{C}{t} \leq 50 \quad \Rightarrow \quad \frac{10}{1.2} = 8.33 < 50 \quad \Rightarrow$ **O.K**

$45° \leq \alpha \leq 135° \quad \Rightarrow \quad 45° \leq 90° \leq 135° \quad \Rightarrow$ **O.K**

$0.2 \leq \frac{C}{B} \leq 0.6 \quad \Rightarrow \quad 0.2 \leq \frac{10}{40} \leq 0.6 \quad \Rightarrow \quad 0.2 < 0.25 < 0.6 \quad \Rightarrow$ **O.K**

$\frac{r}{t} \leq 5 \quad \Rightarrow \quad \frac{2.1}{1.2} = 1.75 < 5 \quad \Rightarrow$ **O.K**

$\frac{r}{b_p} \leq 0.1 \quad \Rightarrow \quad \frac{2.1}{38.76} = 0.05 < 0.1 \quad \Rightarrow$ **O.K**

A.3 CALCULATION OF THE GROSS-SECTION FOR THE BACK-TO-BACK MODEL

$A_s = 2[(2 \times t \times b_p) + 2[t \times (C-t)] + t[H-(2 \times t)]]$

$A_s = 2[(2 \times 1.2 \times 20) + 2[1.2 \times (10-1.2)] + 1.2[75-(2 \times 1.2)]]$

$A_s = 312.48mm^2$

A.4 CALCULATION OF THE EFFECTIVE SECTION

A.4.1 First step

A.4.1.1 Effective width of the upper flange

The stress ratio is $\psi = 1$ (uniform compression), so the buckling coefficient is $K_\sigma = 4$ for an internal compression element.

$$\varepsilon = \sqrt{\frac{235}{f_y}} = \sqrt{\frac{235}{250}}$$

ε = 0.97

$$\overline{\lambda_{bp1}} = \frac{b_p / t}{28.4 \times \varepsilon \sqrt{K_\sigma}} = \frac{38.76 / 1.2}{28.4 \times 0.97 \sqrt{4}} = \mathbf{0.59} < 0.673 \Rightarrow \rho_{bp1} = \mathbf{1}$$

$b_{eff1} = \rho_{bp1} \times b_p = 1 \times 38.76 =$ **38.76mm**

$b_{e1} = b_{e2} = 0.5 \times b_{eff1} = 0.5 \times 38.76 =$ **19.38mm**

A.4.1.2 Effective width of the lower flange

$$\overline{\lambda_{bp2}} = \frac{b_p / t}{28.4 \times \varepsilon \sqrt{K_\sigma}} = \frac{38.76 / 1.2}{28.4 \times 0.97 \sqrt{4}} = \mathbf{0.59} < 0.673 \Rightarrow \rho_{bp2} = \mathbf{1}$$

$b_{eff2} = \rho_{bp2} \times b_p = 1 \times 38.76 =$ **38.76mm**

$b_{e3} = b_{e4} = 0.5 \times b_{eff2} = 0.5 \times 38.76 =$ **19.38mm**

A.4.1.3 Effective width of the upper dropped edge

$$\frac{C_p}{b_p} \le 0.35 \quad \Rightarrow \quad K_\sigma = 0.5$$

$$0.35 \le \frac{C_p}{b_p} \le 0.6 \quad \Rightarrow \quad K_\sigma = 0.5 + 0.83 \sqrt{\frac{C_p}{b_p} - 0.35^2}$$

$$\frac{C_p}{b_p} > 0.6 \quad \Rightarrow \quad K_\sigma = 0.33$$

$$\frac{C_p}{b_p} = \frac{9.38}{38.76} = 0.24 < 0.35 \Rightarrow \mathbf{K_\sigma = 0.5}$$

$$\overline{\lambda_{cp1}} = \frac{C_p / t}{28.4 \times \varepsilon \sqrt{K_\sigma}} = \frac{9.38 / 1.2}{28.4 \times 0.97 \sqrt{4}} = \mathbf{0.40} < 0.673 \Rightarrow \rho_{Cp1} = \mathbf{1}$$

$C_{eff1} = \rho_{Cp1} \times C_p = 1 \times 9.38 =$ **9.38mm**

$A_{s1} = t\left(b_{e1} + C_{eff1}\right) = 1.2\left(19.38 + 9.38\right) =$ **34.512mm²**

A.4.1.4 Effective width of the lower dropped edge

$$\frac{C_p}{b_p} = \frac{9.38}{38.76} = 0.24 < 0.35 \Rightarrow \mathbf{K_\sigma = 0.5}$$

$$\overline{\lambda_{cp2}} = \frac{C_p / t}{28.4 \times \varepsilon \sqrt{K_\sigma}} = \frac{9.38 / 1.2}{28.4 \times 0.97 \sqrt{4}} = \mathbf{0.40} < 0.673 \Rightarrow \rho_{Cp2} = \mathbf{1}$$

$C_{eff2} = \rho_{Cp2} \times C_p = 1 \times 9.38 = \mathbf{9.38mm}$

$$A_{s2} = t\left(b_{e2} + C_{eff\,2}\right) = 1.2\left(19.38 + 9.38\right) = \mathbf{34.512mm^2}$$

A.4.2 Second step

A.4.2.1 Effective width of the upper dropped edge

b_1 and b_2 are the distance between the web-flange junction and the centroid of the effective area of the edge stiffener.

$$b_1 = b_p - \frac{b_{e1} \times t \times b_{e1}/2}{\left(b_{e1}^2 + C_{eff\,1}\right)t} = 38.76 - \frac{19.38 \times 1.2 \times 19.38/2}{\left(19.38^2 + 9.38\right) \times 1.2} = \mathbf{32.23mm}$$

$$b_2 = b_p - \frac{b_{e2} \times t \times b_{e2}/2}{\left(b_{e2}^2 + C_{eff\,1}\right)t} = 38.76 - \frac{19.38 \times 1.2 \times 19.38/2}{\left(19.38^2 + 9.38\right) \times 1.2} = \mathbf{32.23mm}$$

$$I_{s1} = \frac{b_{e1} \times t^3}{12} + \frac{C_{eff\,1}^3 \times t}{12} + b_{e1} \times t \times \left[\frac{C_{eff\,1}^2}{2\left(b_{e2} + C_{eff\,1}\right)}\right]^2 + C_{eff\,1} \times t \times \left[\frac{C_{eff\,1}}{2} - \frac{C_{eff\,1}^2}{2\left(b_{e2} + C_{eff\,1}\right)}\right]^2$$

$$I_{s1} = \frac{19.38 \times 1.2^3}{12} + \frac{9.38^3 \times 1.2}{12} + 19.38 \times 1.2 \times \left[\frac{9.38^2}{2\left(19.38 + 9.38\right)}\right]^2 + 9.38 \times 1.2 \times \left[\frac{9.38}{2} - \frac{9.38^2}{2\left(19.38 + 9.38\right)}\right]^2$$

$\mathbf{I_{s1} = 252.16mm^4}$

$$K_f = \frac{A_{s2}}{A_{s1}} = \frac{34.512}{34.512} = \mathbf{1}$$

$$K_1 = \frac{Et^3}{4\left(1 - \upsilon^2\right)} \times \frac{1}{b_p \times h_p + b_1^3 + 0.5 \times b_1 \times b_2 \times h_p \times K_f}$$

$$K_1 = \frac{210000 \times 1.2^3}{4\left(1 - 0.3^2\right)} \times \frac{1}{38.76 \times 73.76 + 32.23^3 + 0.5 \times 32.23 \times 32.23 \times 73.76 \times 1} = \mathbf{0.67}$$

$$\sigma_{cr,s1} = \frac{2\sqrt{K_1 E I_{s1}}}{A_{s1}} = \frac{2\sqrt{0.67 \times 210000 \times 252.16}}{34.512} = \mathbf{345.62MPa}$$

Reduction coefficient χ_d for edge stiffeners:

$$\overline{\lambda_{d1}} = \sqrt{\frac{f_y}{\sigma_{cr,s1}}} = \sqrt{\frac{250}{345.62}} = \mathbf{0.85 > 0.65} \Rightarrow \quad \chi_{d1} = 1.47 - \left(0.723 \times \overline{\lambda_{d1}}\right)$$

$$\chi_{d1} = 1.47 - \left(0.723 \times 0.85\right) = \mathbf{0.855}$$

A.4.2.2 Effective width of the lower dropped edge

b_3 and b_4 are the distance between the web-flange junction and the centroid of the effective area of the edge stiffener.

$$b_3 = b_p - \frac{b_{e3} \times t \times {b_{e3}}/{2}}{\left(b_{e3}^2 + C_{eff\,2}\right)t} = 38.76 - \frac{19.38 \times 1.2 \times {19.38}/{2}}{\left(19.38^2 + 9.38\right) \times 1.2} = \mathbf{32.23mm}$$

$$b_4 = b_p - \frac{b_{e4} \times t \times {b_{e4}}/{2}}{\left(b_{e4}^2 + C_{eff\,2}\right)t} = 38.76 - \frac{19.38 \times 1.2 \times {19.38}/{2}}{\left(19.38^2 + 9.38\right) \times 1.2} = \mathbf{32.23mm}$$

$$I_{s2} = \frac{b_{e3} \times t^3}{12} + \frac{C_{eff\,2}^3 \times t}{12} + b_{e3} \times t \times \left[\frac{C_{eff\,2}^2}{2\left(b_{e4} + C_{eff\,2}\right)}\right]^2 + C_{eff\,2} \times t \times \left[\frac{C_{eff\,2}}{2} - \frac{C_{eff\,2}^2}{2\left(b_{e4} + C_{eff\,2}\right)}\right]^2$$

$$I_{s2} = \frac{19.38 \times 1.2^3}{12} + \frac{9.38^3 \times 1.2}{12} + 19.38 \times 1.2 \times \left[\frac{9.38^2}{2\left(19.38 + 9.38\right)}\right]^2 + 9.38 \times 1.2 \times \left[\frac{9.38}{2} - \frac{9.38^2}{2\left(19.38 + 9.38\right)}\right]^2$$

I_{s2} = 252.16mm^4

$$K_f = \frac{A_{s2}}{A_{s1}} = \frac{34.512}{34.512} = \mathbf{1}$$

$$K_2 = \frac{Et^3}{4\left(1 - \upsilon^2\right)} \times \frac{1}{b_p \times h_p + b_3^3 + 0.5 \times b_3 \times b_4 \times h_p \times K_f}$$

$$K_2 = \frac{210000 \times 1.2^3}{4\left(1 - 0.3^2\right)} \times \frac{1}{38.76 \times 73.76 + 32.23^3 + 0.5 \times 32.23 \times 32.23 \times 73.76 \times 1} = \mathbf{0.67}$$

$$\sigma_{cr,s2} = \frac{2\sqrt{K_2 E I_{s2}}}{A_{s2}} = \frac{2\sqrt{0.67 \times 210000 \times 252.16}}{34.512} = \mathbf{345.62MPa}$$

Reduction coefficient χ_d for edge stiffeners:

$$\overline{\lambda_{d2}} = \sqrt{\frac{f_y}{\sigma_{cr,s2}}} = \sqrt{\frac{250}{345.62}} = \mathbf{0.85 > 0.65} \Rightarrow \quad \chi_{d2} = 1.47 - \left(0.723 \times \overline{\lambda_{d2}}\right)$$

$$\chi_{d2} = 1.47 - \left(0.723 \times 0.85\right) = \mathbf{0.855}$$

A.4.3 Third step

A.4.3.1 Effective width of the web

$$\overline{\lambda_{hp}} = \frac{h_p / t}{28.4 \times \varepsilon \sqrt{K_\sigma}} = \frac{73.76 / 1.2}{28.4 \times 0.97 \sqrt{4}} = \mathbf{1.17} > 0.673 \Rightarrow \rho_{hp} = \frac{\overline{\lambda_{hp}} - 0.055(3+\psi)}{\overline{\lambda_{hp}}^2}$$

$$\rho_{hp} = \frac{1.17 - 0.055(3+1)}{1.17^2} = \mathbf{0.72}$$

$h_{eff} = \rho_{hp} \times h_p = 0.72 \times 73.76 =$ **53.06mm**

$h_{e1} = h_{e2} = 0.5 \times h_{eff} = 0.5 \times 53.06 =$ **26.53mm**

A.4.4 Effective section of back-to-back model

$$A_{eff\,1} = t \times \left[(2 \times b_{e1}) + (2 \times b_{e3}) + h_{e1} + h_{e2} + 2 \times \left[(b_{e2} + C_{eff\,1}) \times \chi_{d1} \right] + 2 \times \left[(b_{e4} + C_{eff\,2}) \times \chi_{d2} \right] \right]$$

$$A_{eff\,1} = 1.2 \times \left[(2 \times 19.38) + (2 \times 19.38) + 26.53 + 26.53 + 2 \times \left[(19.38 + 9.38) \times 0.855 \right] + 2 \times \left[(19.38 + 9.38) \times 0.855 \right] \right]$$

A_{eff1} = 274.73mm^2

A.4.5 Effective section of face-to-face model

$$A_{eff\,2} = t \times \left[(2 \times b_{e1}) + (2 \times b_{e3}) + (2 \times h_{e1}) + (2 \times h_{e2}) + \left[(b_{e2} + C_{eff\,1}) \times \chi_{d1} \right] + \left[(b_{e4} + C_{eff\,2}) \times \chi_{d2} \right] \right]$$

$$A_{eff\,2} = 1.2 \times \left[(2 \times 19.38) + (2 \times 19.38) + (2 \times 26.53) + (2 \times 26.53) + \left[(19.38 + 9.38) \times 0.855 \right] + \left[(19.38 + 9.38) \times 0.855 \right] \right]$$

A_{eff2} = 279.38mm^2

A.4.6 Effective section of box model

$$A_{eff\,3} = t \times \left[b_{e1} + b_{e3} + (2 \times h_{e1}) + (2 \times h_{e2}) + 2 \times \left[(b_{e2} + C_{eff\,1}) \times \chi_{d1} \right] + 2 \times \left[(b_{e4} + C_{eff\,2}) \times \chi_{d2} \right] \right]$$

$$A_{eff\,3} = 1.2 \times \left[19.38 + 19.38 + (2 \times 26.53) + (2 \times 26.53) + 2 \times \left[(19.38 + 9.38) \times 0.855 \right] + 2 \times \left[(19.38 + 9.38) \times 0.855 \right] \right]$$

A_{eff3} = 291.89mm^2

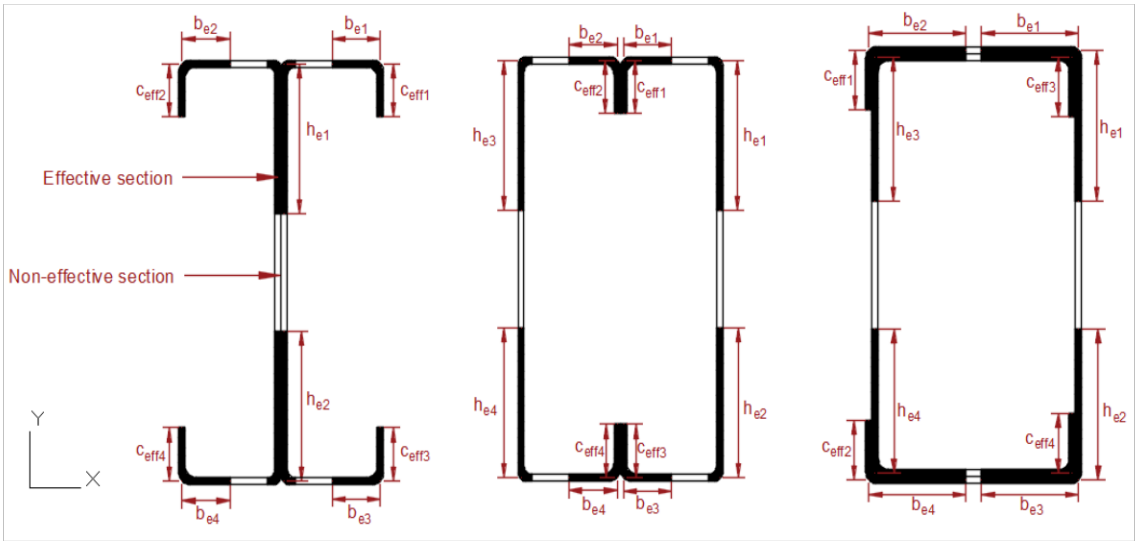

Figure A.1. The effective cross-sections of the studied columns.

A.5 CALCULATION OF THE CRITICAL LOAD FOR UNFILLED BACK-TO-BACK MODEL

A.5.1 Calculation of the buckling length

For L = 600mm $\Rightarrow$ L = l_f **= 600mm** (bi-articulated supports)

A.5.2 Calculation of the radius of gyration

$$i = \sqrt{\frac{I_s}{A_s}}$$

After the hygiene theory, we find that: $\mathbf{I_s = 283340.63mm^4}$

$$i = \sqrt{\frac{283340.63}{312.48}} \mathbf{= 30.11mm}$$

A.5.3 Calculation of the slenderness

$$\lambda = \frac{l_f}{i} = \frac{600}{30.11} \mathbf{= 19.63}$$

A.5.4 Calculation of the reduced slenderness

$$\bar{\lambda} = \frac{\lambda}{\lambda_r}\sqrt{\beta_A}$$

With:

$$\lambda_r = \pi\sqrt{\frac{E}{f_y}} = 3.14\sqrt{\frac{210000}{250}} = \mathbf{91.05}$$

$$\beta_A = \frac{A_{eff}}{A_s} = \frac{274.73}{312.48} = \mathbf{0.88}$$

$$\bar{\lambda} = \frac{\lambda}{\lambda_r}\sqrt{\beta_A} = \frac{19.63}{91.05}\sqrt{0.88} = \mathbf{0.18 < 0.2}$$

$$\bar{\lambda} < 0.2 \qquad \Rightarrow \qquad N_{c,Rd} = A_{eff}\frac{f_y}{\gamma_{M1}} \quad \text{(Class 4)}$$

A.5.5 Calculation of the critical load

$$N_{c,Rd} = A_{eff}\frac{f_y}{\gamma_{M1}} = 274.73 \times \frac{250}{1.1} = \mathbf{76864.63N}$$

$N_{c,Rd}$ = 76.86kN

The same method for the other unfilled models.

A.6 CALCULATION OF THE CRITICAL LOAD FOR BACK-TO-BACK ENCASED WITH CONCRETE MODEL

$$N_{c,Rd} = \chi N_{Pl,Rd}$$

A.6.1 Calculation of the plastic force

Back-to-back model is encased with concrete so:

$$N_{Pl,Rd} = A_{eff}\frac{f_y}{\gamma_{M1}} + 0.85A_c\frac{f_c}{\gamma_c}$$

With: $A_c = 2(B' \times H') = 2(18.8 \times 72.6) = 2729.76 \quad \Rightarrow$ **A_c = 2729.76mm^2**

$$N_{Pl,Rd} = A_{eff}\frac{f_y}{\gamma_{M1}} + 0.85A_c\frac{f_c}{\gamma_c} = 274.73 \times \frac{250}{1.1} + 0.85 \times 2729.76 \times \frac{25}{1.5} = 172581.39\text{N}$$

$N_{Pl,Rd}$ = 172.58kN

A.6.2 Calculation of the reduced slenderness

$$\bar{\lambda} = \sqrt{\frac{N_{Pl,R}}{N_{cr}}}$$

With:

$$N_{Pl,R} = A_{eff}\frac{f_y}{1} + 0.85A_c\frac{f_c}{1} = 274.73\times\frac{250}{1} + 0.85\times 2729.76\times\frac{25}{1} = 198160.2\text{N}$$

$N_{Pl,R}$ = 198.16kN

$$N_{cr} = \frac{\pi^2 (EI)_e}{l_f^2}$$

Where:

$$(EI)_e = E_s I_s + 0.8E_{cd}I_c = (210000\times 283340.63) + (0.8\times 22592.59\times 1406250) = \mathbf{8.49\times 10^{10}\ N.mm^2}$$

$$E_{cd} = \frac{E_{cm}}{\gamma_c} = \frac{30500}{1.35} = \mathbf{22592.59MPa}$$

After the hygiene theory, we find that: **I_c = 1406250mm^4**

$$N_{cr} = \frac{\pi^2 (EI)_e}{l_f^2} = \frac{3.14^2\times 8.49\times 10^{10}}{600^2} = 2327581.70\text{N}$$

N_{cr} = 2327.58kN

$$\bar{\lambda} = \sqrt{\frac{N_{Pl,R}}{N_{cr}}} = \sqrt{\frac{198.16}{2327.58}} = \mathbf{0.27 > 0.2}$$

A.6.3 Calculation of the reduction coefficient χ

$$\chi = \frac{1}{\phi + \sqrt{\phi^2 + \bar{\lambda}^2}} = \frac{1}{0.55 + \sqrt{0.55^2 + 0.27^2}} = 0.86 \quad \Rightarrow \quad \mathbf{\chi = 0.86}$$

Where:

$$\phi = 0.5\left[1 + \alpha(\bar{\lambda} - 0.2) + \bar{\lambda}^2\right] = 0.5\left[1 + 0.34(0.27 - 0.2) + 0.27^2\right] = \mathbf{0.55}$$

α=0.34 ⇒ according to buckling curve b in Table II.2 and Table III.4 in the case of encased with concrete model.

A.6.4 Calculation of the critical load

$$N_{c,Rd} = \chi N_{Pl,Rd} = 0.86\times 172.58 = 148.42$$

$N_{c,Rd}$ = 148.42kN

The same method for the other concrete-filled models.